Controlling Annual Grasses in Sagebrush Communities with Higher Resistance and Resilience is Crucial to Prevent Fire Risk and Invasion Expansion

A Dissertation
Presented in Partial Fulfillment of the Requirements for the
Degree of Doctor of Philosophy
with a
Major in Plant Sciences
in the
College of Graduate Studies
University of Idaho
by
Georgia R. Harrison

Approved by:
Co-Major Professors: Timothy S. Prather, Ph.D,; Eva K. Strand, Ph.D
Committee Members: Lisa M. Ellsworth, Ph.D.; Matthew J. Germino, Ph.D.
Department Administrator: Juliet M. Marshall, Ph.D.

August 2023

Abstract

Invasive annual grasses, such as cheatgrass (*Bromus tectorum*), pose a significant threat to western rangelands by outcompeting native plants and increasing the frequency and intensity of wildfires. Frequent fires have reduced or eliminated native shrubs as annual grasses have invaded rangelands. This research aimed to quantify three aspects of the management of cheatgrass-invaded rangelands: (1) control of annual grasses, native plant community response, and modeled fire behavior after an aerial application of the herbicide indaziflam, (2) flammability of cheatgrass and two native perennial grasses, and (3) classification of shrub canopy volume with structure-from-motion photogrammetry techniques.

Invasive annual grasses pose a significant fire risk and can quickly expand, even in low elevation mountain big sagebrush (*Artemisia tridentata* ssp. *vaseyana*) plant communities that have naturally high resistance to invasion and resilience to disturbance. Reducing the impact of annual grasses requires an effective tactic for annual grass control. The chosen tactic must minimize any negative effects and be maintained long enough to reduce plants emerging from the soil seedbank. One potential solution is the use of indaziflam, a new pre-emergent herbicide that has demonstrated promising results in reducing annual grasses for at least three years in natural areas throughout the western United States. The first chapter of this dissertation evaluated the efficacy of indaziflam in reducing annual grass foliar cover and its impact on native plant foliar cover and fuel continuity in mountain big sagebrush plant communities near Hailey, Idaho. A total of 19 ha were treated with indaziflam in September 2020, and 32, 900 m^2 permanent assessment plots were established within treated and untreated areas. Foliar cover and fuel continuity were measured one and two years post-treatment along 3, 30-m long transects per plot. To better understand the potential impact of control measures on fire behavior, customized fuel beds based on field measurements were developed to model fire behavior across the treated and untreated areas under three different environmental scenarios. The results showed that indaziflam treatment significantly reduced annual grass foliar cover across all plant community types, while not affecting fuel continuity or native perennial plant foliar cover, even in areas with dense shrub cover. Mean untreated annual grass foliar cover was 11% and 38% one- and two-years post-treatment, while treated cover was 4% and 10%, respectively. Total and herbaceous fuel loading did not differ by indaziflam application, and shrubs contributed the most to total fuels. Indaziflam treated areas had slightly lower modeled rates of spread, flame lengths, and reaction intensity than untreated areas, but these differences were only present in areas with low shrub cover. These findings suggest that indaziflam application is an effective tactic for controlling annual

grasses with minimal impacts to resident native plants in high resistance and resilience sagebrush communities for at least two years.

Cheatgrass increases fire risk and alters plant communities in the sagebrush steppe grasslands of the Great Basin (USA) and adjacent sagebrush steppe areas, yet no studies have contrasted its flammability to native perennial grasses. The second dissertation chapter focused on the flammability of cheatgrass compared to two native perennial grasses, Columbia needlegrass (*Achnatherum nelsonii*) and bluebunch wheatgrass (*Pseudoroegneria spicata*), across a range of fuel moistures. Cheatgrass increased overall mass consumption, flaming duration, and flame length when combined with the two perennial grass species. The extent of flammability increase was influenced by the proportion of cheatgrass in the mixture, with flaming duration and thermal dose being particularly sensitive to cheatgrass fuel moisture. Maximum temperature and flame length during perennial grass combustion remained similar, regardless of the presence of cheatgrass. Furthermore, the flammability of Columbia needlegrass was higher when burned with cheatgrass than anticipated based on the flammability of each species alone. Cheatgrass may pre-heat Columbia needlegrass, leading to increased mass consumption, flaming duration, and thermal dose. This study provides experimental evidence supporting previous qualitative observations of cheatgrass altering fire behavior and increasing fire risk. Cheatgrass increased flammability of these two native perennial bunchgrasses throughout a range of fuel moistures and should be considered in fire management decisions.

Shrub canopy volume is an important ecological indicator in rangeland ecosystems and is closely related to biomass, fuel loading, wildlife habitat, site productivity, and ecosystem structure. Traditional field techniques for estimating shrub canopy volume are tedious and time-consuming and pose challenges that alternate methods may alleviate. The third dissertation chapter explored the suitability of using drone-collected data to estimate shrub canopy volume for seven dominant shrub species within mountain big sagebrush plant communities in southern Idaho, USA. First, height and canopy widths of 103 shrubs of eight species was measured in the field. Then, canopy volume for each individual shrub was re-estimated using two techniques (allometric or volumetric) from a 3D representation of the study area which was created using structure-from-motion photogrammetry. The volumetric method, which involved converting point clouds to raster canopy height models, outperformed the allometric method and was more reproducible and robust to user-related variability. Drone-estimated volume closely matched field-estimated volume ($R^2 > 0.9$) for three larger shrub species: *A. tridentata* subsp. *tridentata*, *A. tridentata* subsp. *vaseyana*, and *Purshia tridentata*. These findings demonstrate that drone-collected images can be used to assess shrub canopy volume for at least five upland sagebrush steppe shrub species and support the integration of drone data-collection

into rangeland vegetation and fuels monitoring. Additionally, the study demonstrates the potential for automating canopy volume estimates using point cloud-based automatic shrub detection algorithms.

The research presented here provides compelling evidence of the threat posed by invasive annual grasses in sagebrush plant communities with naturally high resistance and resilience. The presence of cheatgrass increases the flammability of two native perennial grasses across various fuel moisture levels. The interaction across fuel types (grasses and shrubs) emphasizes the importance of low cost, accurate assessment of shrub canopy volume through use of unmanned aerial systems. Rangeland condition, fuel abundance and fuel distribution are important parameters measured with this drone-based technique. Mitigating the risk of annual grasses is imperative, and indaziflam is an effective tool for controlling them for at least two years, with minimal impact on native species.

Acknowledgments

I would like to express my sincere gratitude to the individuals and organizations who have been instrumental in supporting my academic pursuits and the completion of this project. Their contributions, guidance, and assistance have been invaluable, and I am truly thankful for their support. First and foremost, I extend my deepest appreciation to my two co-advisors, Tim Prather and Eva Strand. Their expertise, mentorship, and continuous guidance have shaped the direction of this research and have been instrumental in its successful completion. I am grateful for their unwavering support and valuable insights throughout this journey. I would also like to acknowledge the valuable contributions of Lisa Ellsworth and Matthew Germino, members of my dissertation committee. Their expertise and feedback have significantly enhanced the quality of this work. I am grateful for their thoughtful insights and guidance.

To Kayla Johnston and Lisa Jones, I extend my heartfelt thanks for your assistance throughout the entire project. From the initial planning stages to fieldwork and data analysis, your support has been invaluable. I would like to express my gratitude to the field assistants who played a crucial role in data collection: Ian Luehr-Sele, Aaron Johnston, Sage Huggins, Fisher Reis, Kaemen West, and Nichole Cussins. Their hard work, diligence, and attention to detail have been vital to the completion of this project.

Furthermore, I am thankful to Envu and the Joint Fire Science Program for their financial support, which made this research possible.

Dedication

I would like to extend my heartfelt thanks to Bryce, my family and friends.

Your belief in me has made all the difference, and I am fortunate to have you in my life.

Table of Contents

List of Tables

List of Figures

List of Equations

List of Supplemental Information

Statement of Contribution

Chapter 3, *A comparison and development of methods for estimating sagebrush shrub volume using drone imagery-derived point cloud*, is a collaborative work involving multiple authors, including Georgia Harrison, Abhinav Shrestha, Eva K. Strand, and Jason W. Karl. This chapter has been prepared as a multi-authored article for submission to the journal *Ecosphere*, where Georgia Harrison will serve as the first author.

In accordance with the guidelines for collaborative work submission, Georgia Harrison hereby provides a clear statement of her specific contribution to the collaborative work. Georgia's primary responsibilities and authorship in Chapter 3 include designing the research methodology, leading the collection and processing of field data and drone imagery-derived point cloud data, conducting data analysis, and interpreting the results. Georgia conducted statistical analyses and developed the results section of the manuscript. Furthermore, Georgia lead the writing of the manuscript and lead funding efforts for this project (Joint Fire Science Program Graduate Research Innovation award #L23AC00043-01).

Abhinav Shrestha contributed to the development and implementation of novel methods for estimating sagebrush shrub volume using the drone imagery-derived point cloud data. Abhinav assisted with processing the drone imagery-derived point cloud data and creating data visualizations to articulate the process. In addition, Abhinav conducted additional analysis to provide a proof of concept for automating canopy volume estimates using point cloud-based automatic shrub detection algorithms. Overall, Abhinav's expertise in remote sensing and image processing greatly contributed to the advancement of the research.

Eva K. Strand played a significant role in the collaborative work by contributing to the development of project ideas and securing funding through the Joint Fire Science Program. Her expertise and insights were valuable in shaping the research questions and ensuring the successful acquisition of funding for the project.

Jason W. Karl provided guidance and expertise in drone-based analysis, especially within the context of rangeland ecosystems. Jason conducted the drone flights for image collection. His input was instrumental in refining the research questions and ensuring the scientific rigor of the study. Jason also contributed to the interpretation of the results and provided critical feedback during the manuscript drafting process.

Introduction

Invasive annual grasses, particularly cheatgrass (*Bromus tectorum*), pose a significant threat to western rangelands by outcompeting native plants and increasing the frequency and intensity of fires. These fires have resulted in the reduction or elimination of native vegetation as cheatgrass continues to invade rangelands. Understanding the impact of cheatgrass invasion on rangeland condition and plant community composition, as well as developing effective management strategies, is crucial for the preservation and restoration of these ecosystems.

The primary goal of this research is to enhance our comprehension of annual grass invasion by exploring plant community response after annual grass removal. Additionally, this work aims to develop tools and resources to support effective land management strategies within mountain big sagebrush plant communities that have been invaded by annual grasses while maintaining their ecological integrity. By addressing key aspects of managing cheatgrass-invaded rangelands, including controlling annual grasses, assessing fire risk and flammability, and estimating shrub canopy volume using drone-based techniques, we can gain a comprehensive understanding of cheatgrass invasion and develop practical solutions for preserving the ecological balance of these ecosystems.

Chapter 1, *Indaziflam application reduced invasive annual grass cover and modeled fire behavior while maintaining native species richness in Mountain Big Sagebrush steppe,* describes the efficacy and results of an application of an herbicide, indaziflam, for controlling invasive annual grasses. We report control efficacy, impact on native plant communities, and resulting shifts in modeled fire behavior. Chapter 1 is in preparation for the scientific journal *Rangeland Ecology and Management.*

The impact of cheatgrass on fire potential in sagebrush shrublands is further quantified in Chapter 2. Chapter 2, *Cheatgrass alters flammability of native perennial grasses in laboratory combustion experiments,* describes flammability of cheatgrass and two native perennial grass species (*Achnatherum nelsonii* and *Pseudoroegneria spicata*) alone and in combination with each other. Chapter 2 is in preparation for the scientific journal *Fire Ecology*.

Chapter 3, *A comparison and development of methods for estimating sagebrush shrub volume using drone imagery-derived point cloud,* compares canopy volume estimates from field-based measurements with drone-collected imagery for seven dominant shrub species. Chapter 3 is in preparation for the scientific journal *Ecosphere*.

Chapter 1: Indaziflam application reduced invasive annual grass cover and modeled fire behavior while maintaining native species richness in Mountain Big Sagebrush steppe

Abstract

Invasive annual grasses, such as cheatgrass (*Bromus tectorum*), have detrimental effects on western rangelands, including competition with native plants and alteration of fire patterns. To address this issue, the herbicide indaziflam, known for its long-lasting soil residual, was applied to a study area in mountain big sagebrush (*Artemisia tridentata* ssp. *vaseyana*) plant communities near Hailey, Idaho. Foliar cover, fuel continuity, and fuel loading were assessed one and two years after treatment (YAT) within 32, 900 m^2 assessment plots within treated and untreated areas. Indaziflam treatment significantly reduced annual grass foliar cover across all plant community types (mean untreated cover: 11% and 38%; treated cover: 4% and 10% 1 and 2 YAT, respectively), and annual grass control was highest two YAT. Annual grass control was maintained even in areas with over 25% shrub cover. Perennial grass cover was 7% greater in treated areas. We observed higher species richness and diversity two YAT, but there was an overall reduction of annual forb foliar cover in treated areas (2 and 16% reduction 1 and 2 YAT). There were no differences in canopy gap size or native plant species richness between treated and untreated plots. Total and herbaceous fuel loading did not differ by indaziflam application, and shrubs contributed the most to total fuels. Indaziflam treated areas had slightly lower modeled rates of spread, flame lengths, and reaction intensity than untreated areas, but these differences were only present in areas with low shrub cover. Overall, this research supports the use of indaziflam as an effective method for reducing annual grasses without compromising the richness of native plant communities. The findings contribute to our understanding of managing invasive grasses and their impact on rangeland ecosystems, providing insights for more effective strategies in conserving and restoring these ecosystems.

Introduction

Around 23 million hectares of western public lands are infested with invasive annual grasses, including cheatgrass (*Bromus tectorum*), field brome (*B. arvensis),* medusahead (*Taeniatherum caput-medusae*), and ventenata (*Ventenata dubia;* (Duncan et al. 2004, Kleinhesselink et al. 2023). Among these invasive grasses, cheatgrass is particularly problematic in Great Basin rangelands, infesting over 22.6 million hectares and spreading at an estimated rate of 14% annually. The invasion of these winter annual grasses has significant impacts on the structure, function, and disturbance patterns of the affected ecosystem, as they outcompete native plants by capturing moisture and nutrients earlier in the season compared to their native counterparts (Knapp 1996).

Annual grasses take advantage of an open niche during fall germination, utilizing moisture and nutrients throughout the winter and early spring when most desirable native species remain dormant (Sebastian et al. 2017b). As a result, cheatgrass has profoundly altered sagebrush (*Artemisia* spp.) steppe plant communities and ecological functioning. This alteration has adverse effects on wildlife populations and rural economies (Duncan et al. 2004). The introduction of cheatgrass in sagebrush communities exemplifies biological impoverishment, where the invader can replace native grasses and forbs (D'Antonio and Vitousek 1992, Knapp 1996).

One of the greatest consequences of annual grass invasion is the shift in fire regime to the grass-fire cycle. The grass-fire cycle is driven by higher fine fuel biomass, increased continuity and flammability of grasses, and faster postfire recovery of non-native grasses compared to native species (Balch et al. 2013). This phenomenon is pronounced in semiarid ecosystems with historically low fire occurrence (D'Antonio and Vitousek 1992, Brooks et al. 2004, Balch et al. 2013). The fire activity following cheatgrass invasion in the US Great Basin is one of the most widely cited examples of this phenomenon (Knapp 1996). For example, Whisenant (1990) estimated a fire return interval of 3–5 years in cheatgrass-dominated rangelands, compared with 60–100 years in native sagebrush communities.

Altered, invasive annual grass-driven fire cycles are known to have increased fire size, fire season length, spread rate, numbers of individual fires, and likelihood of fires spreading into surrounding native or managed ecosystems (D'Antonio and Vitousek 1992, Balch et al. 2013). Cheatgrass can change the properties of fire regimes through several mechanisms. It increases fine fuel continuity (Whisenant 1990, Davies and Nafus 2013), enabling fire spread (Link et al. 2006). It also increases fine fuel biomass, particularly following wet years (Bradley and Mustard 2006, Davies and Nafus 2013). Balch et al. (2013) examined the impact of cheatgrass on fire activity from 1980-2009 on a regional scale in the arid western US and found that cheatgrass areas were more likely to burn, and

fires started in cheatgrass were more likely to burn for multiple days and contribute to the largest fires of the year.

Cheatgrass-altered fire cycles have significant economic costs. The economic impact of controlling cheatgrass fueled fire, in southern Idaho alone, is estimated at 10 to 15 million dollars every year (Duncan et al. 2004). These costs include direct firefighting suppression, pre-fire fuels treatments, decreased forage availability, post-fire restoration, and habitat loss. On the individual rancher scale, increased fire frequency limits grazing availability on public land allotments since grazing is excluded for at least two growing seasons post-fire to allow for soil stabilization and plant recovery (Knapp 1996). Larger fires caused by cheatgrass may require additional years to recover following a fire, further reducing cattle forage availability (Maher et al. 2013). When an area is burned more frequently and continuously, post-fire restoration efforts (i.e., seeding) are less successful and require repeated action, increasing cost (Pilliod et al. 2021).

Historically, herbicidial control of annual grasses in rangelands has been inconsistent, and when successful, control is short-lived (DiTomaso 2000, Koby et al. 2019). The three most common herbicides used for annual grass control in US rangelands are imazapic, rimsulfuron, and glyphosate (DiTomaso 2000, Wallace and Prather 2016). Application of these products can occur either pre- or post-seedling emergence. When controlled for only one year, winter annual grasses often re-establish from the soil seedbank, where their seeds can remain viable for up to five years (Sebastian et al. 2017b). These treatments can provide control for up to a year but vary afterwards and require re-application or integration with additional management actions, such as prescribed fire or targeted grazing (Wallace and Prather 2016).

Indaziflam is a broad-spectrum, pre-emergent herbicide first released in 2011 for use in perennial cropping systems and later for control in turfgrass, ornamentals, forestry, and non-crop industrial sites (Anonymous 2011). A supplemental label for indaziflam was approved in 2016 for the release or restoration of desirable vegetation in natural areas, open spaces, wildlife management areas, pastures, and fire rehabilitation areas, specifically targeting invasive winter annual grass control (Anonymous 2016). Grazing restrictions on indaziflam were lifted in 2020 when applied at 291.7 mL/ha (5 oz/acre) (Anonymous 2020). Indaziflam is a cellulose biosynthesis inhibitor, which prevents cell division and thus root elongation primarily in developing root tips of seedlings (Anonymous 2016). This is a novel herbicide mechanism, distinct from previously used modes of action (Sebastian et al. 2016b, Clark et al. 2019). Additionally, indaziflam is lipophilic and has low water solubility, which contributes to increased residual soil activity (Sebastian et al. 2017a). Indaziflam has a longer soil residual than

other herbicides commonly used for annual grass management, providing three or more years of control (Sebastian et al. 2016a, 2017c).

Indaziflam has been shown to successfully control winter annual grasses for at least two, but often three years (Sebastian et al. 2016b, 2017c, 2017d, Clark et al. 2019, Koby et al. 2019, Fowers and Mealor 2020, Seedorf et al. 2022, Courkamp et al. 2022b). First year annual grass control is often best achieved by mixing indaziflam with a post-emergent herbicide such as imazapic. Indaziflam has limited negative impact to non-target species and generally results in a net positive response of perennial bunchgrass and forb biomass, cover, and production by removing annual grass competition (Clark et al. 2019, Koby et al. 2019, Fowers and Mealor 2020, Courkamp et al. 2022a). However, negative effects on native annual forbs (Meyer-Morey et al. 2021), lower seedbank species richness and diversity (Courkamp et al. 2022b) and reduced emergence of seeded native perennial bunchgrasses (Terry et al. 2021) have also been observed. In some cases, indaziflam application represents a tradeoff between effective, long-term annual grass control and non-target species impacts.

Indaziflam is potentially a powerful tool for controlling annual grasses and may allow land managers to tackle the scope of annual grass invasion, but there are few studies that have examined landscape-scale, aerially applied indaziflam treatments. In addition, there has been no research into the impact of indaziflam on fuel continuity and fire behavior. This chapter addresses the efficacy of indaziflam application for annual grass control in mesic mountain big sagebrush plant communities and assesses the impact of treatment on fuels and fire behavior. To address these gaps, we posed four research questions:

1. Does indaziflam provide effective annual grass control even with high shrub cover?
2. What is the impact of indaziflam application to other plant species?
3. What effect does indaziflam application have on fuel continuity?
4. How does fuel load and modeled fire behavior differ after indaziflam application?

From these questions, we developed four research predictions:

1. Annual grass cover will be reduced in indaziflam treated areas, but control will be best in areas with fewer shrubs since the herbicide is able to better reach the soil surface.
2. Indaziflam treated areas will have lower annual plant cover, but perennial herbaceous and shrub vegetation cover will not be reduced.
3. Areas treated with indaziflam will have less continuous fuels due to the reduction of annual grasses.

4. Modeled rate of spread, flame lengths, and reaction intensity will be lower in areas treated with indaziflam due to a reduction in herbaceous fuels.

Methods

Study site

This study was conducted at the University of Idaho's Rinker Rock Creek Ranch in southern Idaho (43.4139 °N, 114.3946 °W). The 4210-ha working ranch is a collaborative research effort among the University, Wood River Land Trust, and Idaho Chapter of The Nature Conservancy. Three pastures were selected for this study due to their mix of representative plant communities, presence of annual grasses, and accessibility. The dominant shrubs are *Artemisia tridentata* ssp. *vaseyana, Purshia tridentata, Chrysothamnus viscidiflorus, Ericameria nauseosa, Tetradymia canescens*, and *A. arbuscula.*

Soils in the study area are in the Povey-Vitale association (gravelly loam, very gravelly loam, extremely cobbly loam, bedrock) or Peevywell-Simonton complex (loam, clay loam, clay, cemented material, very gravelly sandy loam) (NRCS 2023). Both soils have parent material mixed alluvium and/or colluvium. Mean elevation is 1,575 m, and ranged from 1,534 to 1,615 m (USGS 2023). Mean annual precipitation based on the 30-yr mean (1991 to 2020) is 375 mm (PRISM Climate Group, Oregon State University 2023). For years 2020, 2021, and 2022, annual precipitation was 217, 375, and 345 mm, respectively (PRISM Climate Group, Oregon State University 2023).

In September 2020, 19.4 ha across three areas were treated aerially by helicopter with indaziflam. Indaziflam was applied at a rate of 369.4 ml/ha across a 7.62 m spray swath and 468.2 L/ha of water as the carrier. Treated areas contained annual grass and forbs, native perennial grasses and forbs, and sagebrush. The untreated study area was selected based on (1) proximity to treated area and (2) equal representation of aspect and slope.

The study areas were stratified by shrub and perennial vegetation cover within treated and untreated areas. Vegetation cover data were gathered from the rangeland analysis platform (rangelands.app, Allred et al. 2021). Fractional cover (version 2.0) from 2020 was used to delineate study areas (Allred et al. 2021). Areas of high and low cover were delineated at 25% cover for shrubs and 30% cover for perennial vegetation. This resulted in four vegetation sampling strata each within the treated and untreated areas: high shrub, high perennial herbaceous (HSHP); high shrub, low perennial herbaceous (HSLP); low shrub, high perennial herbaceous (LSHP); and low shrub, low perennial herbaceous (LSLP). Once the strata were delineated on the landscape within each treated and untreated areas, plots were located within unique polygons. Four plot replicates (four in treated,

four in untreated) were located within the HSHP, HSLP, and LSHP strata. The LSLP strata had low representation, which only allowed for three plot replicates. This yielded 30 total plots (15 treated and 15 untreated).

From each sampling point (plot center), continuous environmental variables were extracted. Slope, aspect, and elevation (USGS 2023) using publicly available remote sensing data within ESRI's Living Atlas. Aspect was transformed into eastness and northness using a sine and cosine transformation, respectively. Soil properties (either percent sand or sand) were sourced from Ramcharan et al. (2018) and were extracted at the 100 m scale from SoilGrids (soilgrids.org).

Field data collection

Plant communities were surveyed using a modified SageSTEP method as outlined in Bourne and Bunting (2011a). Plots were 30 m by 30 m in size. Three parallel 30 m vegetation transects were located within the plot (Fig. 1.1). Plots were located such that transect lines ran parallel to topographical contour lines.

Total plant foliar cover was derived from 180 intercept points per plot using the line point intercept method (60 points on each of the three vegetation transects). Starting at the 0 m mark and repeating every 0.5 m on each transect, a pin flag was freely dropped from above the tallest vegetation. Each vascular plant that touched the pin flag was recorded by species from the top canopy down. Presence or absence of herbaceous or woody litter was recorded. The soil surface cover was also noted. Standing dead plants were identified to the functional group level. Plant community sampling occurred 1 and 2-years post-treatment in May-July 2021 and 2022. Percent foliar cover was summarized for each species on the transect and then averaged for the plot. Species richness by plant habit (grass, forbs, or shrub), longevity (annual or perennial), and nativity (native or invasive) were summarized for transect and averaged at the plot level. Shannon diversity was summarized for each plot and year with *diversity* function in package vegan (Oksanen et al. 2020).

A canopy gap intercept sampling method was also performed on the three vegetation transects to provide improved estimation of fuel continuity (Fig. 1.1). Gaps of at least 20 cm in standing vegetation (live or dead) were recorded. A gap was broken if over half of a 5 cm section contained vegetation. Litter and duff did not break a gap. For each transect, number of gaps, total gap length, and median gap length were summarized and then averaged for each plot.

Overstory fuels were made up of all live and dead shrubs. Shrub biomass was measured within either three or five nested circular frames placed evenly on the 15 m transect. Shrubs taller than 15 cm with >10% live canopy were measured for height, greatest width, and width perpendicular to the greatest width. The number of subplots (three or five per transect) and subplot radius (1-, 2-, or 3-m), was selected based on shrub density such that at least 15 individuals would be measured. Shrub

fuel load was computed using allometric equations (Bourne and Bunting 2011) and averaged across all subplots.

Shrub density was derived from counts within a 1-m belt on both sides of the three vegetation transects (Fig. 1.1). Shrubs were counted by species and within two height classes (5–15 cm or >15 cm tall). Dead shrubs greater than 15 cm tall were tallied but not separated by species.

Understory fuels were subdivided and quantified in the following categories: live herbaceous plant material, standing dead herbaceous plant material, herbaceous detached plant material (litter), and downed woody debris (DWD). Biomass of live herbaceous plant material, standing dead herbaceous plant material, and herbaceous detached plant materials (litter), were derived through destructive sampling within 8 quadrats (50 by 50 cm) along one, 30 m fuels transect per plot (Fig. 1.1). All herbaceous vegetation, standing litter, and surface litter was collected within the quadrats. Heights of the tallest perennial grass, annual grass and forb were measured before clipping. Vegetation was sorted by life form (annual grass, perennial grass, forb) and whether it was alive or dead. Samples were oven-dried at 58°C for 48 hours. Herbaceous dry mass was weighed and dry matter loading (kg/ha) was calculated by life form.

Downed woody debris was measured using a modified planar intersect method (Brown 1974, 1982) on the three vegetation transects (Fig. 1.1). Along each of these transects, 1-hr (0 to 6.4 mm diameter) and 10-hr (6.5 to 25 mm) fuels were counted along the first 2 m of the transect and 100-hr (25 to 76 mm) fuels were counted along the first 4 m of the transect. There were no 1000-hr (76 to 203 mm) fuels in the study area and thus they were not counted. Brown's (1974) equations were used to assign loadings, by size class, for each plot. Downed woody debris fuel loading was averaged across the three transects for each plot.

Analysis of plant community composition

Species composition of field plots was explored using two techniques. First, functional group abundance in each plot was classified along two trait-based axes as described in Wainwright et al. (2020). Second, species abundance was classified using a nonmetric multidimensional scaling (NMDS) ordination.

Methods outlined in Wainwright et al. (2020) were used to quantify community resilience using trait-based attributes. Plant community composition was classified by relative abundance of each plant functional type, and communities were grouped based on shrub cover and level of annual grass invasion. Plant community composition was quantified using relative abundance of shrubs and annual grasses (Wainwright et al. 2020). The position of each community (plot) each year is plotted using a Shrub index [1.1] and annual grass invasion index [1.2]:

Equation 1.1. Shrub index

$$Shrub\ Index = \frac{S}{S + H}$$

Equation 1.2. Annual Grass Invasion index

$$Annual\ Grass\ Invasion\ Index = \frac{I}{I + N}$$

Where S = total cover of shrub species, H = total cover of non-shrub species, I = total cover of invasive annual grass species, and N = total cover of all species other than invasive annual grasses. Wainwright et al. (2020) included all invasive plants in their plot classification, but for this study we focused on nonnative annual grasses only. These indices are bound by 0 and 1, with values closer to one indicating more shrubs or annual grass, respectively. Together, they form a bivariate "S-I space" that can describe community structure and can allow tracking community movement over time, where stable communities will move the least over time (Wainwright et al. 2020). Each sampling point (transect) was plotted on an S-I axis. The position of each sample point was assessed using a 2D kernel density estimates produced with *kde2d* function in package MASS (Venables et al. 2002).

Additionally, species composition of plots were visualized using a NMDS produced with *metaMDS* function in package vegan (Oksanen et al. 2020). Foliar cover of each plant species was transformed to relative abundance using a Wisconsin-double transformation. Transformed data were displayed using a Bray-Curtis dissimilarity matrix with hierarchical clustering. A three-dimensional solution was chosen to reduce stress. Both the S and I indices were included as environmental vectors in the NMDS to highlight how the shrub and invasion index can be used to separate plant communities. Additionally, slope, elevation, percent clay of soil, percent sand of soil, and eastness and northness (aspect) were also included as environmental vectors.

The impact of indaziflam treatment and sampling strata on plant community composition was visualized by placing 95% confidence ellipses on the first two NMDS axes. A permutational multivariate analysis of variance (PERMANOVA) was used to compare communities across treatments and sampling strata. We performed nonparametric linear regression of environmental variables (slope, aspect, elevation, soil components, and both shrub and annual grass invasion indices) against the ordination axes using function *envfit* (Oksanen et al. 2020). Vectors proportional to regression coefficients were plotted on the ordination to illustrate the strength and direction of their relationship with each axis.

Fire behavior modeling

To assess the impact of indaziflam application on fire behavior, fire behavior modeling was performed using the fire behavior modeling system FCCS in the Fuel and Fire Tool (FFT) (Prichard et al. 2013). Fuel beds were parameterized with in situ data, following methods outlined by Ellsworth

et al. (2022a). Fuel beds were initialized using the standard fuel bed *56:Sagebrush shrubland – exotic species*, and then customized to represent the quantity and arrangement of fuels in each treatment plot, yielding individual custom fuel models for each treatment plot (Prichard et al. 2013). Shrub and herbaceous height were calculated as 80% of maximum plant height measured in the field. Shrub percent live (density) was calculated as a ratio of live to dead individuals as measured during shrub density belt transects. Herbaceous percent live (biomass) was calculated using destructively sampled herbaceous plant biomass, and all annual plant biomass was considered dead. Cover for all shrub and herbaceous species that had greater than 1% proportional foliar cover for each plot were included for each plot by year fuel bed. Fire simulations were done at the plot level for each of the two years of field sampling. This resulted in 60 total fuel beds, since each plot (n=30) was modeled for both sampling years. Fuel bed inputs for each survey plot are reported in Supplemental Information 1.1-3.

Four environmental scenarios were selected for fire behavior modeling. Environmental scenarios in the FFT model are calculated by inclusion of a moisture dampening coefficient to impact fire behavior such that drier fuels result in more intense modeled fire behavior (Prichard et al. 2013). Four environmental scenarios were chosen to represent the range of fuel moisture expected as vegetation phenology progresses from the active growing season, from green through partially curing stages (1/3 cured and 2/3 cured), to late in the summer, when fuels are completely dry (Ellsworth et al. 2022a). Fuel moistures for each fuels class are reported in Table 1.1. Slope assumptions were based on average percent slope as recorded in the field along plot center. Wind speed was based on the 80^{th} and 97^{th} percentile wind speed over the summer (June-September) from the nearest remote automated weather station for the study years. Independent model runs were done for each custom fuel model for each environmental scenario. Model outputs chosen to characterize fire behavior were rate of spread (ROS), flame length (FL), and reaction intensity (RI; the rate of heat release per unit area of the flaming front).

Statistical analysis

Differences in plant functional group (annual grasses, annual forbs, perennial grasses, perennial forbs, and shrubs) foliar cover were examined by indaziflam treatment and sample year using multiple, simple linear regressions. Additionally, within each of these models, the density of large shrubs (>15 cm height), remotely sensed and field recorded shrub cover, and sampling strata (high or low shrub and high or low perennial herbaceous vegetation) were all examined as potential predictor variables for plant functional group cover. Independent model runs were conducted with indaziflam treatment and sample year and each of the potential shrub or strata classifications. Akaike information criterion (AIC)-based model selection was implemented to select between these predictor variables (Zuur et al. 2011). Similarly, differences in total native species richness, and Shannon

Diversity were examined by indaziflam treatment, sample year and sampling strata using multiple, simple linear regressions. An interaction between treatment and both year and sampling strata was also included in all these models.

Differences in fuel continuity (total gap length, gap abundance, and median gap size) and total fuel loading and fuels by strata (shrubs, herbaceous, litter or woody) were examined by indaziflam treatment, sample year, and sampling strata using multiple, linear regressions. Within herbaceous fuels, differences in load for each herbaceous fuels category (annual grass, alive forbs, dead forbs, alive perennial grasses, or dead perennial grasses) were examined by indaziflam treatment and sampling strata using multiple, simple linear regressions. Modeled flame length, rate of spread, and reaction intensity were examined by indaziflam treatment, sampling strata, and year, but also by modeled environmental scenario (categorical covariate) using analysis of variance (ANOVA). All statistical analysis was performed in R (version 4.3.3; R Core Team 2023). An alpha level of 0.05 was used to determine statistical significance.

Results

Plant community response to Indaziflam treatment

Indaziflam treatment significantly reduced annual grass foliar cover across all plant community types ($P<0.001$; mean untreated cover: 11% (± 2.7) and 38 % (± 3.4); treated cover: 4% (± 1.0) and 10% (± 3.7) in 2021 and 2022, respectively; Fig. 1.2). Annual grass control was on average 14% higher two years after treatment in 2022 ($P<0.001$; Fig. 1.2). The cover of the two target annual grass species (*B. tectorum* and *B. arvensis*) differed, but overall followed similar trends (Fig. 1.3). Cover of *B. arvensis* was higher and more variable than *B. tectorum* in 2022. *B. tectorum* cover was greatest in areas classified within the low shrub, low perennial herbaceous (LSLP) vegetation strata. For both species, cover was lowest in areas treated with indaziflam in 2022.

Annual forb cover across the study site was 13% higher two years after treatment than one year after treatment ($P<0.001$; Fig. 1.2). Annual forb cover was 9% lower in treated areas than untreated areas in 2022 ($P<0.001$; mean untreated cover: 1.3% (± 0.5) and 20% (± 1.9); treated cover: 2.5% (± 0.6) and 11% (± 1.6) in 2021 and 2022, respectively; Fig. 1.2). This reduction in cover was only present within the HSHG sampling strata two years after treatment, where annual forb cover was 10.0% (± 2.6) in treated areas and 26.5% (± 4.3) in untreated areas ($P<0.001$; Fig. 1.2).

Perennial grass cover was 7% higher in indaziflam treated areas than in untreated areas for both study years ($P<0.001$; mean untreated cover: 32% (± 1.9) and 40% (± 2.3); treated cover: 38% (± 2.4) and 47% (± 3) in 2021 and 2022, respectively; Fig. 1.2). Perennial grass cover was lower in the LSLP strata than either of the high shrub (HS) strata ($P<0.005$; Fig. 1.2). Perennial forb cover was 10%

higher in 2022 (27% ± 2) than 2021 (16% ± 2; P<0.001; Fig. 1.2). There were no differences in perennial forb cover by strata or indaziflam treatment. Shrub cover was on average 38% (± 4.1) and did not differ by treatment nor year (P<0.0001; Fig. 1.2).

Total species richness and Shannon Diversity Index values were highest in 2022, but for both survey years there were no differences in native plant species richness nor diversity by indaziflam treatment (see Table 1.2 for species richness and Table 1.3 for diversity). The LSHP strata had the highest plant diversity (P<0.005; Table 1.3). The LSHP strata in 2021, but not 2022, had greater diversity than both of the HS sampling strata (P<0.005; Table 1.3). One hundred twenty nine species were observed across all treatments, years, and sample strata in this study. Eighty two species were observed in both treated and untreated areas. Twenty two species were observed only in untreated areas, and 25 species were observed only in treated areas. For a full species list in treated and untreated areas by year, see Supplemental Information 1.4 and 1.5. The dominant species within treated areas in 2021 in rank abundance order were *Artemisia tridentata* ssp. *tridentata,, Poa secunda, Bromus tectorum, Pseudoroegneria spicata, Artemisia arbuscula, Bromus arvensis, Nestotus stenophyllus, Phlox longifolia, Achnatherum nelsonii, Eriogonum caespitosum*, and *Elymus elymoides*. The dominant species within untreated areas in 2021 in rank abundance order were *Artemisia tridentata* ssp., *Poa secunda, Pseudoroegneria spicata, Achnatherum nelsonii, Lupinus* sp., *Festuca idahoensis, Bromus tectorum, Phlox longifolia, Purshia tridentata*, and *Leymus cinereus* (Supplemental Information 1.4). The dominant species within treated areas in 2022 in rank abundance order were *Artemisia tridentata* ssp *tridentata, Poa secunda, Pseudoroegneria spicata, Bromus tectorum, Phlox longifolia, Lupinus* sp., *Festuca idahoensis, Collinsia parviflora, Bromus arvensis, Carex douglassai, Achnatherum nelsonii* and *Purshia tridentata.* The dominant species within untreated areas in 2022 in rank abundance order were *Artemisia tridentata* ssp. *tridentata, Poa secunda, Bromus tectorum, Bromus arvensis, Collinsia parviflora, Pseudoroegneria spicata, Phlox longifolia,* and *Collomia linearis* (Supplemental Information 1.5).

The shrub and annual grass invasion index revealed differences in plant communities by sample year, strata, and indaziflam treatment (Fig. 1.3). In both sample years, HS strata were overlapping with high shrub index values. Plots in the LSLP strata were the most variable (largest ellipse; Fig. 1.3). The untreated LSLP strata plots also had the highest annual grass invasion index values in 2021, which was distinct from plots in all other strata. However, in 2022, this pattern did not persist; plots within the untreated LSLP had similar (overlapping) annual grass invasion index to all the other strata (Fig. 1.3). In 2021, when overall annual grass cover was lower, annual grass cover varied more strata,

than in 2022, when annual grass cover was higher. Due to the reduction in annual grass cover within indaziflam treated areas, the treated plots had lower annual grass invasion index values (Fig. 1.3).

Results from NMDS showed that plant communities treated with indaziflam were not distinct from untreated communities ($P>0.05$; Fig. 1.4). Sampling strata, however, was significant in separating plant communities ($P=0.024$; Fig. 1.4). Both of the HS strata were highly overlapping (Fig. 1.4). For both sample years, the LSLP vegetation strata was more variable and less overlapping with other strata (Fig. 1.4). Additionally, both the shrub index ($R^2 = 0.589$ for 2021; $R^2 = 0.454$ for 2022; $P<0.001$) and annual grass index ($R^2 =0.255$ for 2021; $R^2 = 0.45$ for 2022; $P<0.001$) were important predictors of differentiating plant communities, as was northness of plot aspect ($R^2 = 0.236$ for 2021; $R^2 = 0.158$ for 2022; $P<0.005$; Fig. 1.4). Other environmental factors (slope, eastness, elevation, and both percent clay and sand) were not significant in differentiating plant communities and thus were not included in the NMDS visualizations (Fig. 1.4). Stress values for the three-dimensional NMDS for 2021 and 2022 were 0.119 and 0.127, respectively.

Fuels and fire behavior

Median foliar gap size was 40.1 cm, there were on average 17 gaps per 30 m, and average total gap length was 929 cm. Fuel continuity did not differ by indaziflam treatment, year, or sampling strata ($P>0.05$; Fig. 1.5)

Average aboveground total fuel loading was 8,476 kg/ha. Areas within the HS vegetation strata had greater fuel load than those within low shrub (LS) vegetation strata (17,432 vs 3,991 kg/ha, respectively; $P<0.001$; Fig. 1.6). There was no difference in total fuel loading by treatment nor year ($P> 0.05$; Fig. 1.6). Shrub fuels made up the greatest fuel component (68% of total fuel), and loading was greater in areas classified as high shrub than low shrub ($P<0.001$; Fig. 1.6). There were no differences in shrub, herbaceous (5% of total fuel), litter (15%), or downed wood (12%) proportional fuels between indaziflam treated or untreated areas ($P>0.05$; Fig. 1.6).

Total herbaceous fuel load was on average 330.76 kg/ha ± 39.9. Within herbaceous fuels, there were no differences in fuel loading of annual grass (17.54 kg/ha ± 6.4), live perennial grass (122.9 kg/ha ± 17.2), dead perennial grass (10.61 kg/ha ± 4.1), live forb (154.2 kg/ha ± 27.2), nor dead forb (34.5 kg/ha ± 17.9) fuel loading by indaziflam treatment or sampling strata ($P>0.05$; Fig. 1.7)

Modeled flame lengths, rates of spread, and reaction intensities differed by environmental scenario, sampling strata and indaziflam treatment. Within treated areas, average flame lengths, rates of spread, and reaction intensity were 0.88 (± 0.027) m, 2.24 (± 0.025) m/min, and 8,792 (± 509) $kW/m^2/min$, respectively (Fig. 1.8). Within untreated areas, average flame lengths, rates of spread,

and reaction intensity were 0.85 (± 0.03) m, 1.95 (± 0.06) m/min, and 9,014 (± 546) kW/m^2/min, respectively (Fig. 1.8).

Modeled flame lengths, rates of spread, and reaction intensities did not differ by sample year ($P>0.05$; Fig. 1.8). Modeled flame length and reaction intensity differed by environmental condition. The green environmental scenario (Table 1.1) had minor but significantly lower flame lengths (range of differences: 0.17 – 0.20 m) than the two-thirds cured and fully cured environmental scenarios ($P<0.01$; Fig. 1.8). There were no differences in flame length among the cured environmental scenarios. Similar differences were observed with modeled reaction intensity: the green scenario had lower reaction intensity than all three levels of cured environmental scenarios (range of differences 2,645 – 4,527 kW/m^2/min; Fig. 1.8). Modeled rates of spread did not differ by environmental scenario (Fig. 1.8).

Modeled flame length was higher (range of differences 0.37 – 0.44 m) in both of the HS strata than the LS strata ($P<0.05$; Fig. 1.8) Within each strata, the only difference in flame length by indaziflam treatment was within the LSHG strata, where treated plots had on average 0.24 m taller flame lengths than untreated areas. Reaction intensity was also higher (range of differences 5,574 – 6,336 kW/m^2/min) in both of the HS strata than the LS strata ($P<0.05$; Fig. 1.8). There were no differences in reaction intensity by indaziflam treatment. Modeled rate of spread was higher (range of difference 0.29 – 0.54 m/min) in both of the HS strata than the LS strata ($P<0.05$; Fig. 1.8). Within the HSLG strata, untreated areas had on average 0.31 m/min higher rate of spread than treated. In the LSHG strata, the treated area has on average 0.98 m/min higher rate of spread than untreated.

Discussion

This study is the first of its kind to investigate landscape-scale application of indaziflam within mountain big sagebrush plant communities. Indaziflam effectively reduced annual grass cover with minimal impacts to resident native plant communities over two years. The control of annual grasses led to slightly lower modeled flame lengths, rates of spread, and reaction intensities, within the treated areas, particularly in regions with low shrub cover. After one year of treatment, the most successful control of annual grasses was observed in areas with less shrub canopy. However, after two years of treatment, the annual grass cover in the treated areas was lower than in untreated areas.

Mountain big sagebrush plant communities commonly have high ecological resistance to invasion by annual grasses and high resilience to fire (Chambers et al. 2014a, 2014b, 2017, 2019). However, even in plant communities with high inherent resistance and resilience, annual grasses still present a threat. Effective annual grass control which minimizes impact to native plant communities and

bolsters natural resistance and resilience is needed to minimize annual grass expansion to higher elevation plant communities.

One of the primary concerns regarding the application of indaziflam is its potential impact on the native plant community, particularly native annual species. In our study, we did not observe any differences in native species richness as a result of indaziflam treatment. However, we did notice a reduction in annual forb cover in 2022. Meyer-Morey et al. (2021) also reported a similar decrease in annual forbs following indaziflam application in their study conducted in sagebrush steppe plant communities within Yellowstone National Park. Although there was a decrease in forb cover two years after treatment, it is important to note that the treated areas still exhibited a variety of native annual forbs, including *Mentzelia albicaulis, Amsinckia menziesii, Amsinckia retorsa, Collinsia parviflora, Collomia linearis, Polygonum douglasii, Microsteris gracilis, Epilobium brachycarpum, Mertensia oblongifolia, Phacelia linearis,* and *Descurainia pinnata*. While the cover of annual forbs was reduced, the high species richness and persistence of these native annual forbs suggest few impacts to plant species composition. Courkamp et al. (2022b) reported a decrease in soil seedbank species richness in areas treated with indaziflam but did not observe similar trends in the aboveground plant community. These findings parallel our findings, suggesting that the reduction in native annual forb abundance may be temporary. Additionally, our NMDS analysis did not reveal any distinct separation between plant communities within the same sampling strata that were treated or untreated. While indaziflam reduced annual forb cover, this reduction may be a worthwhile trade-off for the benefit of annual grass control, especially in areas with intact native vegetation.

In areas treated with indaziflam, we observed equivalent perennial grass species richness and higher cover compared to untreated areas in both survey years. Other studies of indaziflam use in rangelands have reported damage to or reduction of perennial grasses, especially one year after treatment (Clark et al. 2019, Koby et al. 2019, Fowers and Mealor 2020). However, it is important to note that in all of those studies, indaziflam was applied in combination with another herbicide, such as glyphosate, imazapic, picloram, and aminocyclopyrachlor (Clark et al. 2019, Koby et al. 2019, Fowers and Mealor 2020). Clark et al. (2019) and Fowers and Mealor (2020) reported damage to perennial grasses and/or forbs one year after treatment but attributed these results to the non-indaziflam component of their herbicide mixture. Clark et al. (2019) and Fowers and Mealor (2020) reported damage to perennial grasses and/or forbs one year after treatment but attributed these results to the non-indaziflam component of their herbicide mixture. They also mentioned that after two or more years following treatment, no significant differences in non-target native plants were observed (Clark et al. 2019, Fowers and Mealor 2020).

The reduction in annual grass cover observed in areas treated with indaziflam did not result in any noticeable differences in fuel continuity. In our measurements of gaps, we only considered the presence of vegetation (live or dead) or non-vegetated gaps (such as bare ground, rocks, or litter). It is worth noting that annual vegetation was grouped together with all other fuels, which means that it could fill in the gaps. We could improve the accuracy of our method and allow for better comparison with percent cover observations, by using smaller minimum gap sizes, distinguishing between shrub and fine fuels, or even conducting double sampling on each transect: once for gaps in perennial vegetation and a second time for annuals.

Some previous studies have reported differences in fuel continuity as a result of annual grasses. For instance, Davies and Nafus (2013) observed greater fuel continuity (longer patch length) and smaller fuel gaps (lower patch density) in areas invaded by cheatgrass in southeastern Oregon compared to adjacent non-invaded sites. In their study, Davies and Nafus (2013) categorized vegetation into fine fuels or shrubs, which helped differentiate potential variations. One notable difference between their study and ours is that the invaded areas they examined had experienced recent burns within the past 5 years and were nearly monocultures of *Bromus tectorum*. In our study, untreated areas had on average 11% annual grass coverage, but annual grasses were still relatively minor components of the overall ecosystem (Supplemental Information 1.2 and 1.3). Other research investigating the use of indaziflam for annual grass control in rangelands has not included measures or comparisons of fuel continuity. However, incorporating these indicators could enhance our understanding of indaziflam's effectiveness, particularly for management goals related to herbaceous fuel reduction.

Reduction in annual grass cover in indaziflam treated areas did not translate to reduced herbaceous fuel loading. While annual grasses were present in both treated and untreated areas, they were a relatively minor component of total herbaceous fuel loading (Supplemental Information 1.2 and 1.3). Similar results were observed by Ellsworth et al. (2022a), who noted that the herbicide imazapic suppressed herbaceous vegetation (2 and 3 years following treatment), but that there was ultimately no impact on total fuels. Areas treated with indaziflam had lower flame lengths and reaction intensity, however these differences were only observed in the low shrub and low perennial vegetation sampling strata. In areas with high shrub cover, fire behavior did not differ by indaziflam treatment, treatment, likely because of the large amounts of shrub fuel loads. These findings are consistent with Schachtschneider (2016), who reported that alterations (by grazing) to the herbaceous fuels had little effect on fire behavior when shrub cover was high (>25-30%).

Conclusions

The use of indaziflam for annual grass control in mountain big sagebrush plant communities has significant implications for the management and conservation of these valuable ecosystems. In our study, aerial indaziflam treatment effectively reduced annual grass foliar cover across all plant community types, with the highest control observed two years after treatment. Notably, annual grass control was maintained even in areas with high shrub cover. Furthermore, treated areas showed a 7% increase in perennial grass cover, indicating potential benefits for native grass species. Although there was a reduction in annual forb foliar cover in treated areas, we observed higher total species richness and no differences in diversity in treated areas, two years after treatment. Total and herbaceous fuel loading did not differ significantly between indaziflam-treated and untreated areas, likely due to the minor contribution by weight of herbaceous fuels in these systems.

Overall, our research supports the use of indaziflam as an effective method for reducing annual grasses for multiple years without compromising the richness or native perennial plant cover of native plant communities in mountain big sagebrush ecosystems. These findings contribute to our understanding of managing invasive grasses and their impact on rangeland ecosystems, providing insights for more effective strategies in conserving and restoring these valuable ecosystems.

References

Allred, B. W., B. T. Bestelmeyer, C. S. Boyd, C. Brown, K. W. Davies, M. C. Duniway, L. M. Ellsworth, T. A. Erickson, S. D. Fuhlendorf, T. V. Griffiths, V. Jansen, M. O. Jones, J. Karl, A. Knight, J. D. Maestas, J. J. Maynard, S. E. McCord, D. E. Naugle, H. D. Starns, D. Twidwell, and D. R. Uden. 2021. Improving Landsat predictions of rangeland fractional cover with multitask learning and uncertainty. Methods in Ecology and Evolution 12:841–849.

Anonymous. 2011. Indaziflam 500 SC herbicide product label. Page 2. Bayer CropScience, Research Triangle Park, NC.

Anonymous. 2016. Esplanade® 200SC supplemental label- for release or restoration of desirable vegetation. Page 11. Bayer CropScience, Research Triangle Park, NC.

Anonymous. 2020. Esplanade 200SC product label. Page 9. Bayer CropScience, Research Triangle Park, NC.

Balch, J. K., B. A. Bradley, C. M. D'Antonio, and J. Gómez-Dans. 2013. Introduced annual grass increases regional fire activity across the arid western USA (1980-2009). Global Change Biology 19:173–183.

Bourne, A., and S. C. Bunting. 2011. Post-treatment Fuels in the Sagebrush Steppe and Juniper Woodlands of the Great Basin. Page 115. Technical Note, Bureau of Land Management, Denver, CO.

Bradley, B. A., and J. F. Mustard. 2006. Characterizing the Landscape Dynamics of an Invasive Plant and Risk of Invasion Using Remote Sensing. Ecological Applications 16:1132–1147.

Brooks, M. L., C. M. D'Antonio, D. M. Richardson, J. B. Grace, J. E. Keeley, J. M. DiTomaso, R. J. Hobbs, M. Pellant, and D. Pyke. 2004. Effects of Invasive Alien Plants on Fire Regimes. BioScience 54:677.

Brown, J. K. 1974. Handbook for inventorying downed woody material. Page 24. General Technical Report, U.S. Department of Agriculture, Forest Service, Intermountain Forest and Range Experiment Station, Ogden, UT.

Brown, J. K. 1982. Fuel and fire behavior prediction in big sagebrush. Page INT-RP-290. U.S. Department of Agriculture, Forest Service, Intermountain Forest and Range Experiment Station, Ogden, UT.

Chambers, J. C., B. A. Bradley, C. S. Brown, C. D'Antonio, M. J. Germino, J. B. Grace, S. P. Hardegree, R. F. Miller, and D. A. Pyke. 2014a. Resilience to Stress and Disturbance, and Resistance to Bromus tectorum L. Invasion in Cold Desert Shrublands of Western North America. Ecosystems 17:360–375.

Chambers, J. C., M. L. Brooks, M. J. Germino, J. D. Maestas, D. I. Board, M. O. Jones, and B. W. Allred. 2019. Operationalizing Resilience and Resistance Concepts to Address Invasive Grass-Fire Cycles. Frontiers in Ecology and Evolution 7:185.

Chambers, J. C., J. D. Maestas, D. A. Pyke, C. S. Boyd, M. Pellant, and A. Wuenschel. 2017. Using Resilience and Resistance Concepts to Manage Persistent Threats to Sagebrush Ecosystems and Greater Sage-grouse. Rangeland Ecology & Management 70:149–164.

Chambers, J. C., R. F. Miller, D. I. Board, D. A. Pyke, B. A. Roundy, J. B. Grace, E. W. Schupp, and R. J. Tausch. 2014b. Resilience and Resistance of Sagebrush Ecosystems: Implications for State and Transition Models and Management Treatments. Rangeland Ecology & Management 67:440–454.

Clark, S. L., D. J. Sebastian, S. J. Nissen, and J. R. Sebastian. 2019. Effect of indaziflam on native species in natural areas and rangeland. Invasive Plant Science and Management 12:60–67.

Courkamp, J. S., P. J. Meiman, and S. J. Nissen. 2022a. Indaziflam reduces downy brome (*Bromus tectorum*) density and cover five years after treatment in sagebrush-grasslands with no impact on perennial grass cover. Invasive Plant Science and Management 15:122–132.

Courkamp, J. S., P. J. Meiman, and M. W. Paschke. 2022b. Indaziflam Reduces Seed Bank Richness and Density but not Sagebrush-Grassland Plant Diversity. Rangeland Ecology & Management 84:31–44.

D'Antonio, C. M., and P. M. Vitousek. 1992. Biological Invasions by Exotic Grasses, the Grass/Fire Cycle, and Global Change. Annual Review of Ecology and Systematics 23:63–87.

Davies, K. W., and A. M. Nafus. 2013. Exotic annual grass invasion alters fuel amounts, continuity and moisture content. International Journal of Wildland Fire 22:353.

DiTomaso, J. M. 2000. Invasive weeds in rangelands: Species, impacts, and management. Weed Science 48:255–265.

Duncan, C. A., J. J. Jachetta, M. L. Brown, V. F. Carrithers, J. K. Clark, J. M. DiTOMASO, R. G. Lym, K. C. McDANIEL, M. J. Renz, and P. M. Rice. 2004. Assessing the Economic, Environmental, and Societal Losses from Invasive Plants on Rangeland and Wildlands [1]. Weed Technology 18:1411–1416.

Ellsworth, L. M., B. A. Newingham, S. E. Shaff, C. L. Williams, E. K. Strand, M. Reeves, D. A. Pyke, E. W. Schupp, and J. C. Chambers. 2022. Fuel reduction treatments reduce modeled fire intensity in the sagebrush steppe. Ecosphere 13.

Fowers, B., and B. A. Mealor. 2020. Indaziflam effects on seed production for established perennial grasses. Native Plants Journal 21:290–298.

Kleinhesselink, A. R., E. J. Kachergis, S. E. McCord, J. Shirley, N. R. Hupp, J. Walker, J. C. Carlson, S. L. Morford, M. O. Jones, J. T. Smith, B. W. Allred, and D. E. Naugle. 2023. Long-Term Trends in Vegetation on Bureau of Land Management Rangelands in the Western United States. Rangeland Ecology & Management 87:1–12.

Knapp, P. A. 1996. Cheatgrass (Bromus tectorum L) dominance in the Great Basin Desert. Global Environmental Change 6:37–52.

Koby, L. E., T. S. Prather, H. Quicke, J. Beuschlein, and I. C. Burke. 2019. Management of *Ventenata dubia* in the inland Pacific Northwest with indaziflam. Invasive Plant Science and Management 12:223–228.

Link, S. O., C. W. Keeler, R. W. Hill, and E. Hagen. 2006. Bromus tectorum cover mapping and fire risk. International Journal of Wildland Fire 15:113.

Maher, A. T., J. A. Tanaka, and N. Rimbey. 2013. Economic Risks of Cheatgrass Invasion on a Simulated Eastern Oregon Ranch. Rangeland Ecology & Management 66:356–363.

Meyer-Morey, J., M. Lavin, J. Mangold, C. Zabinski, and L. J. Rew. 2021. Indaziflam controls nonnative Alyssum spp. but negatively affects native forbs in sagebrush steppe. Invasive Plant Science and Management 14:253–261.

NRCS. 2023. Web Soil Survey. Natural Resources Conservation Service, United States Department of Agriculture.

Oksanen, J., F. G. Blanchet, M. Friendly, R. Kindt, P. Legendre, D. McGlinn, P. R. Minchin, R. B. O'Hara, G. L. Simpson, P. Solymos, M. H. H. Stevens, E. Szoecs, and H. Wagner. 2020, November 28. vegan: Community Ecology Package.

Pilliod, D. S., M. A. Jeffries, J. L. Welty, and R. S. Arkle. 2021. Protecting restoration investments from the cheatgrass-fire cycle in sagebrush steppe. Conservation Science and Practice 3.

Prichard, S. J., D. V. Sandberg, R. D. Ottmar, E. Eberhardt, A. Andreu, P. Eagle, and K. Swedin. 2013. Fuel Characteristic Classification System version 3.0: technical documentation. Gen. Tech. Rep. PNW-GTR-887. Portland, OR: U.S. Department of Agriculture, Forest Service, Pacific Northwest Research Station. 79 p. 887.

PRISM Climate Group, Oregon State University. 2023. https://prism.oregonstate.edu.

Ramcharan, A., T. Hengl, T. Nauman, C. Brungard, S. Waltman, S. Wills, and J. Thompson. 2018. Soil Property and Class Maps of the Conterminous United States at 100-Meter Spatial Resolution. Soil Science Society of America Journal 82:186–201.

Schachtschneider, C. L. 2016. Targeted Grazing Applied to Reduce Fire Behavior Metrics and Wildfire Spread. Text, University of Idaho.

Sebastian, D. J., M. B. Fleming, E. L. Patterson, J. R. Sebastian, and S. J. Nissen. 2017a. Indaziflam: a new cellulose-biosynthesis-inhibiting herbicide provides long-term control of invasive winter annual grasses: Indaziflam: a new cellulose-biosynthesis-inhibiting herbicide. Pest Management Science 73:2149–2162.

Sebastian, D. J., S. J. Nissen, and J. D. S. Rodrigues. 2016a. Pre-emergence Control of Six Invasive Winter Annual Grasses with Imazapic and Indaziflam. Invasive Plant Science and Management 9:308–316.

Sebastian, D. J., S. J. Nissen, J. R. Sebastian, and K. G. Beck. 2017b. Seed Bank Depletion: The Key to Long-Term Downy Brome (Bromus tectorum L.) Management. Rangeland Ecology & Management 70:477–483.

Sebastian, D. J., S. J. Nissen, P. Westra, D. L. Shaner, and G. Butters. 2017c. Influence of soil properties and soil moisture on the efficacy of indaziflam and flumioxazin on *Kochia scoparia* L.: Effect of soil properties and moisture on indaziflam and flumioxazin efficacy. Pest Management Science 73:444–451.

Sebastian, D. J., S. J. Nissen, P. Westra, D. L. Shaner, and G. Butters. 2017d. Influence of soil properties and soil moisture on the efficacy of indaziflam and flumioxazin on *Kochia scoparia* L. Pest Management Science 73:444–451.

Sebastian, D. J., J. R. Sebastian, S. J. Nissen, and K. G. Beck. 2016b. A Potential New Herbicide for Invasive Annual Grass Control on Rangeland. Rangeland Ecology & Management 69:195–198.

Seedorf, R. H., S. L. Clark, and S. J. Nissen. 2022. Prescribed burning followed by indaziflam enhances downy brome (*Bromus tectorum*) control. Invasive Plant Science and Management 15:72–80.

Terry, T. J., M. D. Madsen, R. A. Gill, V. J. Anderson, and S. B. St. Clair. 2021. Herbicide effects on the establishment of a native bunchgrass in annual grass invaded areas: Indaziflam versus imazapic. Ecological Solutions and Evidence 2:e12049.

USGS. 2023. National Elevation Dataset for Idaho (1/3 arc second, ~10-meter).

Venables, W. N., B. D. Ripley, and W. N. Venables. 2002. Modern applied statistics with S. 4th ed. Springer, New York.

Wainwright, C. E., G. M. Davies, E. Dettweiler-Robinson, P. W. Dunwiddie, D. Wilderman, and J. D. Bakker. 2020. Methods for tracking sagebrush-steppe community trajectories and quantifying resilience in relation to disturbance and restoration. Restoration Ecology 28:115–126.

Wallace, J. M., and T. S. Prather. 2016. Herbicide Control Strategies for *Ventenata dubia* in the Intermountain Pacific Northwest. Invasive Plant Science and Management 9:128–137.

Whisenant, S. G. 1990. Changing fire frequencies on Idaho's Snake River Plains: ecological and management implications. General Technical Report, US Department of Agriculture, Forest Service, Intermountain Research Center, Logan, UT.

Zuur, A. F., E. N. Ieno, N. J. Walker, A. A. Saveliev, and G. M. Smith. 2011. Mixed effects models and extensions in ecology with R. Springer, New York, NY.

Tables

Table 1.1. Fuel moistures for each fuels class for the four environmental scenarios used in the fuel characteristic classification system in Fuel Fire Tools.

Environmental Scenario	FFT scenario	Fuel moisture (%)					
		Herbaceous	Shrub	Crown	1 hour	10 hour	100 hour
Green	D2L4	120	150	90	6	7	8
1/3 cured	D2L3	90	120	60	6	7	8
2/3 cured	D2L2	60	90	60	6	7	8
Fully cured	D2L1	30	60	60	6	7	8

Table 1.2 Species richness (per survey plot) of native and nonnative (in parenthesis) species both survey years, within areas treated and untreated with indaziflam.

	2021		2022	
Functional group	Treated	Untreated	Treated	Untreated
Annual forbs	4 (1)	3 (1)	15 (6)	14 (6)
Perennial forbs	28 (0)	28 (0)	43 (2)	43 (0)
Perennial grasses	10 (0)	7 (0)	13 (2)	11 (3)
Shrubs	6 (0)	6 (0)	6 (0)	6 (0)

Table 1.3. Mean and standard error of Shannon Diversity indices by indaziflam treatment and year within the four sampling strata.

	2021		2022	
Sampling Strata*	Treated	Untreated	Treated	Untreated
HSHP	1.96 (±0.14)	1.62 (±0.10)	2.48 (±0.21)	2.44 (±0.16)
HSLP	1.93 (±0.09)	1.94 (±0.12)	2.18 (±0.13)	2.48 (±0.19)
LSHP	2.26 (±0.07)	2.28 (±0.05)	2.56 (±0.08)	2.51 (±0.04)
LSLP	2.2 (±0.16)	2.23 (±0.12)	2.33 (±0.11)	2.31 (±0.02)

*Sampling strata is either high (H) or low (L) shrub (S) and perennial herbaceous (P) vegetation.

Figures

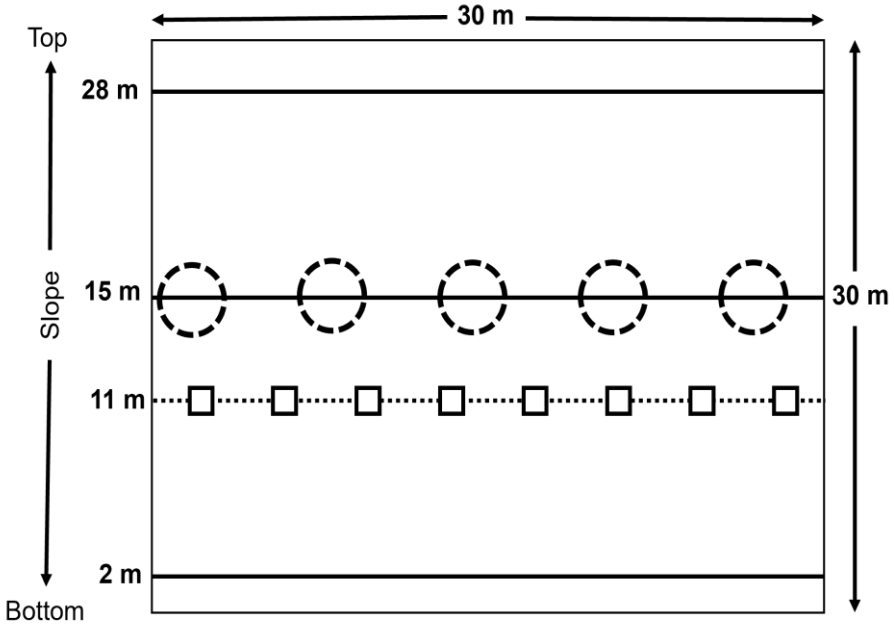

Figure 1.1 Diagram of plot and vegetation sampling regime, a modified SageSTEP sampling protocol (Bourne and Bunting 2011a).
Each plot was 30 x 30 m and contained three transects where vegetation cover and canopy gaps were measured (solid, dark lines) and one transect where herbaceous biomass was measured (dashed). Foliar cover and canopy gaps were measured using line point intercept and canopy gap intercept sampling methods, respectively. Herbaceous biomass was destructively sampled within 8 50x50 cm quadrat per plot along the fuels transect. Shrub volume was recorded within variable radius circular plots on the central vegetation transect.

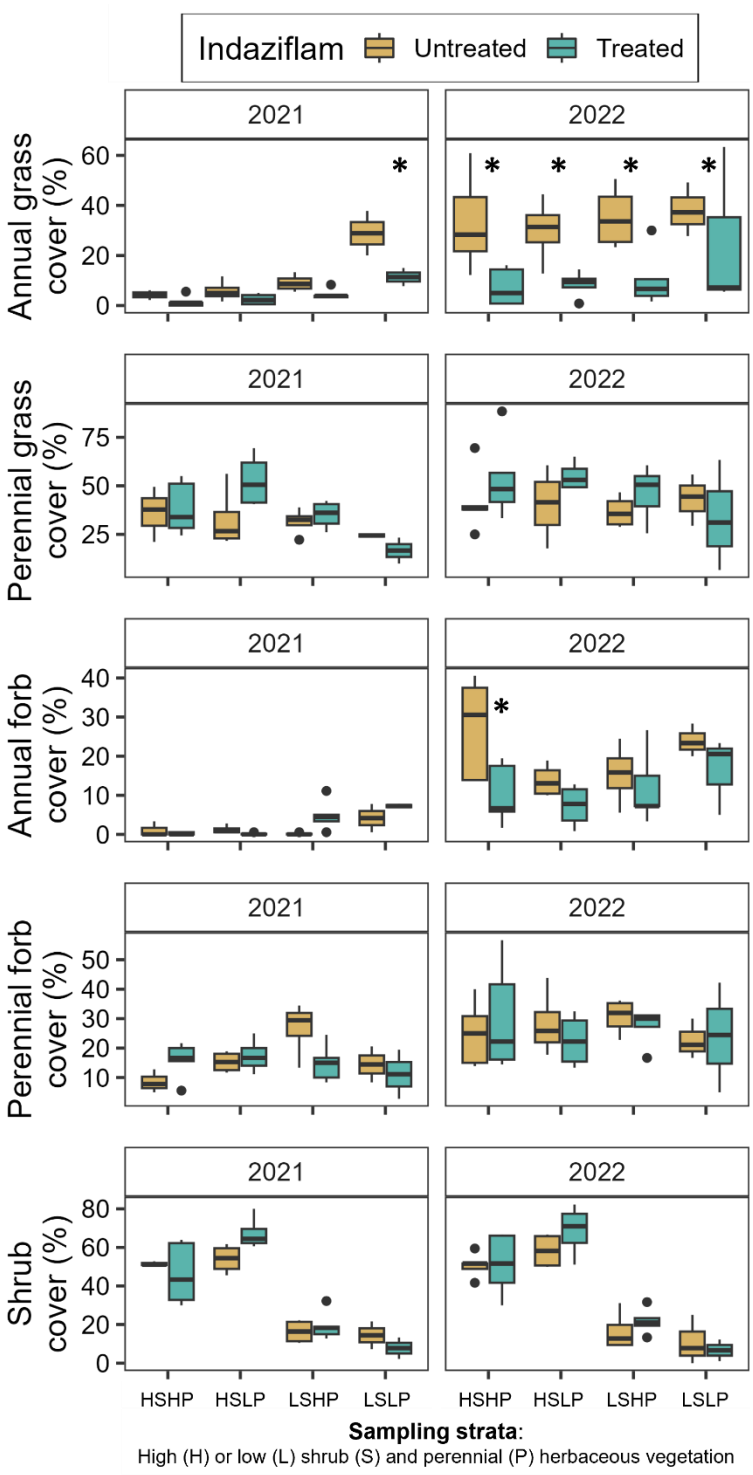

Figure 1.2. Plant functional group cover in 2021 and 2022 in areas treated and untreated with indaziflam.
Asterisks indicate statistical differences in cover between indaziflam treated and untreated areas within sampling strata and year ($P<0.001$).

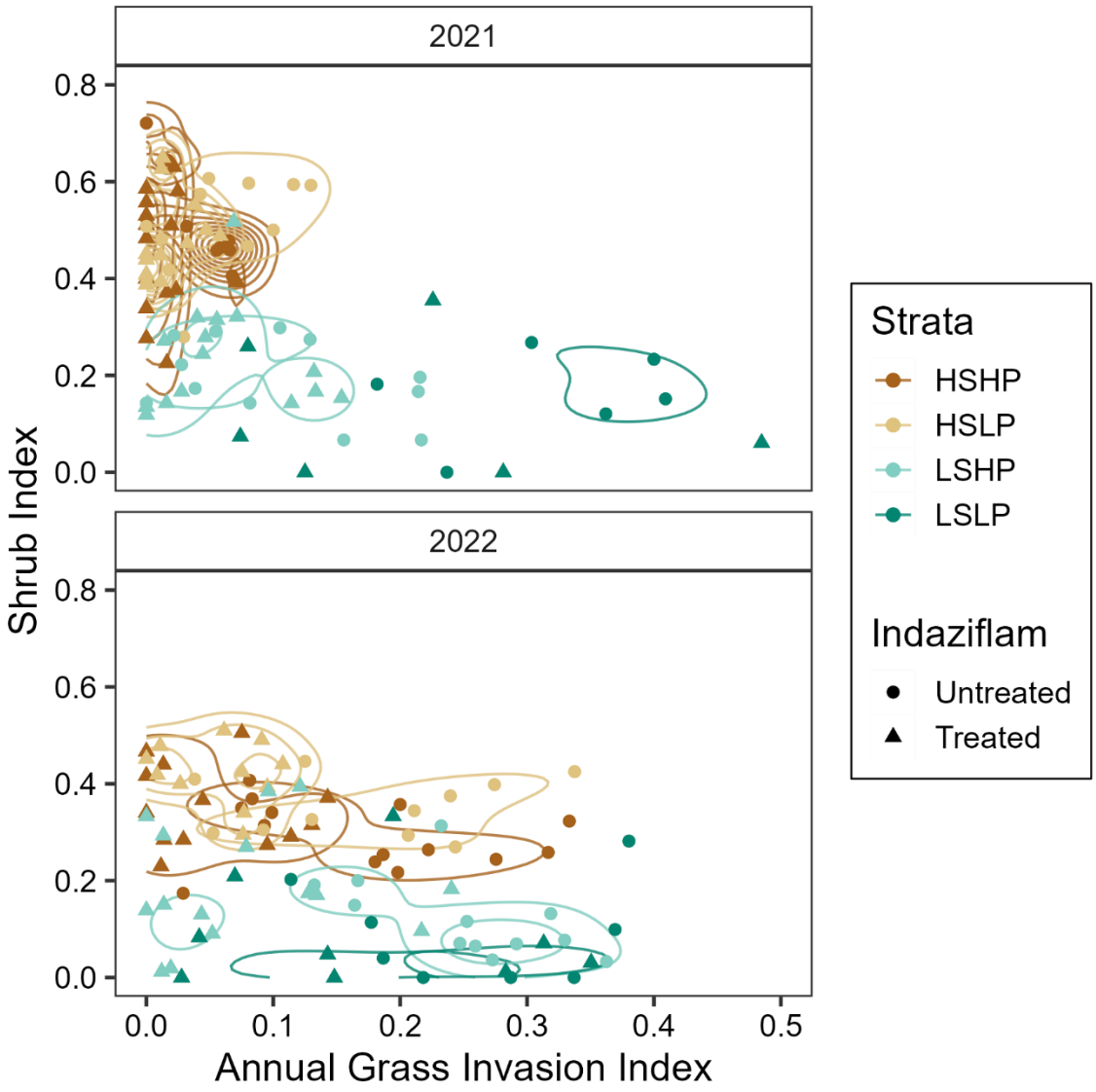

Figure 1.3. Plant community classification by sampling strata and indaziflam application along the shrub and annual grass invasion index.
Sampling strata is either high (H) or low (L) shrub (S) and perennial herbaceous (P) vegetation. Both sample years, strata with high shrub cover (HS) were overlapping, and as would be expected, had high shrub index values. Plots within low shrub low perennial herbaceous vegetation strata were more different from the rest of the plots. In 2021, when overall annual grass cover was lower, there were greater differences in plot location by strata, than in 2022 when annual grass cover was higher.

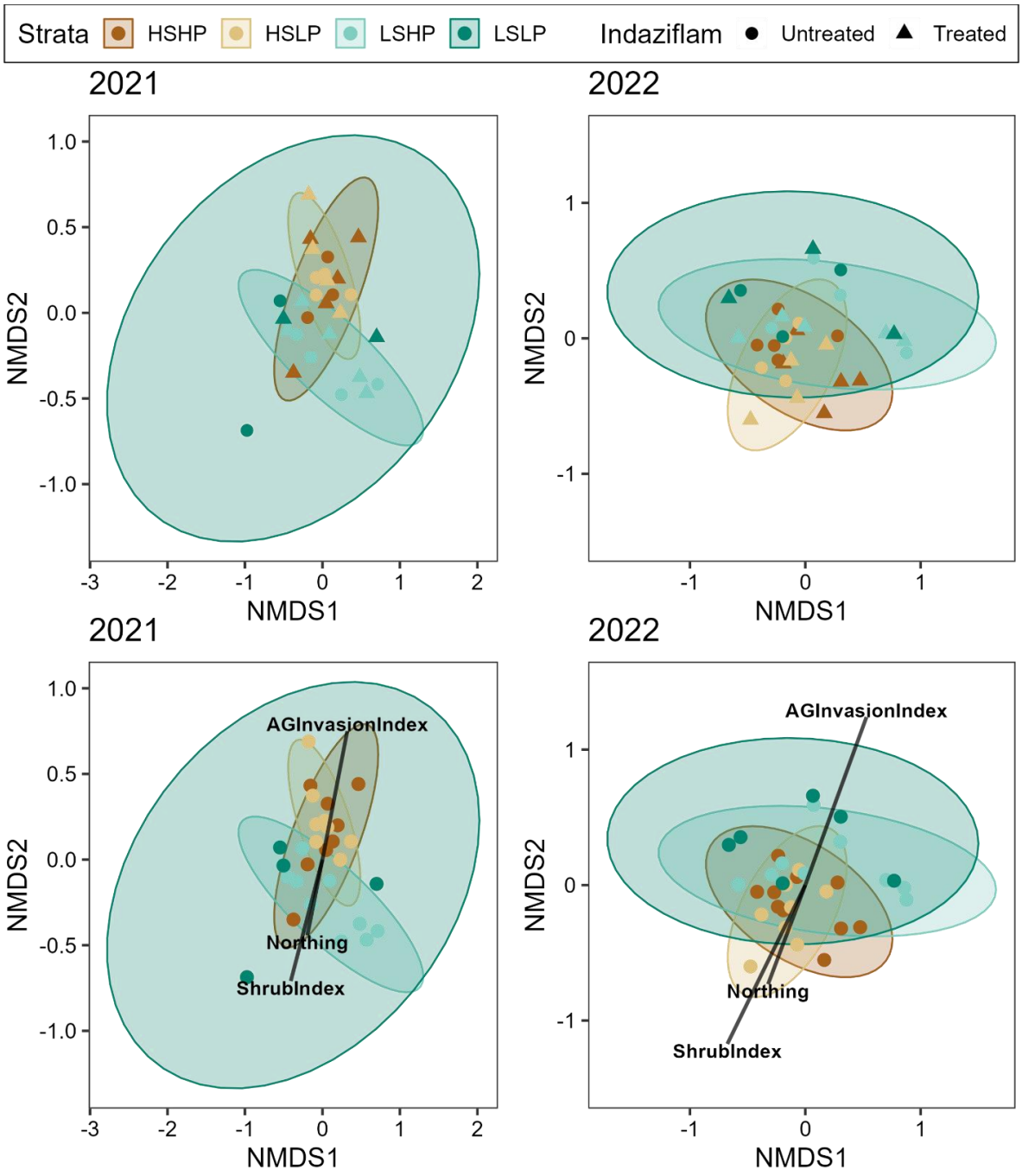

Figure 1.4. NMDS plots for both sample years, including sampling strata and indaziflam treatment (top) and environmental vectors which were significant predictors of community differentiation (bottom).
Sampling strata (high (H) or low (L) shrub (S) and perennial herbaceous (P) vegetation), and not indaziflam application, separated plant communities. Environmental attributes slope, eastness, elevation, and both percent clay and sand were not significant in differentiating plant communities. Ellipsoids represent 95% confidence intervals for each sampling strata.

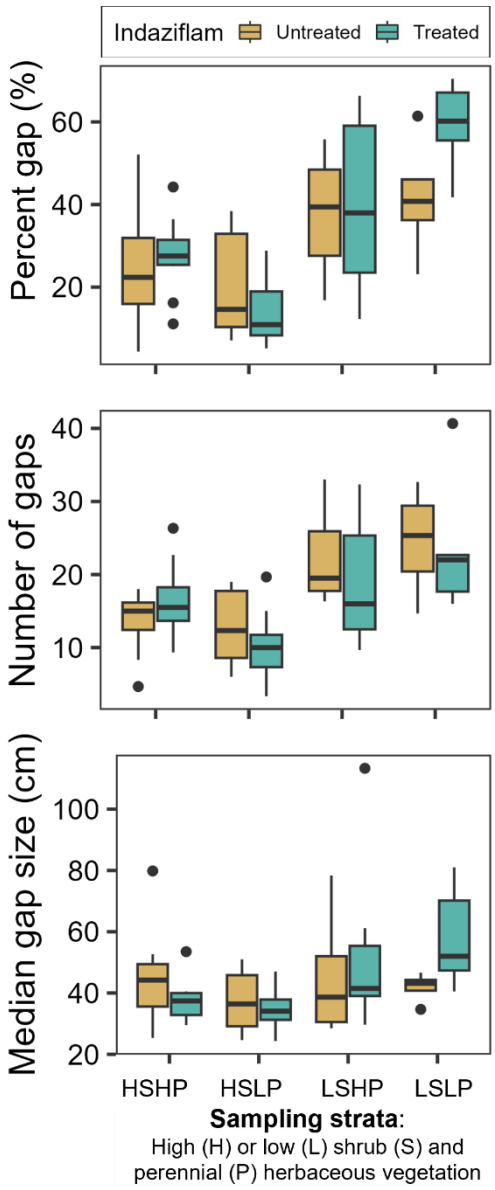

Figure 1.5. Gap size, abundance, and percent in areas treated and untreated with indaziflam. There were no differences in gap length (%), abundance, or median size by indaziflam treatment. There were no differences by year, so data from both years are shown together. Only gaps 20 cm or greater were recorded.

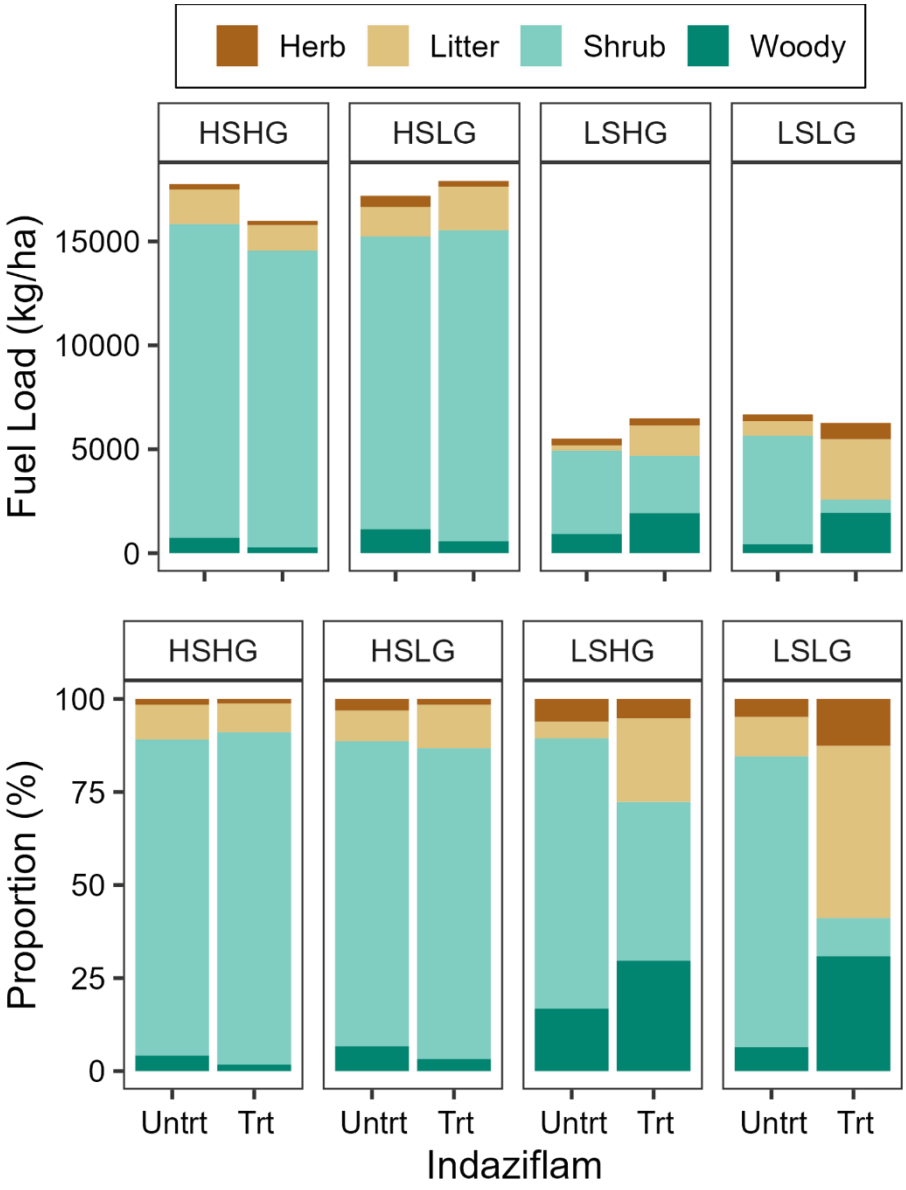

Figure 1.6. Total and proportional fuel load of herbaceous, shrub, litter, and woody fuels within areas treated (trt) and untreated (untrt) with indaziflam.
Load is displayed in four sampling strata: high (H) or low (L) shrub (S) and perennial herbaceous (P) vegetation.

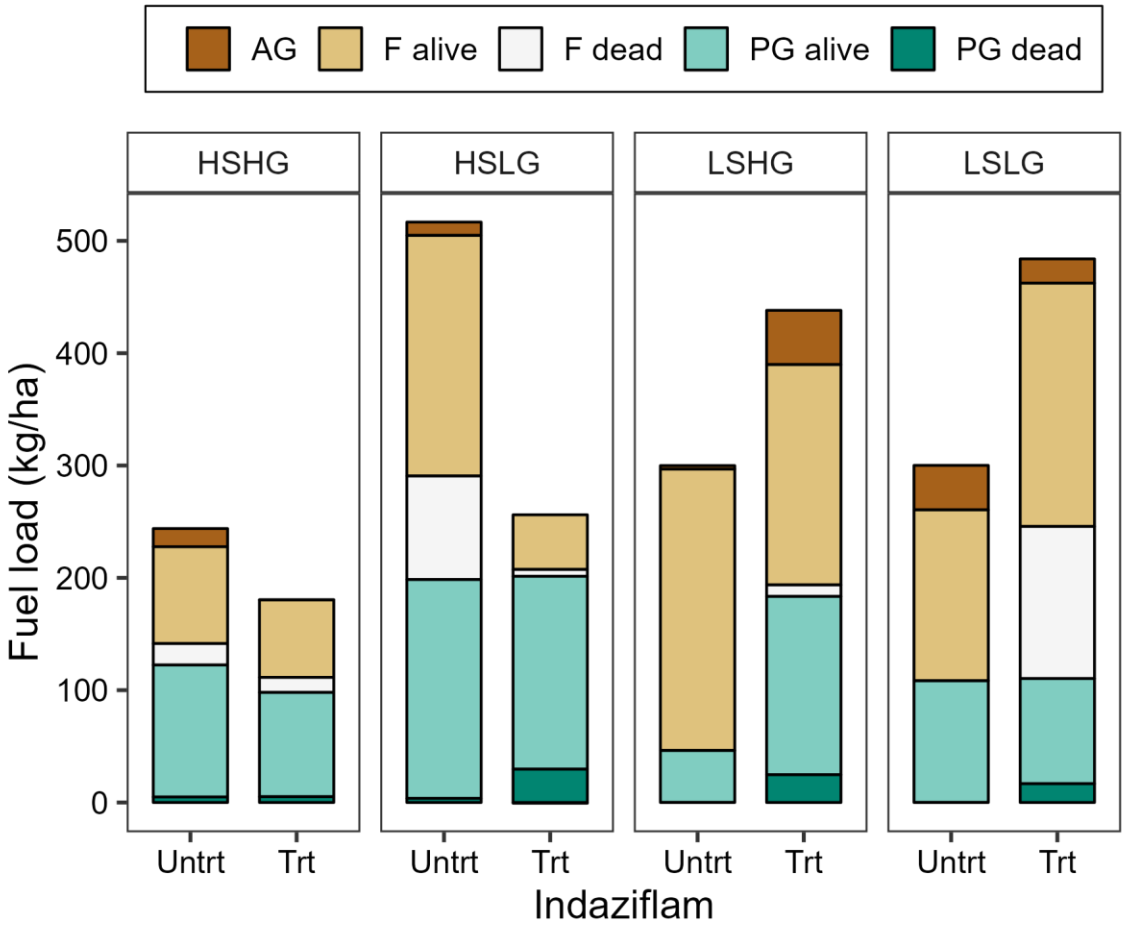

Figure 1.7 Herbaceous fuel load of annual grasses (AG), alive and dead forbs (F), and alive and dead perennial grasses (PG) by indaziflam treatment.
Load is displayed in four sampling strata: high (H) or low (L) shrub (S) and perennial herbaceous (P) vegetation. Within each sampling strata, there were no differences in fuels by indaziflam treatment.

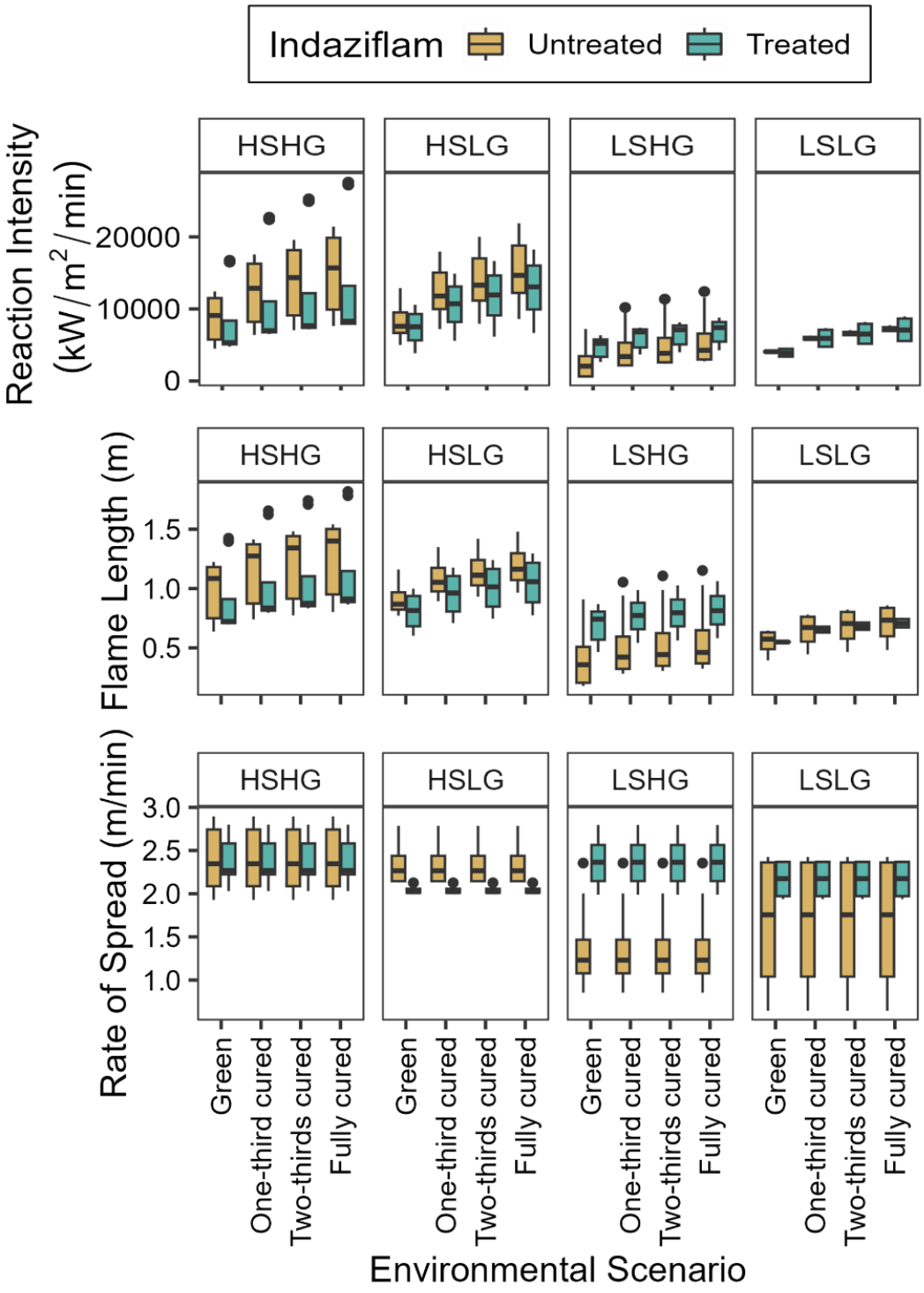

Figure 1.8. Modeled flame length, rate of spread, and reaction intensity under four environmental scenarios.
Each attribute of fire behavior is divided into four sampling strata: high (H) or low (L) shrub (S) and perennial herbaceous (P) vegetation. Both flame length and reaction intensity increased in drier fuel moisture scenarios.

Supplemental Information

Supplemental Information 1.1. Inputs for shrub layer for custom fuel beds in FFT.

PlotID	Strata	Trt	shrub cover (%) 2021	shrub cover (%) 2022	shrub height (m)	shrub percent live (%)	shrub fuel load (kg/ha)
101C	HSHG	C	50.6	48.9	1.016	100.0	17034
101T	HSHG	T	43.3	41.7	0.976	94.5	21855
102C	HSHG	C	51.7	51.7	0.712	88.4	9036
102T	HSHG	T	62.2	66.1	0.776	96.0	7504
103C	HSHG	C	51.1	51.7	0.848	93.9	12912
103T	HSHG	T	63.9	51.7	0.816	97.7	7567
104C	HSHG	C	52.8	41.7	0.584	91.1	3528
104T	HSHG	T	30.0	30.0	0.84	78.6	5322
201C	HSLG	C	45.6	50.0	1	92.7	18000
201T	HSLG	T	80.0	82.2	0.968	97.2	17929
202C	HSLG	C	61.7	65.6	0.832	96.6	10612
202T	HSLG	T	66.1	66.1	0.896	97.3	14278
203C	HSLG	C	50.0	66.7	0.808	97.7	9584
203T	HSLG	T	62.8	75.8	0.896	98.4	7533
204C	HSLG	C	58.9	50.8	0.904	91.8	3460
204T	HSLG	T	60.6	51.1	0.768	98.0	4283
301C	LSHG	C	21.1	31.1	0.848	84.4	8164
301T	LSHG	T	15.0	13.3	0.576	79.3	595
302C	LSHG	C	11.7	9.4	0.416	69.9	454
302T	LSHG	T	18.9	19.4	0.64	92.0	2908
303C	LSHG	C	22.2	16.1	0.392	70.2	1882
303T	LSHG	T	18.3	23.3	0.864	98.3	3680
304C	LSHG	C	10.6	9.4	0.416	66.1	2070
304T	LSHG	T	12.8	21.1	0.808	91.1	1410
305T	LSHG	T	32.2	31.7	0.776	92.8	3998
401C	LSLG	C	21.7	25.0	0.696	98.2	3993
401T	LSLG	T	2.2	1.1	0.74	100.0	682
402C	LSLG	C	7.2	7.8	0.584	59.5	3705
402T	LSLG	T	13.3	12.2	0.696	70.6	269

Supplemental Information 1.2. Inputs for herbaceous layer for custom fuel beds in FFT.

PlotID	Strata	Trt	herb cover (%)	herb height (m)	herb percent live (%)	herb fuel load (kg/ha)
101C	HSHG	C	30.6	0.384	81.2	150.4
101T	HSHG	T	33.9	0.448	0.0	183.1
102C	HSHG	C	63.3	0.376	80.1	232.1
102T	HSHG	T	63.3	0.28	80.7	146.6
103C	HSHG	C	52.8	0.408	93.6	269.8
103T	HSHG	T	43.9	0.224	0.0	84.9
104C	HSHG	C	58.9	0.296	83.6	323.3
104T	HSHG	T	41.1	0.68	95.8	307.8
201C	HSLG	C	33.9	0.184	100.0	129.9
201T	HSLG	T	50.6	0.376	100.0	97.9
202C	HSLG	C	51.1	0.36	92.8	380.8
202T	HSLG	T	56.7	0.312	100.0	144.6
203C	HSLG	C	65.6	0.752	81.0	1077.5
203T	HSLG	T	79.4	0.496	66.4	543.8
204C	HSLG	C	40.0	0.448	72.9	478.8
204T	HSLG	T	68.3	0.272	100.0	235.8
301C	LSHG	C	52.2	0.304	100.0	244.2
301T	LSHG	T	50.0	1.152	83.5	423.2
302C	LSHG	C	66.1	0.104	100.0	448.9
302T	LSHG	T	57.2	0.256	100.0	194.7
303C	LSHG	C	60.6	0.152	100.0	257.2
303T	LSHG	T	51.7	0.416	87.3	674.8
304C	LSHG	C	57.2	0.288	100.0	249.6
304T	LSHG	T	42.8	0.352	0.0	327.6
305T	LSHG	T	60.6	0.408	100.0	570.5
401C	LSLG	C	66.1	0.496	100.0	388.1
401T	LSLG	T	48.3	0.728	67.5	1055.1
402C	LSLG	C	56.7	0.352	100.0	212.2
402T	LSLG	T	40.0	0.648	69.2	484.0

Supplemental Information 1.3. Inputs for herbaceous and woody layer for custom fuel beds in FFT.

PlotID	Strata	Trt	litter cover (%) 2021	litter cover (%) 2022	litter fuel load (kg/ha)	1 hr fuel load (kg/ha)	10 hr fuel load (kg/ha)	100 fuel load (kg/ha)
101C	HSHG	C	95.4	78.2	1169.1	0.385	0.092	0.000
101T	HSHG	T	95.8	77.8	788.6	0.027	0.277	0.000
102C	HSHG	C	98.3	89.1	1195.2	0.093	0.092	0.000
102T	HSHG	T	98.3	97.2	1276.7	0.040	0.000	0.000
103C	HSHG	C	88.4	91.9	738.7	0.066	0.000	0.000
103T	HSHG	T	90.6	79.6	1610.9	0.027	0.000	0.000
104C	HSHG	C	91.6	76.1	2374.9	0.173	0.277	0.000
104T	HSHG	T	90.8	69.0	494.8	0.040	0.092	0.000
201C	HSLG	C	95.8	79.9	1371.2	0.119	0.277	0.000
201T	HSLG	T	97.8	98.3	1863.0	0.040	0.369	0.000
202C	HSLG	C	92.9	90.1	1490.5	0.080	0.092	0.000
202T	HSLG	T	96.5	88.0	1737.9	0.053	0.000	0.000
203C	HSLG	C	97.7	87.6	1175.4	0.119	0.092	0.492
203T	HSLG	T	97.2	94.1	2112.1	0.040	0.092	0.000
204C	HSLG	C	86.7	81.9	774.4	0.133	0.646	0.000
204T	HSLG	T	96.1	86.0	1531.1	0.066	0.369	0.000
301C	LSHG	C	96.2	64.3	409.6	0.040	0.462	0.000
301T	LSHG	T	98.8	79.6	1147.7	0.066	0.369	0.000
302C	LSHG	C	74.4	45.6	101.1	0.027	0.000	0.000
302T	LSHG	T	97.1	81.1	1142.5	0.080	0.277	0.492
303C	LSHG	C	83.0	45.6	55.4	0.013	0.185	0.492
303T	LSHG	T	97.1	86.9	791.4	0.226	0.554	0.492
304C	LSHG	C	77.1	52.1	57.4	0.093	0.185	0.492
304T	LSHG	T	97.6	84.9	1836.0	0.226	0.646	0.000
305T	LSHG	T	98.8	87.0	1049.1	0.080	0.277	0.000
401C	LSLG	C	92.6	80.5	1079.5	0.066	0.000	0.000
401T	LSLG	T	99.4	81.4	3926.1	0.066	0.277	0.492
402C	LSLG	C	75.4	28.1	70.7	0.040	0.277	0.000
402T	LSLG	T	100.0	89.0	1136.0	0.119	0.277	0.492

*Two model inputs for litter were sourced from FCCS 56: Litter depth of 0.25 cm and 75% grass litter

Supplemental Information 1.4 2021 species list in rank abundance order by proportional (P) cover separated by year and indaziflam treatment.

Untreated					Treated				
Rank	P	Species	Life form	Nativity	P	Species	Life form	Nativity
1	28.4	*Artemisia tridentata*	SH	N	32.4	*Artemisia tridentata*	SH	N
2	20.4	*Poa secunda*	PG	N	17.4	*Poa secunda*	PG	N
3	6.5	*Bromus tectorum*	AG	I	6.4	*Pseudoroegneria spicata*	PG	N
4	5	*Pseudoroegneria spicata*	PG	N	6.4	*Achnatherum nelsonii*	PG	N
5	4.5	*Artemisia arbuscula*	SH	N	4.8	*Lupinus* sp.	PF	N
6	3.8	*Bromus arvensis*	AG	I	4	*Festuca idahoensis*	PG	N
7	3.6	*Nestotus stenophyllus*	PF	N	3.7	*Bromus tectorum*	AG	I
8	3.5	*Phlox longifolia*	PF	N	3.5	*Phlox longifolia*	PF	N
9	3.4	*Achnatherum thurberianum*	PG	N	2.4	*Purshia tridentata*	SH	N
10	2.1	*Eriogonum caespitosum*	PF	N	2.3	*Leymus cinereus*	PG	N
11	2.1	*Elymus elymoides*	PG	N	1.9	*Carex douglassai*	PG	N
12	1.6	*Festuca idahoensis*	PG	N	1.4	*Chrysothamnus viscidiflorus*	SH	N
13	1.2	*Lupinus* sp.	PF	N	1.2	*Eriogonum heracleoides*	PF	N
14	1.2	*Chrysothamnus viscidiflorus*	SH	N	1.2	*Tragopogon dubius*	AF	I
15	1.2	*Agoseris glauca*	PF	N	1.2	*Elymus elymoides*	PG	N
16	1	*Lomatium triternatum*	PF	N	1	*Lupinus sericeus*	PF	N
17	0.8	*Leymus cinereus*	PG	N	0.8	*Ericameria nauseosa*	SH	N
18	0.8	*Lomatium cous*	PF	N	0.8	*Tetradymia canescens*	SH	N
19	0.8	*Tetradymia canescens*	SH	N	0.7	*Mentzelia albicaulis*	AF	N
20	0.8	*Crepis atribarba*	PF	N	0.5	*Penstemon* sp.	PF	N
21	0.7	*Eriogonum heracleoides*	PF	N	0.5	*Crepis acuminata*	PF	N
22	0.7	*Tragopogon dubius*	AF	I	0.5	*Agoseris glauca*	PF	N
23	0.5	*Purshia tridentata*	SH	N	0.3	*Eriogonum umbellatum*	PF	N
24	0.5	*Lomatium nudicaule*	PF	N	0.3	*Achillea millefolium*	PF	N
25	0.4	*Eriogonum wrightii*	PF	N	0.3	*Lomatium triternatum*	PF	N
26	0.4	*Achillea millefolium*	PF	N	0.3	*Balsamorhiza sagittata*	PF	N
27	0.3	*Balsamorhiza sagittata*	PF	N	0.2	*Nestotus stenophyllus*	PF	N
28	0.3	*Lomatium dissectum*	PF	N	0.2	*Zigadenus paniculatus*	PF	N
29	0.3	*Eriogonum umbellatum*	PF	N	0.2	*Eriogonum caespitosum*	PF	N
30	0.2	*Ericameria nauseosa*	SH	N	0.2	*Amsinckia menziesii*	AF	N
31	0.2	*Mentzelia albicaulis*	AF	N	0.2	*Viola purpurea*	PF	N
32	0.2	*Allium acuminatum*	PF	N	0.2	*Artemisia ludoviciana*	PF	N
33	0.2	*Antennaria luzuloides*	PF	N	0.2	*Phacelia heterophylla*	PF	N
34	0.1	*Castilleja* sp	PF	N	0.1	*Koeleria macrantha*	PG	N
35	0.1	*Lewisia rediviva*	PF	N	0.1	*Amsinckia retorsa*	AF	N
36	0.1	*Astragalus* sp.	PF	N	0.1	*Collinsia parviflora*	AF	N
37	0.1	*Cirsium undulatum*	PF	N	0.1	*Melica bulbosa*	PG	N
38	0.1	*Zigadenus paniculatus*	PF	N	0.1	*Microseris nutans*	PF	N
39	0.1	*Lithospermum ruderale*	PF	N	0.1	*Senecio integerrimus*	PF	N

Supplemental Information 1.4 2021 species list in rank abundance order by proportional (P) cover separated by year and indaziflam treatment.

	Untreated				Treated			
Rank	P	Species	Life form	Nativity	P	Species	Life form	Nativity
40	0.1	*Amsinckia* sp.	AF	N	0.1	*Eriogonum ovalifolium*	PF	N
41	0.1	*Erigeron aphanactis*	PF	N	0.1	*Cirsium undulatum*	PF	N
42	0.1	*Senecio integerrimus*	PF	N	0.1	*Crepis occidentalis*	PF	N
43	0.1	*Melica bulbosa*	PG	N	0.1	*Poa bulbosa*	PG	I
44	0.1	*Hydrophyllum capitatum*	PF	N	0.1	*Equisetum laevigatum*	PF	N
45	0.1	*Lupinus sericeus*	PF	N	0.1	*Helianthella uniflora*	PF	N
46	0.1	*Crepis acuminata*	PF	N	0.1	*Artemisia arbuscula*	SH	N
47	0.1	*Penstemon* sp.	PF	N	0.1	*Chaenactis douglasii*	PF	N
48					0.1	*Lomatium cous*	PF	N
49					0.1	*Bromus arvensis*	AG	I
50					0.1	*Antennaria luzuloides*	PF	N
51					0.1	*Iva axillaris*	PF	N

Supplemental Information 1.5. 2022 species list in rank abundance order by proportional (P) cover separated by year and indaziflam treatment.

	Untreated			Treated		
Rank	P Species	Life form	Nativity	P Species	Life form	Nativity
1	17.4 *Artemisia tridentata*	SH	N	21.6 *Artemisia tridentata*	SH	N
2	16.3 *Poa secunda*	PG	N	18.1 *Poa secunda*	PG	N
3	11.3 *Bromus tectorum*	AG	I	5.4 *Pseudoroegneria spicata*	PG	N
4	9.9 *Bromus arvensis*	AG	I	5.3 *Bromus tectorum*	AG	I
5	5.9 *Collinsia parviflora*	AF	N	4.8 *Phlox longifolia*	PF	N
6	3.2 *Pseudoroegneria spicata*	PG	N	4.6 *Lupinus* sp.	PF	N
7	3 *Phlox longifolia*	PF	N	4 *Festuca idahoensis*	PG	N
8	2 *Collomia linearis*	AF	N	3.3 *Collinsia parviflora*	AF	N
9	1.9 *Artemisia arbuscula*	SH	N	2.8 *Bromus arvensis*	AG	I
10	1.7 *Festuca idahoensis*	PG	N	2.4 *Carex douglassai*	PG	N
11	1.6 *Purshia tridentata*	SH	N	2.2 *Achnatherum nelsonii*	PG	N
12	1.6 *Achnatherum nelsonii*	PG	N	2 *Purshia tridentata*	SH	N
13	1.3 *Lomatium triternatum*	PF	N	1.9 *Crepis atribarba*	PF	N
14	1.2 *Elymus elymoides*	PG	N	1.4 *Leymus cinereus*	PG	N
15	1.2 *Eriogonum caespitosum*	PF	N	1.3 *Elymus elymoides*	PG	N
16	1.1 *Agoseris glauca*	PF	N	1.2 *Agoseris glauca*	PF	N
17	1.1 *Crepis atribarba*	PF	N	1 *Tragopogon dubius*	AF	I
18	1 *Nestotus stenophyllus*	PF	N	0.9 *Ericameria nauseosa*	SH	N
19	0.9 *Lupinus* sp.	PF	N	0.9 *Calochortus* sp.	PF	N
20	0.9 *Draba verna*	AF	I	0.8 *Sisymbrium altissimum*	AF	I
21	0.9 *Allium* sp.	PF	N	0.8 *Artemisia arbuscula*	SH	N
22	0.9 *Chrysothamnus viscidiflorus*	SH	N	0.8 *Eriogonum thymoides*	PF	N
23	0.8 *Lomatium nudicaule*	PF	N	0.8 *Melica bulbosa*	PG	N
24	0.7 *Microsteris gracilis*	AF	N	0.7 *Allium* sp.	PF	N
25	0.6 *Carex douglassai*	PG	N	0.7 *Poa bulbosa*	PG	I
26	0.6 *Alyssum alyssoides*	AF	I	0.6 *Lomatium triternatum*	PF	N
27	0.5 *Eriogonum heracleoides*	PF	N	0.5 *Crepis occidentalis*	PF	N
28	0.5 *Poa bulbosa*	PG	I	0.5 *Collomia linearis*	AF	N
29	0.5 *Crepis occidentalis*	PF	N	0.5 *Chrysothamnus viscidiflorus*	SH	N
30	0.5 *Lupinus arbustus*	PF	N	0.5 *Polygonum douglasii*	AF	N
31	0.4 *Melica bulbosa*	PG	N	0.4 *Viola purpurea*	PF	N
32	0.4 *Eriogonum thymoides*	PF	N	0.4 *Eriogonum heracleoides*	PF	N
33	0.4 *Senecio integerrimus*	PF	N	0.4 *Tetradymia canescens*	SH	N
34	0.4 *Paeonia brownii*	PF	N	0.3 *Penstemon* sp.	PF	N
35	0.4 *Eriogonum microthecum*	PF	N	0.3 *Hesperostipa comata*	PG	N
36	0.4 *Calochortus* sp.	PF	N	0.3 *Koeleria macrantha*	PG	N
37	0.4 *Crepis acuminata*	PF	N	0.3 *Crepis acuminata*	PF	N
38	0.3 *Tragopogon dubius*	AF	I	0.3 *Alyssum alyssoides*	AF	I
39	0.3 *Leymus cinereus*	PG	N	0.3 *Eriogonum caespitosum*	PF	N
40	0.3 *Polygonum douglasii*	AF	N	0.3 *Microsteris gracilis*	AF	N

Supplemental Information 1.5. 2022 species list in rank abundance order by proportional (P) cover separated by year and indaziflam treatment.

	Untreated				Treated		
Rank	P	Species	Life form	Nativity	P Species	Life form	Nativity
41	0.3	*Balsamorhiza sagittata*	PF	N	0.3 *Hydrophyllum capitatum*	PF	N
42	0.3	*Sisymbrium altissimum*	AF	I	0.3 *Penstemon humilis*	PF	N
43	0.3	*Antennaria luzuloides*	PF	N	0.2 *Senecio integerrimus*	PF	N
44	0.3	*Epilobium brachycarpum*	AF	N	0.2 *Balsamorhiza sagittata*	PF	N
45	0.3	*Ericameria nauseosa*	SH	N	0.2 *Astragalus* sp.	PF	N
46	0.2	*Castilleja tenuis*	PF	N	0.2 *Lupinus arbustus*	PF	N
47	0.2	*Tetradymia canescens*	SH	N	0.1 *Amsinckia* sp.	AF	N
48	0.2	*Astragalus* sp.	PF	N	0.1 *Epilobium brachycarpum*	AF	N
49	0.2	*Achillea millefolium*	PF	N	0.1 *Paeonia brownii*	PF	N
50	0.2	*Lactuca serriola*	AF	I	0.1 *Lomatium nudicaule*	PF	N
51	0.2	*Lomatium cous*	PF	N	0.1 *Iva axillaris*	PF	N
52	0.2	*Penstemon* sp.	PF	N	0.1 *Artemisia ludoviciana*	PF	N
53	0.1	*Lomatium grayi*	PF	N	0.1 *Achillea millefolium*	PF	N
54	0.1	*Lappula occidentalis*	AF	N	0.1 *Chaenactis douglasii*	PF	N
55	0.1	*Viola purpurea*	PF	N	0.1 *Equisetum arvense*	PG	N
56	0.1	*Castilleja angustifolia*	PF	N	0.1 *Eriogonum ovalifolium*	PF	N
57	0.1	*Iva axillaris*	PF	N	0.1 *Descurainia sophia*	AF	I
58	0.1	*Machaeranthera grindelioides*	AF	N	0.1 *Nestotus stenophyllus*	PF	N
59	0.1	*Cirsium undulatum*	PF	N	0.1 *Mertensia oblongifolia*	AF	N
60	0.1	*Mentzelia albicaulis*	AF	N	0.1 *Phacelia hastata*	PF	N
61	0.1	*Phacelia linearis*	AF	N	0.1 *Viola beckwithii*	PF	N
62	0.1	*Viola beckwithii*	PF	N	0.1 *Lithospermum ruderale*	PF	N
63	0.1	*Amsinckia* sp.	AF	N	0.1 *Phacelia linearis*	AF	N
64	0.1	*Delphinium* sp.	PF	N	0.1 *Alopecurus pratensis*	PG	I
65	0.1	*Zigadenus paniculatus*	PF	N	0.1 *Poa compressa*	PF	I
66	0.1	*Navarretia breweri*	AF	N	0.1 *Castilleja angustifolia*	PF	N
67	0.1	*Lewisia rediviva*	PF	N	0.1 *Chorispora tenella*	AF	I
68	0.1	*Lithospermum ruderale*	PF	N	0.1 *Descurainia pinnata*	AF	N
69	0.1	*Artemisia ludoviciana*	PF	N			

Chapter 2: Cheatgrass alters flammability of native perennial grasses in laboratory combustion experiments

Abstract

The invasive annual grass cheatgrass (*Bromus tectorum*) increases fuel continuity, alters patterns of fire spread, and changes plant communities in sagebrush shrublands of the Great Basin (USA) and adjacent sagebrush steppe areas, yet no studies have contrasted its flammability to native perennial grasses. Understanding cheatgrass flammability is crucial for predicting fire behavior, informing management decisions, and assessing fire potential in invaded areas. This study aimed to determine the flammability of cheatgrass compared to two native perennial grasses (Columbia needlegrass (*Achnatherum nelsonii*) and bluebunch wheatgrass (*Pseudoroegneria spicata*)) across a range of typical fire season fuel moistures. All three grass species had decreased flammability with increasing fuel moisture. Columbia needlegrass had on average 11% lower mass consumption than cheatgrass, and both perennial grasses had on average 13.5 s longer flaming durations and higher thermal doses (temperature over time) than cheatgrass. The addition of cheatgrass to the perennial grasses increased combined mass consumption, flaming duration, and thermal dose. For these three attributes, flammability increased with greater amounts of cheatgrass in the mixture, but flaming duration and thermal dose were not sensitive to cheatgrass fuel moisture. Maximum temperature and flame length of perennial grass combustion were similar with and without cheatgrass addition.Flammability of Columbia needlegrass was higher when burned with cheatgrass than expected based on the flammability of each respective species, suggesting that Columbia needlegrass may be susceptible to pre-heating from cheatgrass, causing increased mass consumption, flaming duration, and thermal dose. Conversely, flammability of bluebunch wheatgrass and cheatgrass together had no interactive effects. This study provides experimental evidence supporting previous qualitative observations of high cheatgrass flammability. Even at high fuel moisture, cheatgrass increased perennial grass flammability, suggesting that cheatgrass poses a significant threat to native grasses. The study's findings provide crucial data for informing invasive plant management and fire potential, as well as guiding efforts to prevent and mitigate cheatgrass-induced fires.

Background

Annual grasses in the western US are spreading at an alarming rate (Germino et al. 2016), and land managers require science-based information on best practices to address this problem (Boyd and Svejcar 2009, Sayre et al. 2012). One significant consequence of annual grass invasion is the shift in fire regime towards an increased invasive grass-wildfire feedback cycle, driven by increased fine fuel continuity, flammability of grasses, and faster postfire recovery of non-native species (D'Antonio and Vitousek 1992, Knapp 1996, Brooks et al. 2004, Balch et al. 2013). This phenomenon is pronounced in semiarid ecosystems with historically low fire occurrence (D'Antonio and Vitousek 1992, Brooks et al. 2004, Balch et al. 2013).

One way that science may inform management is by directly quantifying flammability of native and invasive plant species. Flammability encompasses four phenomena: (1) ignitability-the time elapsed until ignition once a material is exposed to a known ignition source, (2) sustainability-how well the fuel continues to burn, (3) combustibility-how rapidly or intensely a material burns and (4) consumption-the quantity of material that is consumed (Anderson 1970). Fuel moisture is a major determinant of flammability (Rothermel 1972). Fuel moisture differs by plant functional group, changes throughout the season, and is sensitive to smaller scale changes, such as shade microclimates or daily weather cycles (Rothermel 1972). For example, Cardoso et al. (2018) reported a shift in fire potential within tropical forest-savannahs of Lopé National Park, Gabon due to changes in understory species composition, and therefore flammability. Understanding species' flammability is necessary for understanding how they contribute to fuel loads and therefore potential fire behavior.

One way to assess species flammability is through laboratory combustion experiments. Fuentes-Ramirez et al. (2016) measured the flammability of the fire-intolerant creosote bush *(Larrea tridentata)*, in combination with two invasive annual grasses (*Schismus arabicus* and *Bromus madritensis*) and two native plants (sub-shrub *Ambrosia dumosa* and annual forb *Amsinckia menziesii*). Each species was burned individually and in combination with creosote bush in laboratory combustion experiments. They found that invasive grasses spread fire quickly, burned briefly, and produced more intense fires, while native plants spread fire slowly (Fuentes-Ramirez et al. 2016). As a result, Fuentes-Ramirez et al. (2016) classified invasive and native vegetation by their functional role in creosote bush flammability: invasive grasses served as fire spreaders, and when ignited by "spreaders", native vegetation served as "ignitors" of lower, dead branches of creosote bush (Fuentes-Ramirez et al. 2016). The study concluded that different species have distinct flammability characteristics, and their arrangement on the landscape should be considered when assessing fire risk,

especially in areas where fire-prone invaders are impacting native fire-intolerant species (Fuentes-Ramirez et al. 2016).

Flammability of two species burned together can be influenced not only by the flammability traits of the individual species but also by the interaction between the species. Blauw et al. (2015) investigated the impact of fuel moisture on species flammability, both individually and when burned together. The study involved the combustion of two pleurocarpous moss species (*Hypnum jutlandicum* and *Pleurozium schreberi*) and two shrub species (*Empetrum nigrum* and *Calluna vulgaris*) in various combinations. The results showed that flammability varied depending on the species, but increased overall with lower fuel moisture content. Additionally, non-additive effects - deviations between observed and expected combined flammability - were more pronounced and varied at higher fuel moisture contents. These findings suggest that when modeling fire behavior, it may not be sufficient to consider the flammability of individual species alone, but that species interactions must also be considered in multi-species systems.

Within sagebrush shrublands, introduced winter annual grasses such as cheatgrass (*Bromus tectorum*), have altered fire through several mechanisms, including increasing fine fuel continuity (Whisenant 1990) and enabling fire spread (Link et al. 2006). Cheatgrass forms a highly flammable, continuous, fine fuel bed with a high fuel surface-to-volume ratio that readily ignites and rapidly carries wildfire even under wet early season conditions (Balch et al. 2013). Invasive grass-fueled wildfires often occur earlier in the season than was common historically, because cheatgrass cures before native plants have senesced. More frequent fires can eliminate some sagebrush species, which require longer fire return intervals to reach maturity and produce seed (Whisenant 1990).

Studies which have examined the impact of cheatgrass on fire activity in the Great Basin using remote sending tools have demonstrated that cheatgrass has increased fire regionally, and that invaded areas are more likely to burn. Balch et al. (2013) examined the impact of cheatgrass on fire activity from 1980-2009 on a regional scale in the arid western US and found that areas with cheatgrass were more likely to burn, and fires started in cheatgrass were more likely to burn for multiple days and contribute to the largest fires of the year. Pastick et al. (2021) proposed a risk threshold of 10% invasive annual grass cover to heighten fire risk based on remotely sensed estimates of annual grass cover and fire occurrence. Even relatively small amounts of introduced annual grass on the landscape can increase wildfire risk (Balch et al. 2013, Pastick et al. 2021). However, little is known about the species-level flammability of cheatgrass. Link et al. (2019) experimentally initiated and then quantified flammability of study plots in Grant County, Washington which had been invaded by cheatgrass, but were re-vegetation with large bunchgrasses, but did not observe any differences in

plot-level ignitability due to revegetation or cheatgrass abundance. No studies have quantified cheatgrass flammability, nor compared it to other native species present in the invaded ecosystem. The main goal of this study was to evaluate the flammability of cheatgrass and two native perennial bunchgrasses. To address this, we posed three research questions:

1. How does the flammability of cheatgrass compare to that of Columbia needlegrass and bluebunch wheatgrass species across a range of fuel moistures?
2. What effect does the addition of cheatgrass have on the overall flammability of Columbia needlegrass and bluebunch wheatgrass?
3. When cheatgrass and Columbia needlegrass or bluebunch wheatgrass are burned together, does the combined flammability result from a simple combination of the individual species' attributes, or are there additional interactions between the two species that alter the overall flammability?

From these questions, we developed three research predictions:

1. Cheatgrass will have higher flammability than both Columbia needlegrass and bluebunch wheatgrass due to its high surface area to volume ratio and fine stems.
2. The addition of cheatgrass will increase the overall flammability of Columbia needlegrass and bluebunch wheatgrass due to the higher fuel loads and lower moisture content of the annual grass compared to the perennials.
3. When cheatgrass and Columbia needlegrass or bluebunch wheatgrass are burned together, the combined flammability will not be a simple additive function of the individual species' attributes; rather, there will be greater flammability due to cheatgrass preheating perennial grasses, resulting in an altered overall flammability.

Methods

Collection and processing of plant materials

One invasive annual grass species (*Bromus tectorum)*, and two perennial grass species, bluebunch wheatgrass (*Pseudoroegneria spicata)* and Columbia needlegrass (*Achnatherum nelsonii*), were selected for combustion experiments due to their dominance in sagebrush steppe ecosystems. Plant materials were collected at Rinker Rock Creek Ranch (Blaine County, Idaho) during the last week of June 2021. Grasses were clipped within 1 cm of the soil surface to obtain only aboveground plant material. All materials were oven dried at 38 °C for 72 hours and stored at room temperature until initiation of the combustion experiments in July and August of 2021.

Prior to combustion experiments, samples were rehydrated, following methods from Baluw et al. (2015). Oven dried samples were weighed to a standard mass (20 g for individual species trials and either 2.5, 5, 10, or 15 g for combined species trials), and water was added by weight to achieve the desired percent relative fuel moisture. Samples were sealed in plastic bags for 48 hours before sample combustion. Prior to combustion, plants were weighed to obtain pre-burn wet mass and confirm moisture level. This rehydration method allowed us to achieve variation in percent fuel moisture, but these values should be considered relative to each other, and not necessarily representative of live fuel moisture as would be assessed in the field from freshly collected plants. Cheatgrass was rehydrated to 5, 10, 15, 25, 35, 45, and 55 percent moisture. Perennial grasses were rehydrated to 15, 25, 35, 45, and 55 percent moisture. Moisture ranges were sourced from fuel moisture content reported by Davies and Nafus (2013) from green-up until senescence. A minimum of five replicates of each moisture level for each species were burned.

Both perennial grasses were also burned in combination with cheatgrass. Perennial grass mass was kept consistent (20 g). Two target perennial grass moisture levels were selected for combination experiments: a high (55%) and moderate (35%) moisture. Four levels of both cheatgrass mass and moisture were selected to reflect varying levels of cheatgrass invasion, from relatively low to high under different moisture regimes. The four amounts were 2.5, 5, 10, and 15 g of cheatgrass at 5, 15, 25, and 35% moisture. Bluebunch wheatgrass combination trials were only burned with 2.5, 5, and 10 g of cheatgrass, but still at all four moisture levels. Four replicates of each annual and perennial grass combination were burned.

Combustion experiments

Combustion experiments were conducted inside a combustion chamber at the University of Idaho's iFire laboratory. The chamber, constructed using a 10 cm diameter steel pipe, was elevated 2.5 cm above the ground to facilitate sample ignition (Fig. 2.1). For ventilation, approximately 15 holes, each with a diameter of 0.5 cm, were incorporated into the walls of the chamber. Three Type K thermocouples were inserted into the chamber at distances of 19, 33, and 48 cm from the base (Fig. 2.1).

For each combustion trial, samples were weighed to the nearest 0.01 g pre-burn to assess moisture achieved from rehydration. For trials with two species, perennial and annual grasses were weighed separately since they had been independently rehydrated. Grasses were burned upright inside the combustion chamber to best mimic natural fuel structure. To accomplish this, samples were loaded inside 5 cm diameter PVC pipes, cut longitudinally (Fig. 2.2). Both halves of PVC were

closed around the sample and released into the chamber, standing vertically (Fig. 2.2). Perennial and annual grass species mixtures were mixed homogeneously and loaded into chamber (Fig. 2.2).

Once samples were loaded into chamber, 1 mL of isopropyl alcohol was placed on a watch glass centered under the chamber (Fig. 2.2). The alcohol was ignited using a remote charge through a wire. Each burn was recorded on video. Post-burn plant material was weighed to the nearest 0.01 g. For combined perennial and annual grass trials, post-burn weight was of both species combined. A height board with 10 cm increments was placed behind the combustion chamber, and maximum flame height for each trail was recorded by viewing combustion videos (Fig. 2.1). The majority of flame heights exceeded the height of the chamber. However, for flames that were shorter than the chamber, their height was estimated within a range based on the visibility of chamber vent holes in the recorded video (Fig. 2.1). Temperature was recorded for each thermocouple throughout the experiment at 0.5 second intervals. All temperature data were trimmed at a 100 °C temperature threshold.

Data analysis for individual and combined species trials

Data were summarized to assess four major phenomena of flammability (Table 2.1). Ignitability, was determined by assessing the probability of ignition, i.e., whether the sample ignited or not under standardized experimental conditions. This assessment was done visually during the trials and confirmed using video footage. Information from all trials was used to inform ignitability. For other attributes of flammability, only temperature data from trials which ignited were used. Sustainability was assessed as flaming duration, which was the time in seconds that each thermocouple spent above 100 °C. Combustibility was classified with three traits: maximum temperature, thermal dose, and maximum flame height. Maximum temperature was calculated for each thermocouple. Thermal dose was the sum of each thermocouple's temperatures when they exceeded 100 °C. Maximum flame height was estimated by reviewing the trial videos and approximating the highest point from the high board to the nearest 10 cm. Consumption was calculated as percent mass loss, using equation 2.1

Equation 2.1. Percent mass loss

$$ML_{\%} = \frac{(M_i - M_e)}{M_i} \times 100$$

where M_i is the initial mass and M_e is the end mass for each trial.

To determine if all three thermocouples could be combined for future analysis, an analysis of variance (ANOVA) test was implemented to test for differences in temperature across the three thermocouples. The lowest (19 cm) thermocouple was significantly different from the upper two, and was removed from further analysis. Differences in flammability attributes (ignition probability,

flaming duration, maximum temperature, thermal dose, maximum flame height, and percent mass loss) were first examined across the three species (categorical variable for species: either cheatgrass, Columbia needlegrass, or bluebunch wheatgrass) using an ANOVA. A Tukey post-hoc test was used if ANOVA results yielded significance. Next, differences in flammability attributes were examined across fuel moistures, with fuel moisture as a continuous predictor variable, using linear regression analysis. An interaction between fuel moisture (continuous) and species (categorical) was also examined for each attribute of flammability.

Differences between combined species flammability (ignition probability, flaming duration, maximum temperature, thermal dose, maximum flame height, and percent mass loss) when cheatgrass was added to perennial grasses compared to perennial grass alone was tested using multiple ANOVA tests. For these analyses, each perennial grass species and level of perennial grass fuel moisture (either 35 or 55 % fuel moisture) were examined separately. We tested for differences by cheatgrass amount (continuous) and fuel moisture (continuous) using multiple ANOVA tests. To test for differences between the perennial grass alone (0g of cheatgrass added) and perennial grasses with increasing amounts of cheatgrass, we used a Tukey post-hoc test. For all individual and combined species analysis, separate models were implemented for each combustion response variable. All statistical analysis was performed in R (version 4.3.3; R Core Team 2023).

Additive effects of combustion

To compare the flammability attributes of individual and combined fuel beds, effect size of non-additivity was calculated as $(observed - expected)/expected$. Observed values were obtained directly from trials involving two species, and the expected flammability was calculated as a weighted average based on the results of individual species trials. Weights for each species were assigned based on their relative contribution to the total mass in the two-species trial.

Effect size was examined using a two-sided t-test and μ was set to 0 to determine whether the mean effect size for each trial combination (perennial grass species x perennial grass fuel moisture x cheatgrass mass x cheatgrass fuel moisture) differed significantly from 0. A non-significant result suggests additivity of flammability attributes, meaning that the observed flammability does not differ significantly from what is expected based on individual species fuel beds. A significant effect size indicates a nonadditive interaction between the two species. Positive and negative values of the effect size indicate different directions of non-additivity, and the value represents the strength of the nonadditive effect. A negative effect size means that the expected values are higher than observed, indicating that at least one species has a negative influence on the combined flammability. A positive effect size indicates that the two species together enhance the flammability compared to their

individual species fuel beds. Further, multiple linear regressions were used to examine whether non-additivity differed based on perennial grass species (categorical), perennial grass fuel moisture (categorical), cheatgrass mass (continuous), and cheatgrass fuel moisture (categorical). All statistical analysis was performed in R (version 4.0.3; R Core Team, 2021).

Results

Individual species flammability

Mass consumption, flaming duration, and thermal dose all differed among species (Table 2.2). Columbia needlegrass had lower mass consumption (by 11% on average, $p < 0.01$) than cheatgrass, but bluebunch wheatgrass was similar to cheatgrass for mass consumption, flaming duration, and thermal dose (Fig. 2.3). Both perennial grasses had higher thermal dose and longer flaming duration than cheatgrass, but there were no differences between the two perennial grass species. Columbia needlegrass ($p = 0.008$) and bluebunch wheatgrass ($p = 0.052$) burned for 15.2 and 11.8 s, respectively, longer than cheatgrass (Table 2.2; Fig. 2.3). Columbia needlegrass ($p = 0. 001$) and bluebunch wheatgrass ($p = 0.072$) had greater thermal dose than cheatgrass by 14,382 and 8,645 °C, respectively (Table 2.2; Fig. 2.3). There were no differences in maximum temperature and flame height between the three species (Table 2.2; Fig. 2.3). Flammability decreased for all three grass species with increasing fuel moisture (Table 2.3; Fig. 2.3). All species maintained relatively high ignitability across all fuel moistures tested (Fig 2.3).

Combined species flammability

The addition of cheatgrass to the two perennial grass species altered certain flammability characteristics (Fig. 2.4 and 2.5; refer to Table 2.4 for Columbia needlegrass results and Table 2.5 for bluebunch wheatgrass results). The importance of cheatgrass amount and fuel moisture varied depending on the flammability attribute being observed. When comparing combined trials to those without any cheatgrass added, only mass consumption, flaming duration, and flame height differed from just the perennial grass burned alone (Fig. 2.4 and 2.5; Tables 2.3 and 2.4).

Cheatgrass increased percent mass consumption when combined with the perennial grasses (Tables 2.3 and 2.4). Consumption increased with increasing cheatgrass amount for both Columbia needlegrass ($p < 0.001$) and bluebunch wheatgrass ($p = 0.003$). When Columbia needlegrass was combined with greater than 2.5 g of cheatgrass, consumption was higher than when Columbia needlegrass was burned alone ($p < 0.001$; Fig. 2.4)

When both perennial grass species were burned with increasing amount of cheatgrass, total flaming duration increased. Cheatgrass mass ($p < 0.001$) but not fuel moisture impacted combined

species flaming duration (Tables 2.3 and 2.4). Columbia needlegrass with 10 g of cheatgrass had longer flaming duration than Columbia needlegrass alone ($p = 0.031$; Fig. 2.4). Bluebunch wheatgrass with 10 g of cheatgrass burned for 45 and 43 s longer than with only 2.5 and 5 g of cheatgrass ($p < 0.001$; Fig. 2.4). It's important to note that flaming durations were not normalized to total biomass, and all experiments were conducted in a fixed-size combustion chamber. Therefore, it is challenging to determine whether the increased flaming duration is solely attributable to cheatgrass or if it is a result of overall increased fuel quantity.

For both perennial grass species and perennial fuel moistures, there were no differences in thermal dose between trials where perennial grasses were burned alone and trials where cheatgrass was added (Figs. 2.4 and 2.5). However, cheatgrass mass ($p=0.003$) and fuel moisture ($p=0.31$) were both significant factors in explaining differences in thermal dose for 55% FM perennial grasses (Fig. 2.4; Tables 2.3 and 2.4).

The maximum temperature in combined trials with Columbia needlegrass and cheatgrass did not differ from trials where Columbia needlegrass was burned alone (Fig. 2.3). For bluebunch wheatgrass at 55% FM, the mass of cheatgrass explained some of the variability in maximum temperature ($p = 0.003$; Table 2.5; Fig. 2.4). Similarly, flame height of combined trials with Columbia needlegrass and cheatgrass did not differ from trials where Columbia needlegrass was burned alone (Tables 2.3 and 2.4). For bluebunch wheatgrass at 55% FM, the mass of cheatgrass explained some of the variability in maximum temperature ($p = 0.001$; Fig. 2.4). Bluebunch wheatgrass with 10 g of cheatgrass had significantly higher flame lengths than when bluebunch wheatgrass was burned alone ($p = 0.004$; Table 2.5).

Additive effects of combined flammability

Tests for the additive effects revealed when combined flammability of cheatgrass with one of the two perennial grass species was different than expected based on the flammability of each species. Cheatgrass fuel moisture did not impact any of these additive effects (Table 2.6). However, effects did differ by perennial grass species and fuel moisture, and annual grass mass (Table 2.6). The most significant additive effects were observed in mass consumption, flaming duration, and thermal dose (Fig. 2.6). Greater combined flammability suggests some non-additive interaction among the two fuels within the mixture, resulting in greater overall flammability.

When Columbia needlegrass at 55% FM was burned with more than 5 g of cheatgrass, the combined mass consumption was significantly greater than when each were burned alone. The opposite was true when more than 5 g of cheatgrass were burned with 55% FM bluebunch

wheatgrass: the combined mass consumption was less than was expected from individual species flammability. Similar trends were observed with 35% FM perennial grasses (Fig. 2.7).

Flaming duration with Columbia needlegrass at both 35 and 55% FM with cheatgrass was greater than would be expected from each species' flammability. This phenomenon increased as increasing cheatgrass mass (Fig. 2.6). Combined flaming duration with bluebunch wheatgrass at 55% FM with cheatgrass had either shorter or longer flaming duration than would be expected, depending on cheatgrass mass (Fig. 2.6). Flaming duration of cheatgrass with bluebunch wheatgrass at 35% was greater than would be expected from individual species, but this effect did not differ by cheatgrass mass (Fig. 2.7).

Thermal dose of Columbia needlegrass at 55% FM with all amounts of cheatgrass was greater than would be expected from individual species' flammability (Fig. 2.6). Similar trends were observed at 35% FM for both perennial grass species (Fig. 2.7). Thermal dose of bluebunch wheatgrass at 55% FM with cheatgrass varied by cheatgrass mass: only 10 g of cheatgrass resulted in a different combined thermal dose (Fig. 2.6).

Differences between expected and observed combined maximum temperature were minimal, and differences were due to perennial grass species and fuel moisture, not cheatgrass (Fig. 2.6). Only the lowest amounts of cheatgrass with Columbia needlegrass at 55% FM had a significantly greater maximum temperature than what was expected (Fig. 2.6). For both perennial species at 35% FM with cheatgrass, there were small but positive differences from what would be expected from individual species flammability (Fig. 2.7).

Discussion

Our results show that changes in grass species composition, in our case increased ratios of annual to perennial grass, increased overall flammability. Cheatgrass increased perennial grass mass consumption, flaming duration, and flame height, and increasing cheatgrass biomass increased perennial grass flammability. These results expand on the examinations of invasive grass flammability included in Fuentes-Ramires et al. (2016) but consider multiple mass ratios and fuel moistures of target species.

These experiments provide clear, quantitative evidence for the high flammability of cheatgrass, align with prior qualitative observations, and provide valuable insight into specific flammability attributes. As little as 11% invasive grass biomass (2.5 g of cheatgrass with 20 g of perennial grass) impacted overall mass percent consumption. Cheatgrass was highly flammable, even at high fuel moisture and low mass. At the same initial mass and fuel moisture, the two perennial

grass species burned longer and had a higher thermal dose, but cheatgrass had greater mass consumption than perennials.

Individually, Columbia needlegrass and bluebunch wheatgrass had similar flammability. However, when cheatgrass was added to each perennial grass species, the combined flammability was higher for Columbia needlegrass than bluebunch wheatgrass. This increased combined flammability could be a result of pre-heating of fuels by cheatgrass. Columbia needlegrass was more readily pre-heated to flammable moisture levels, whereas bluebunch wheatgrass seemed to be more resistant to pre-heating. These different pre-heating traits may be due to plant structure as Columbia needlegrass leaves have a greater surface to volume area than bluebunch wheatgrass leaves. While Columbia needlegrass and bluebunch wheatgrass are both native perennial grasses, they have different leaf shapes (Columbia needlegrass leaves are narrower and more needle-like, whereas bluebunch wheatgrass has wider and larger leaves) and can overlap in their distribution within sagebrush grasslands (Trujillo and Strand 2018). Differences in perennial grass combined flammability could be important considerations for seeding post-fire or post-disturbance or within fuel breaks (Shinneman et al. 2019).

Our study evaluated grass flammability across fuel moistures commonly seen during a fire season in a laboratory setting. Although we collected grasses in the field, dried them, and then rehydrated them, this method was consistent with other studies such as Blauw et al. (2015), and provides repeatable measurements and experimental control. However, rehydration with additional water is not the same as intercellular water in live plants. Moreover, cheatgrass was mostly senesced and dry when collected since it is an annual plant. Collecting plant material allowed for low fuel moistures to be obtained, since cheatgrass was already relatively dry when clipped. Differences between live intercellular water in plants versed our methods should be consider when interpreting our experimental results. Experimental fuel moistures should be considered relative to each other, and not necessarily a reproduction of live fuel moisture. Despite these limitations, our results shed light on the increased flammability of cheatgrass and its potential contributions to overall flammability on the landscape. An alternative method could have been to collect and burn grasses in the field, as done in previous studies (Zanzarini et al. 2022), burn plant parts (Simpson et al. 2016), plants from seed in a controlled environment to burn, or burn naturally occurring plants *in situ* (Fill et al. 2016, Cardoso et al. 2018, Newberry et al. 2020). While these methods have their advantages, using a controlled laboratory environment allowed us to obtain consistent measurements within a consistent environment across all grass species.

In this study, cheatgrass and perennial grasses were burned together in a homogenous mixture, with the plant material standing upright to simulate the structure of natural fuels. The main difference between the two fuel sub-layers was the natural height variation between perennials and annuals. However, the spatial distribution of fuels was not examined. Perennial grasses typically grow in tight bunches of live and dead plant material, while cheatgrass fills the plant interspaces (Pilliod et al. 2021). The flammability of each perennial grass species may vary depending on dead plant material within the bunch, which can be influenced by site climate, productivity, and decomposition rate (Bansal et al. 2014). For instance, a perennial grass surrounded by dry dead plant material, including attached and detached litter, could be more susceptible to ignition by cheatgrass in the interspaces. This pre-heating effect from cheatgrass and dead perennial grass material may contribute to increased flammability, as observed with Columbia needlegrass in our study.

Flammability of cheatgrass was only examined in combination with two perennial grass species. To gain a more comprehensive understanding of cheatgrass flammability in sagebrush steppe, future research could explore the flammability of additional dominant species, including those commonly used for fuel breaks (Shinneman et al. 2019). Additionally, flammability experiments could consider the interaction of cheatgrass with other fuels, such as litter and lower shrub branches (Fuentes-Ramirez et al. 2016). It is important to understand how annual and perennial grass species contribute to overall shrub flammability in sagebrush shrublands, as shrub components are a key driver of fire behavior in these ecosystems (Ellsworth et al. 2022). The increased combined flammability (especially mass consumption) observed could suggest increased plant injury and potentially mortality post-fire and could play into potential changes in burn severity.

Conclusions

Cheatgrass flammability impacts the flammability of perennial grass species differently, increasing flammability of Columbia needlegrass more than those with bluebunch wheatgrass. Perennial grass flammability increased as greater amounts of cheatgrass were added to perennial grasses. Cheatgrass increased flammability of these two native perennial bunchgrasses throughout a range of fuel moistures. Flammability with cheatgrass was greater in areas with Columbia needlegrass than those with bluebunch wheatgrass. Establishing a threshold for protection from cheatgrass is challenging and our study suggests that when cheatgrass is more than 11% of the total grass biomass, and efforts to control cheatgrass should be considered to mitigate increased flammability.

References

Anderson, H. E. 1970. Forest fuel ignitibility. Fire Technology 6:312–319.

Balch, J. K., B. A. Bradley, C. M. D'Antonio, and J. Gómez-Dans. 2013. Introduced annual grass increases regional fire activity across the arid western USA (1980-2009). Global Change Biology 19:173–183.

Bansal, S., R. L. Sheley, B. Blank, and E. A. Vasquez. 2014. Plant litter effects on soil nutrient availability and vegetation dynamics: changes that occur when annual grasses invade shrub-steppe communities. Plant Ecology 215:367–378.

Blauw, L. G., N. Wensink, L. Bakker, R. S. P. van Logtestijn, R. Aerts, N. A. Soudzilovskaia, and J. H. C. Cornelissen. 2015. Fuel moisture content enhances nonadditive effects of plant mixtures on flammability and fire behavior. Ecology and Evolution 5:3830–3841.

Boyd, C. S., and T. J. Svejcar. 2009. Managing Complex Problems in Rangeland Ecosystems. Rangeland Ecology & Management 62:491–499.

Brooks, M. L., C. M. D'Antonio, D. M. Richardson, J. B. Grace, J. E. Keeley, J. M. DiTomaso, R. J. Hobbs, M. Pellant, and D. Pyke. 2004. Effects of Invasive Alien Plants on Fire Regimes. BioScience 54:677.

Cardoso, A. W., I. Oliveras, K. A. Abernethy, K. J. Jeffery, D. Lehmann, J. Edzang Ndong, I. McGregor, C. M. Belcher, W. J. Bond, and Y. S. Malhi. 2018. Grass Species Flammability, Not Biomass, Drives Changes in Fire Behavior at Tropical Forest-Savanna Transitions. Frontiers in Forests and Global Change 1:6.

D'Antonio, C. M., and P. M. Vitousek. 1992. Biological Invasions by Exotic Grasses, the Grass/Fire Cycle, and Global Change. Annual Review of Ecology and Systematics 23:63–87.

Davies, K. W., and A. M. Nafus. 2013. Exotic annual grass invasion alters fuel amounts, continuity and moisture content. International Journal of Wildland Fire 22:353.

Ellsworth, L. M., B. A. Newingham, S. E. Shaff, C. L. Williams, E. K. Strand, M. Reeves, D. A. Pyke, E. W. Schupp, and J. C. Chambers. 2022. Fuel reduction treatments reduce modeled fire intensity in the sagebrush steppe. Ecosphere 13.

Fill, J. M., B. M. Moule, J. M. Varner, and T. A. Mousseau. 2016. Flammability of the keystone savanna bunchgrass Aristida stricta. Plant Ecology 217:331–343.

Fuentes-Ramirez, A., J. W. Veldman, C. Holzapfel, and K. A. Moloney. 2016. Spreaders, igniters, and burning shrubs: plant flammability explains novel fire dynamics in grass-invaded deserts. Ecological Applications 26:2311–2322.

Germino, M. J., J. C. Chambers, and C. S. Brown, editors. 2016. Exotic Brome-Grasses in Arid and Semiarid Ecosystems of the Western US: Causes, Consequences, and Management Implications. Springer International Publishing, Cham.

Knapp, P. A. 1996. Cheatgrass (Bromus tectorum L) dominance in the Great Basin Desert. Global Environmental Change 6:37–52.

Link, S. O., C. W. Keeler, R. W. Hill, and E. Hagen. 2006. Bromus tectorum cover mapping and fire risk. International Journal of Wildland Fire 15:113.

Newberry, B. M., C. R. Power, R. C. R. Abreu, G. Durigan, D. R. Rossatto, and W. A. Hoffmann. 2020. Flammability thresholds or flammability gradients? Determinants of fire across savanna–forest transitions. New Phytologist 228:910–921.

Pastick, N. J., B. K. Wylie, M. B. Rigge, D. Dahal, S. P. Boyte, M. O. Jones, B. W. Allred, S. Parajuli, and Z. Wu. 2021. Rapid Monitoring of the Abundance and Spread of Exotic Annual Grasses in the Western United States Using Remote Sensing and Machine Learning. AGU Advances 2.

Pilliod, D. S., M. A. Jeffries, J. L. Welty, and R. S. Arkle. 2021. Protecting restoration investments from the cheatgrass-fire cycle in sagebrush steppe. Conservation Science and Practice 3.

R Core Team. 2023. R: A Language and Environment for Statistical Computing. R Foundation for Statistical Computing, Vienna, Austria.

Rothermel, R. C. 1972. A mathematical model for predicting fire spread in wildland fuels. Page 48. General Technical Report, US Department of Agriculture, Forest Service, Intermountain Forest and Range Experimental Station, Ogden, UT.

Sayre, N. F., W. deBuys, B. T. Bestelmeyer, and K. M. Havstad. 2012. “The Range Problem” After a Century of Rangeland Science: New Research Themes for Altered Landscapes. Rangeland Ecology & Management 65:545–552.

Shinneman, D. J., M. J. Germino, D. S. Pilliod, C. L. Aldridge, N. M. Vaillant, and P. S. Coates. 2019. The ecological uncertainty of wildfire fuel breaks: examples from the sagebrush steppe. Frontiers in Ecology and the Environment 17:279–288.

Simpson, K. J., B. S. Ripley, P.-A. Christin, C. M. Belcher, C. E. R. Lehmann, G. H. Thomas, and C. P. Osborne. 2016. Determinants of flammability in savanna grass species. Journal of Ecology 104:138–148.

Trujillo, J., and E. Strand. 2018. A Field Guide to Grasses and Grass-Like Plants of Idaho. University of Idaho Extension, Moscow, Idaho.

Whisenant, S. G. 1990. Changing fire frequencies on Idaho's Snake River Plains: ecological and management implications. General Technical Report, US Department of Agriculture, Forest Service, Intermountain Research Center, Logan, UT.

Zanzarini, V., A. N. Andersen, and A. Fidelis. 2022. Flammability in tropical savannas: Variation among growth forms and seasons in Cerrado. Biotropica 54:979–987.

Tables

Table 2.1 List of flammability traits and how they were assessed.

Phenomenon	Trait	Technique
Ignitability	Ignition probability	Whether or not the sample ignited under standardized experimental conditions. Visually assessed during trials and verified with video.
Sustainability	Flaming duration	Time above 100 °C temperature threshold (seconds)
Combustibility	Maximum temperature	Maximum temperature for each thermocouple
	Thermal dose	Sum of thermocouple temperatures when above 100 °C threshold
	Maximum flame height	Tallest flame height, assessed using height board in video of combustion
Consumption	Percent mass loss	$ML_{\%} = \frac{(M_i - M_e)}{M_i} \times 100$, where M_i is the initial mass and M_e is the end mass

Table 2.2 Differences between individual species flammability by species as examined using multiple, one-way ANOVA texts.

Flammability	Factor	df	Sum Sq	Mean Sq	f value	P value	Sig
Max. temp	Species	2	668106.4	334053.2	2.63	0.075	
	Residuals	181	23031134.2	127243.8			
Flame length	Species	2	1543.7	771.9	1.13	0.328	
	Residuals	74	50531.0	682.9			
Consumption	Species	2	1806.1	903.1	4.55	0.013	**
	Residuals	89	17664.5	198.5			
Duration	Species	2	7796.9	3898.5	5.31	0.006	**
	Residuals	165	121040.0	733.6			
Thermal dose	Species	2	6.2E+09	3.1E+09	6.89	0.001	**
	Residuals	166	7.5E+10	4.5E+08			

Table 2.3. Differences between individual species flammability by fuel moisture as examined using multiple linear models.

Flammability	Adj.	Coefficient	Estimate	Std.	t value	P value	Sig.
Max. temp	0.161	Intercept	998.47	71.50	13.96	<0.001	***
		Moisture	-87.77	14.62	-6.00	<0.001	***
Flame length	0.222	Intercept	142.54	7.33	19.44	<0.001	***
		Moisture	-7.41	1.55	-4.76	<0.001	***
Consumption	0.209	Intercept	106.50	3.99	26.70	<0.001	***
		Moisture	-4.09	0.82	-5.01	<0.001	***
Duration	0.048	Intercept	91.78	5.97	15.37	<0.001	***
		Moisture	-3.79	1.24	-3.06	0.003	***
Thermal dose	0.161	Intercept	60332.91	4558.58	13.24	<0.001	***
		Moisture	-4334.04	943.28	-4.59	<0.001	***

Table 2.4. Differences in combined flammability of Columbia needlegrass at two fuel moisture levels (categorical covariate) by annual grass (AG) mass (continuous covariate) and moisture (continuous covariate) using multiple ANOVA tests.

Flammability	Columbia needlegrass FM (%)	Factor	df	Sum of squares	Mean sq	F-value	P-value	Sig
Consumption	35	AG mass	2	2911	1456	2.70	0.096	
		AG moisture	1	468	468	0.87	0.365	
		Residuals	17	9171	539			
	55	AG mass	4	10454	2614	16.28	<0.001	**
		AG moisture	3	452	151	0.94	0.428	
		Residuals	61	9793	161			
Duration	35	AG mass	2	3407	1704	1.66	0.204	
		AG moisture	1	790	790	0.77	0.386	
		Residuals	38	39014	1027			
	55	AG mass	4	54132	13533	10.17	<0.001	**
		AG moisture	3	12677	4226	3.18	0.026	*
		Residuals	128	170276	1330			
Flame height	35	AG mass	2	1185	593	0.62	0.551	
		AG moisture	1	27	27	0.03	0.869	
		Residuals	16	15343	959			
	55	AG mass	4	6210	1552	1.52	0.212	
		AG moisture	3	2157	719	0.7	0.555	
		Residuals	46	47004	1022			
Thermal dose	35	AG mass	2	8.02E+08	4E+08	0.62	0.545	
		AG moisture	1	59030442	5.9E+07	0.09	0.765	
		Residuals	38	2.47E+10	6.5E+08			
	55	AG mass	4	1.02E+10	2.6E+09	4.14	0.003	**
		AG moisture	3	5.66E+09	1.9E+09	3.05	0.031	*
		Residuals	128	7.91E+10	6.2E+08			
Max. temp	35	AG mass	2	48933	24466	0.20	0.817	
		AG moisture	1	9810	9810	0.08	0.777	
		Residuals	38	4580669	120544			
	55	AG mass	4	104588	26147	0.35	0.847	
		AG moisture	3	137129	45710	0.6	0.614	
		Residuals	130	9842780	75714			

Table 2.5. Differences in combined flammability of bluebunch wheatgrass at two fuel moisture levels (categorical covariate) by annual grass (AG) mass (continuous covariate) and moisture (continuous covariate) using multiple ANOVA tests.

Flammability	Bluebunch wheatgrass FM (%)	Factor	df	Sum of squares	Mean sq	F-value	P-value	Sig
Consumption	35	AG mass	2	511	256	9.2	0.003	**
		AG moisture	1	15	15	0.53	0.478	
		Residuals	13	361	28			
	55	AG mass	3	4529	1510	5.67	0.002	**
		AG moisture	3	763	254	0.95	0.422	
		Residuals	46	12259	266			
Duration	35	AG mass	2	1096	548	0.82	0.449	
		AG moisture	1	1106	1106	1.66	0.207	
		Residuals	30	19967	666			
	55	AG mass	3	43287	14429	19.57	<0.001	**
		AG moisture	3	4259	1420	1.93	0.13	
		Residuals	97	71508	737			
Flame height	35	AG mass	2	1475	737	2.54	0.117	
		AG moisture	1	78	78	0.27	0.613	
		Residuals	13	3774	290			
	55	AG mass	3	16387	5462	6.46	0.001	**
		AG moisture	3	5324	1775	2.1	0.117	
		Residuals	37	31283	845			
Thermal dose	35	AG mass	2	7.02E+08	3.51E+08	1.17	0.325	
		AG moisture	1	3.35E+08	3.35E+08	1.11	0.3	
		Residuals	30	9.03E+09	3.01E+08			
	55	AG mass	3	1.1E+10	3.67E+09	13.9	<0.001	**
		AG moisture	3	3.22E+09	1.07E+09	4.06	0.009	**
		Residuals	98	2.58E+10	2.64E+08			
Max. temp	35	AG mass	2	221190	110595	1.09	0.348	
		AG moisture	1	6120	6120	0.06	0.807	
		Residuals	30	3037736	101258			
	55	AG mass	3	1339142	446381	4.88	0.003	**
		AG moisture	3	450510	150170	1.64	0.185	
		Residuals	99	9062072	91536			

Table 2.6. Linear models test the difference in effect size for each flammability attribute by perennial grass (PG) species, annual grass (AG) fuel moisture and mass.

Flammability	Subset	Indep. Var.	Estimate	Std error	t value	P value	Sig.
Consumption	All	PG species	-0.32	0.03	-9.86	<0.001	***
		PG FM	0.03	0.04	0.75	0.457	
		AG FM	-0.01	0.01	-0.56	0.575	
		AG mass	0.05	0.02	2.64	0.009	**
	Needlegrass	PG FM	0.18	0.06	2.93	0.005	**
		AG mass	0.03	0.02	1.30	0.2	
	Bluebunch	PG FM	-0.16	0.04	-4.31	<0.001	***
		AG mass	0.06	0.02	3.31	0.002	**
Duration	All	PG species	-0.43	0.07	-6.25	<0.001	***
		PG FM	-0.32	0.09	-3.55	0.001	**
		AG FM	-0.04	0.03	-1.28	0.203	
		AG mass	0.28	0.04	7.63	<0.001	***
	Needlegrass	PG FM	-0.09	0.13	-0.64	0.524	
		AG mass	0.27	0.05	5.38	<0.001	***
	Bluebunch	PG FM	-0.66	0.09	-7.32	<0.001	***
		AG mass	0.28	0.05	6.25	<0.001	***
Max. temp	All	PG species	-0.26	0.09	-2.96	0.004	**
		PG FM	-0.23	0.12	-2.01	0.047	*
		AG FM	0.03	0.04	0.66	0.509	
		AG mass	-0.06	0.05	-1.23	0.221	
	Needlegrass	PG FM	-0.04	0.16	-0.25	0.806	
		AG mass	-0.12	0.06	-1.92	0.059	
	Bluebunch	PG FM	-0.43	0.15	-2.98	0.004	**
		AG mass	0.05	0.07	0.65	0.518	
Thermal dose	All	PG species	-0.59	0.13	-4.75	<0.001	***
		PG FM	-0.31	0.16	-1.92	0.057	
		AG FM	-0.04	0.06	-0.80	0.425	
		AG mass	0.24	0.07	3.56	0.001	**
	Needlegrass	PG FM	0.00	0.25	-0.01	0.99	
		AG mass	0.21	0.10	2.23	0.029	*
	Bluebunch	PG FM	-0.75	0.15	-5.08	<0.001	***
		AG mass	0.26	0.07	3.50	0.001	**

Figures

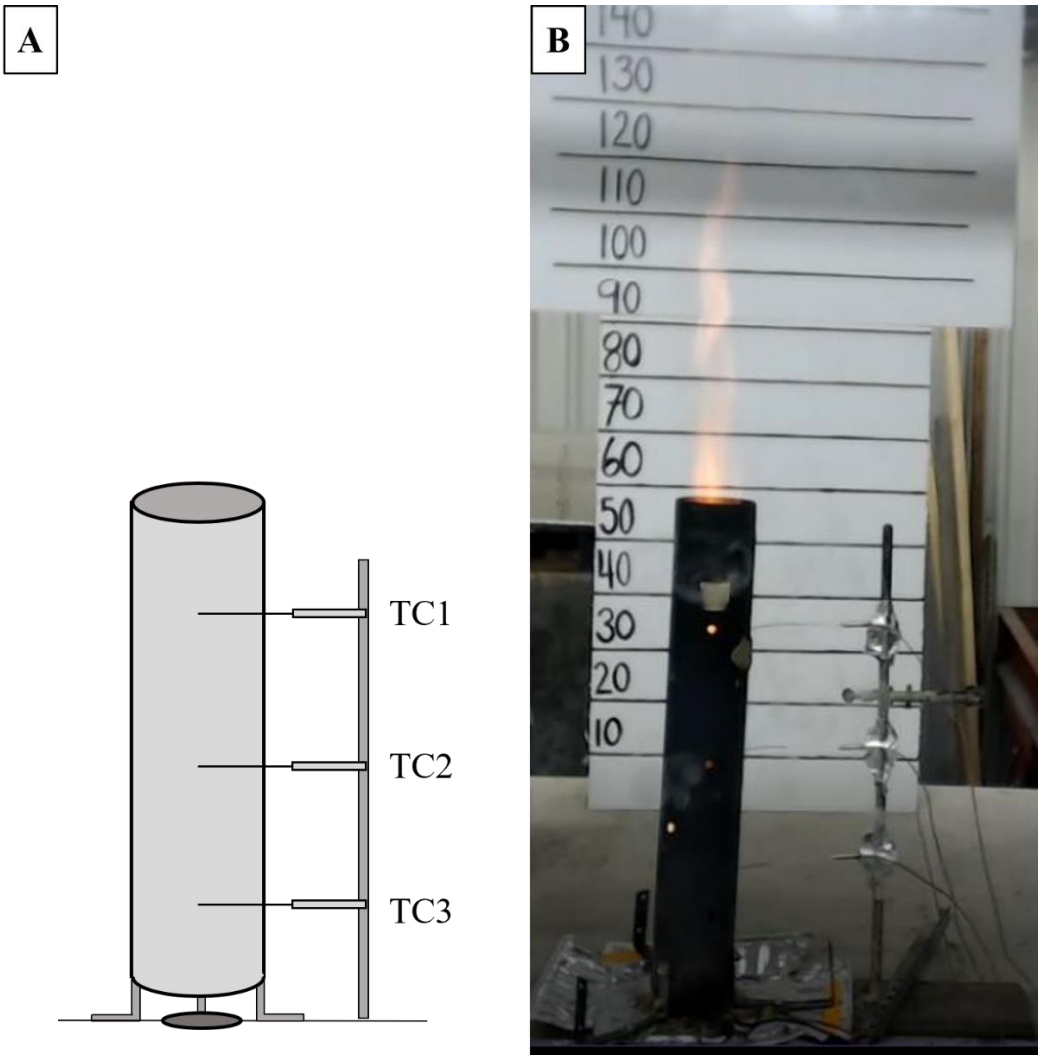

Figure 2.1. Diagram (A) and photo (B) of combustion chamber with three thermocouples (TC). The main chamber is a 10 cm diameter pipe which is raised 2.5 cm off the ground. Thermocouples extend into the chamber at 19, 33, and 48 cm from the base.

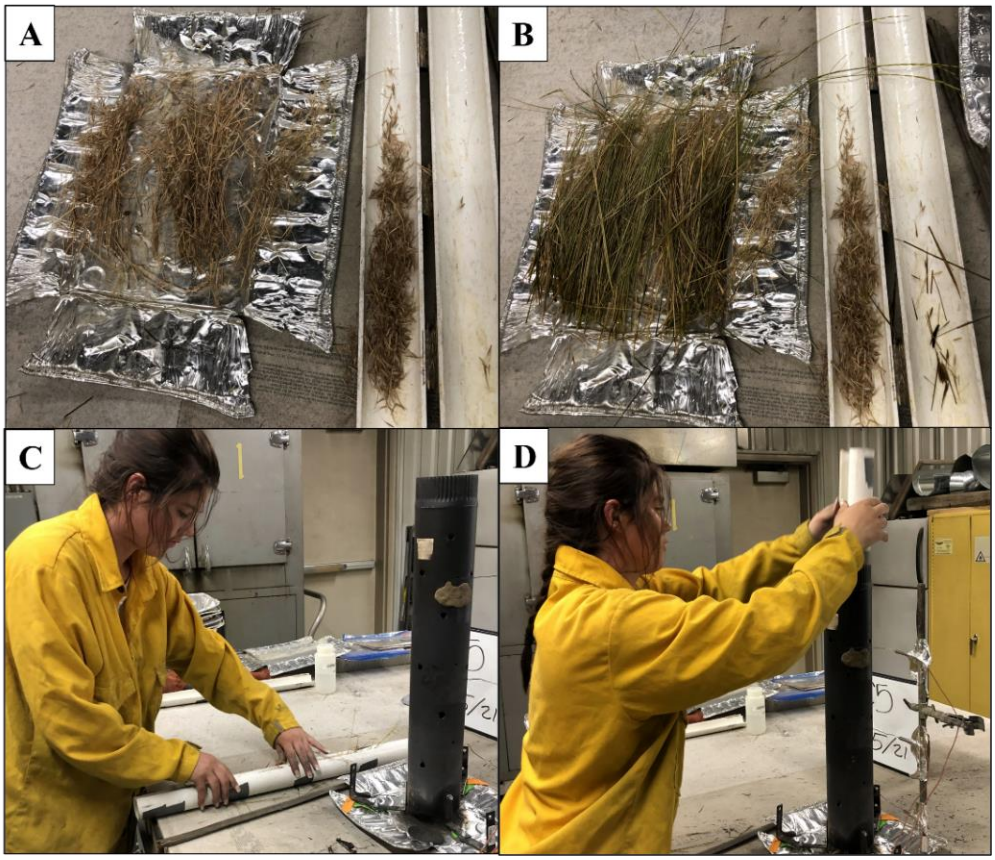

Figure 2.2 Loading plant material into the combustion chamber.
Panels A and B show combining annual (A) and perennial (B) grasses. Panel C and D show vertical sample loading into the combustion chamber.

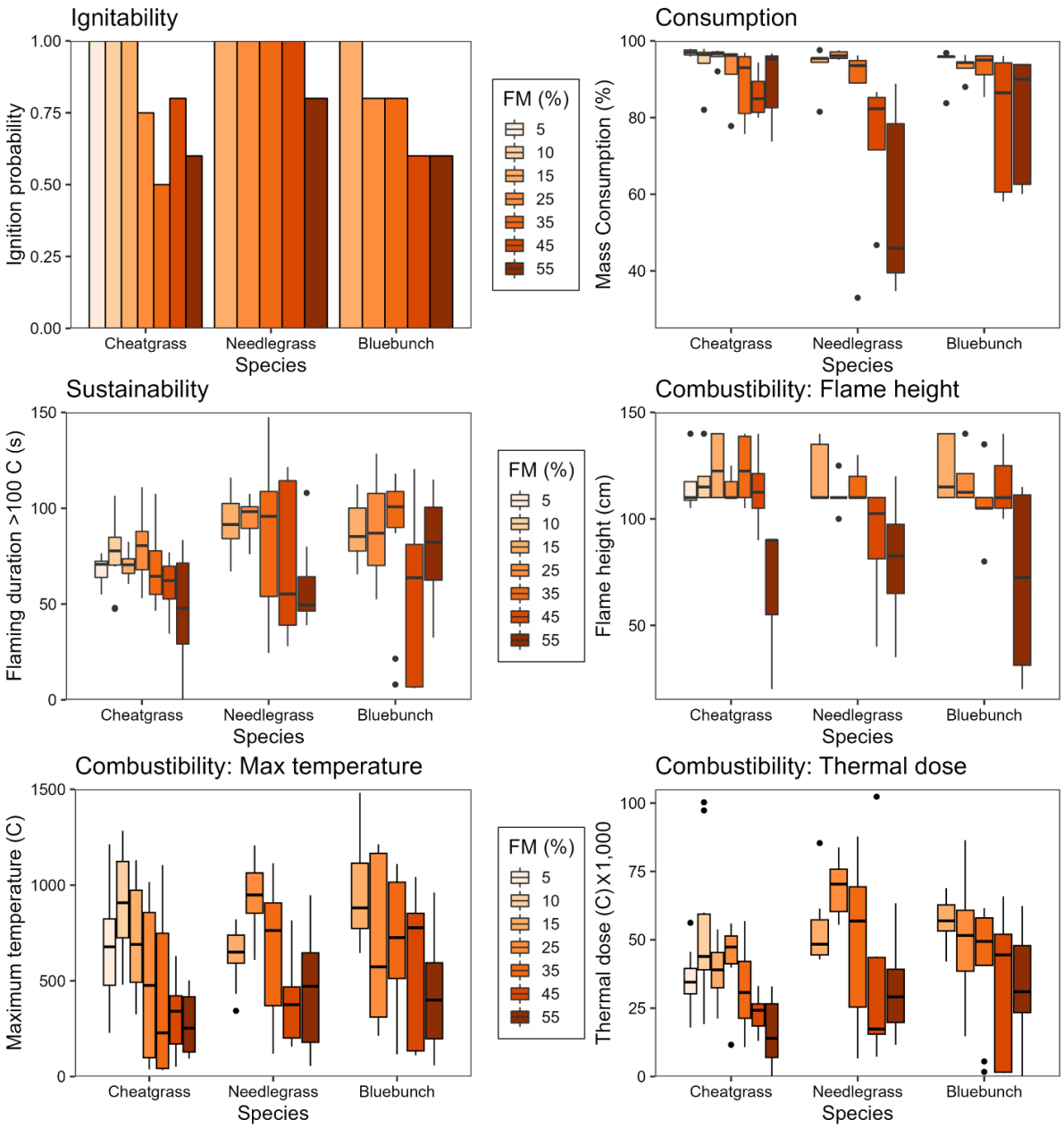

Figure 2.3. Flammability of individual species with increasing fuel moisture (FM).
Across all three species, flammability decreased with increasing fuel moisture. Perennial grass species had lower mass consumption and higher thermal dose and flaming duration than cheatgrass. Columbia needlegrass and bluebunch wheatgrass had the same flammability.

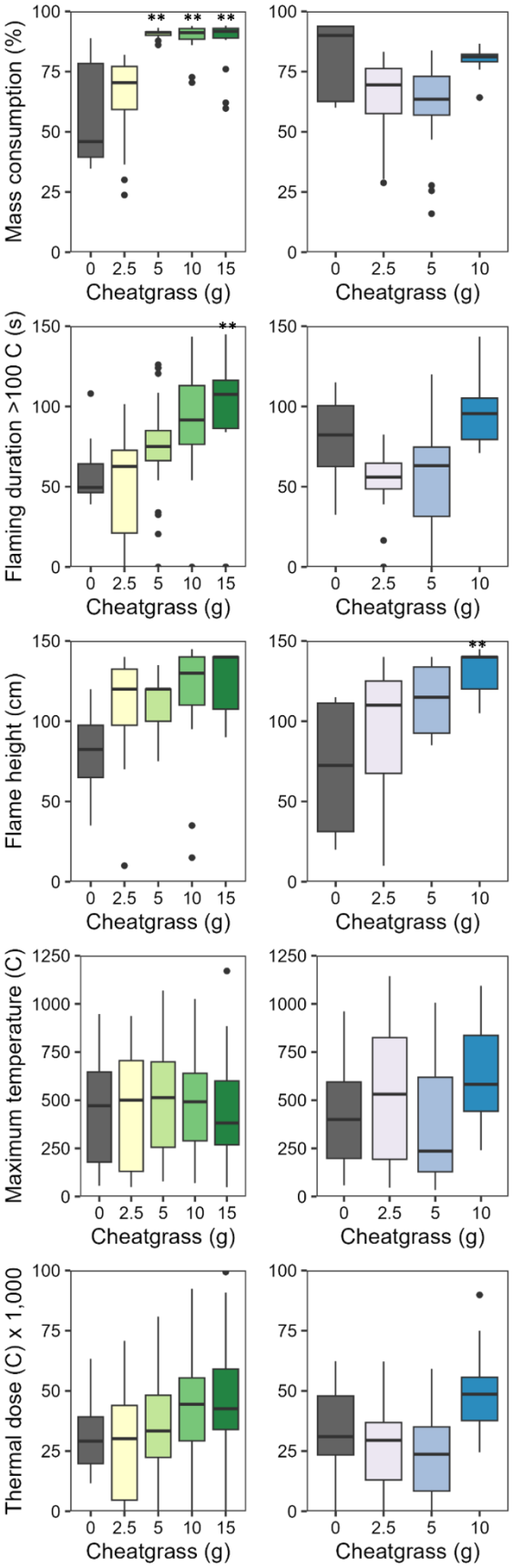

Figure 2.4. Flammability of perennial grasses at 55% FM burned alone (grey boxes) and with increasing amounts of cheatgrass added to the mix. Left column with green boxes is Columbia needlegrass; right column with blue boxes is bluebunch wheatgrass. ** indicates statistical difference from perennials alone. Cheatgrass fuel moisture was non-significant within the evaluated range of moistures, so only differences by cheatgrass mass are displayed.

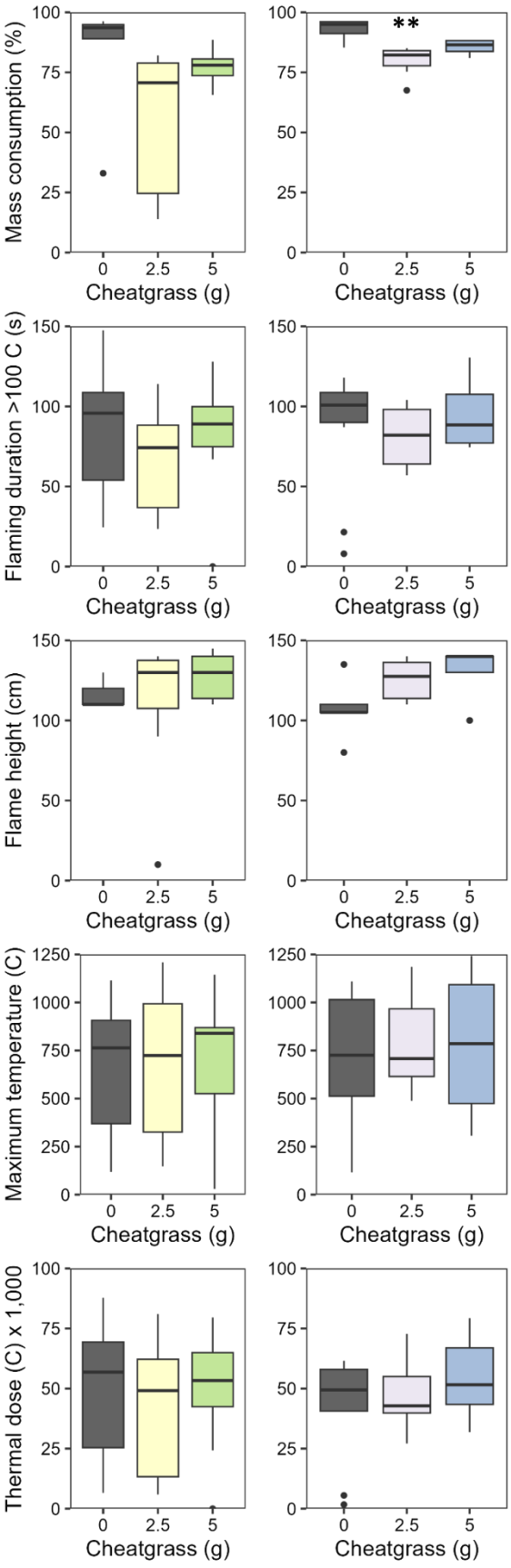

Figure 2.5. Flammability of perennial grasses at 35% FM burned alone (grey boxes) and with increasing amounts of cheatgrass added to the mix. Left column with green boxes is Columbia needlegrass; right column with blue boxes is bluebunch wheatgrass. ** indicates statistical difference from perennials alone. Annual grass fuel moisture was non-significant within the evaluated range, so only differences by annual grass mass are displayed.

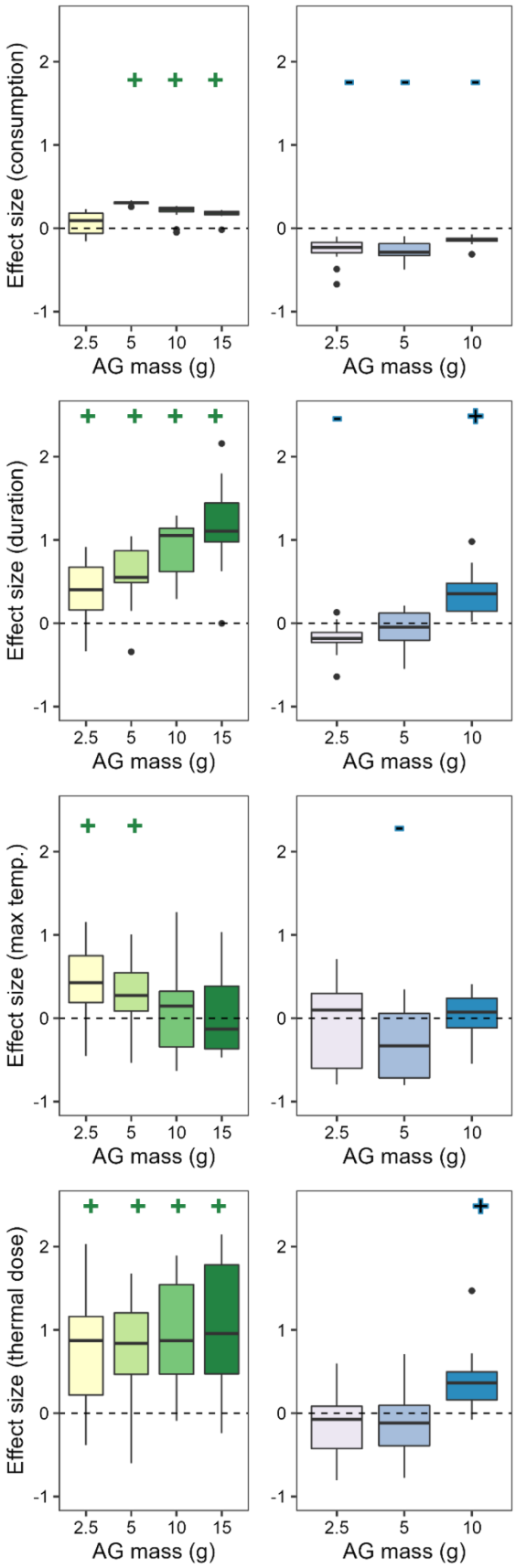

Figure 2.6. Effect size between observed and expected flammability of 55% fuel moisture Columbia needlegrass (green) and bluebunch wheatgrass (blue) with cheatgrass.
Mean effect sizes that do not overlap with 0 (dashed line) indicate the presence of nonadditivity. + or – indicates statistically different from 0 and direction of difference.

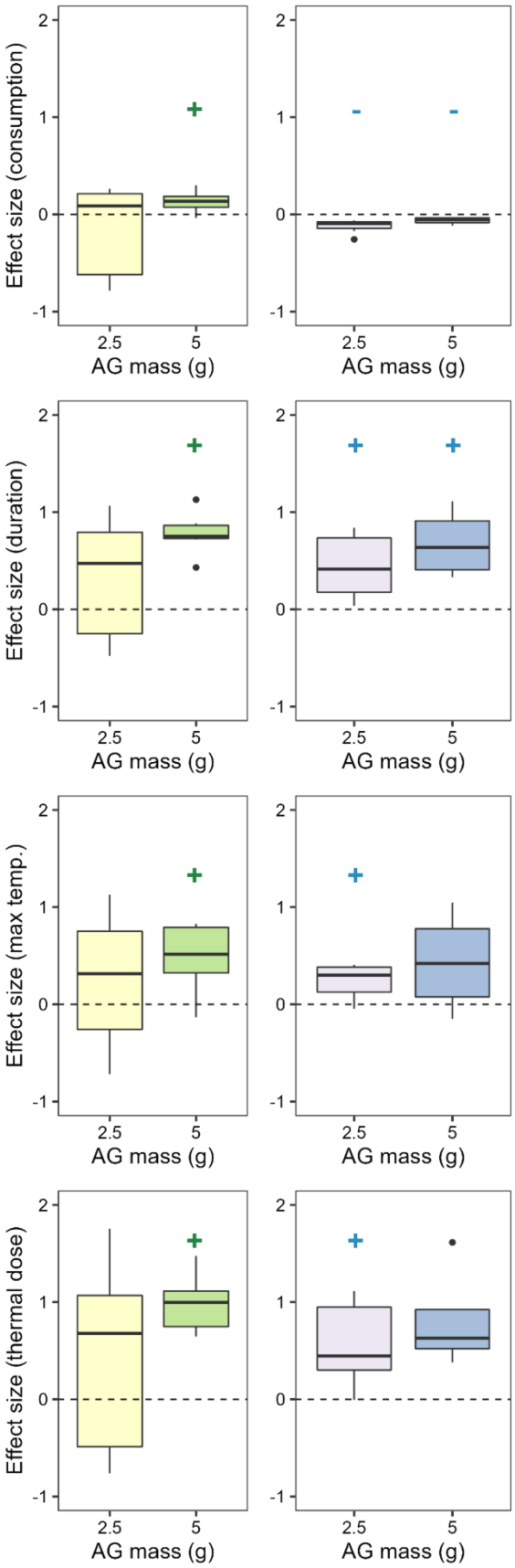

Figure 2.7. Effect size between observed and expected flammability of 35% fuel moisture Columbia needlegrass (green) and bluebunch wheatgrass (blue) with cheatgrass.
Mean effect sizes that do not overlap with 0 indicate the presence of nonaditivity. + or – indicates statistically different from 0 and direction of difference.

Chapter 3: A comparison and development of methods for estimating sagebrush shrub volume using drone imagery-derived point clouds

Abstract

Shrub volume is used to calculate numerous, essential ecological indicators in rangeland ecosystems such as biomass, fuel loading, wildlife habitat, site productivity, and ecosystem structure. Field techniques for biomass estimation, including destructive sampling, ocular estimates, and allometric techniques use shrub height and canopy widths to estimate volume and translate it to biomass with species-specific allometric equations, are tedious, time-consuming, and pose challenges. We compared canopy volume estimates from field-based measurements with drone-collected canopy volume estimates for seven dominant shrub species within mountain big sagebrush (*Artemisia tridentata* subsp. *vaseyana*) plant communities in southern ID, USA. Canopy height and two perpendicular width measurements were taken from 103 shrubs of varying sizes, and volume was estimated using a traditional allometric equation. Overlapping aerial images captured with a DJI Mavic 2 Professional drone were used to create a 3D representation of the study area using structure-from-motion photogrammetry. Each shrub was extracted from the point cloud, and volume was estimated using allometric and volumetric methods. The volumetric method, which involved converting point clouds to raster canopy height models with 2.5 and 5 cm grid cells, outperformed the allometric method ($R^2 > 0.7$), and was more reproducible and robust to user-related variability. Drone-estimated volume best matched field-estimated volume ($R^2 > 0.9$) for three larger species: *A. tridentata* subsp. *tridentata*, *A. tridentata* subsp. *vaseyana*, and *Purshia tridentata*. The volume of smaller shrubs (canopy widths <1 m) was slightly overestimated from drone-based models. We argue that drone-based models provide a suitable alternative to field methods, while having the added benefit of being less time-consuming, with fewer limitations, and more easily scaled to larger study areas than traditional field technique. Finally, we demonstrate a proof of concept for automating canopy volume estimates using point cloud-based automatic shrub detection algorithms. These findings demonstrate that drone-collected images can be used to assess shrub canopy volume for at least five upland sagebrush steppe shrub species and support the integration of drone data-collection into rangeland vegetation monitoring.

Introduction

The sagebrush steppe ecosystem is a semi-arid area in western North America with grassland and high-elevation desert characteristics. However, it is now one of North America's most critically endangered ecosystems due to habitat fragmentation (Anderson and Inouye, 2001; Davies et al.,

2011). Only 56 percent of its original range remains, covering approximately 3 million hectares in the Great Basin region and Columbia Plateau in the United States (Davies et al., 2011; Padgett, 2020). This endangered ecosystem is vital for various wildlife, including the Greater sage-grouse (*Centrocercus urophasianus*), sagebrush sparrow (*Artemisiospiza nevadensis*), and mule deer (*Odocoileus hemionus*). Shrub species composition and size provide valuable ecological information such as wildlife habitat quality, fire risk, ecological state, and site productivity. Monitoring shrub biomass and size is essential to track changes in the sagebrush steppe ecosystem's canopy volume, which informs key ecological indicators such as wildlife habitat and fuel load.

Big sagebrush (*Artemisia tridentata*), a keystone species of the sagebrush-steppe ecosystem, extends further south beyond the sagebrush-steppe into more xeric regions, with more than 350 associated plants identified as being of conservation concern (Davies et al., 2011; Padgett, 2020). Within shrubland ecosystems, shrubs contribute to fire behavior and effects (Sandberg et al., 2001). Invasive grasses, such as cheatgrass (*Bromus tectorum*), alter fuel loading and continuity to a landscape with greater fire spread potential and flammability than the heterogenous mosaic they replace (Ellsworth et al. 2020).

Measuring fuel loading in sagebrush steppe is important because it plays a critical role in determining predicting fire behavior, which is crucial for managing and protecting sagebrush steppe ecosystems (Ellsworth et al., 2022; Germino et al., 2022). Fuel loading refers to the amount and arrangement of live and dead burnable vegetation such as live plants, dead wood, and litter that can ignite and burn during a wildfire (Sandberg et al., 2001). In sagebrush steppe, fuel loading is largely determined by the abundance and structure of shrubs (Ellsworth et al., 2022). Higher shrub fuel loads can result in more intense and severe fires, which can negatively impact wildlife habitat, ecosystem resilience, and threaten human safety and infrastructure (Chambers et al., 2021). Conversely, low fuel loading can lead to a loss of ecological integrity and biodiversity, as many plant and animal species in sagebrush steppe are adapted to fire regimes and depend on live and dead vegetation. Altogether, measuring fuel load in sagebrush shrublands is important for predicting fire behavior, managing invasive species, evaluating management interventions, and protecting wildlife habitat and ecosystem resilience.

Measuring shrub biomass

Numerous techniques are used to estimate shrub biomass and thus fuel loading. Broadly, these methods are either destructive or non-destructive and can be implemented individually or through double sampling. Destructive sampling requires shrubs to be cut at the base, dried in a forced-air oven at 60-70 °C for at least 24-48 hours and weighed (Rittenhouse and Sneva, 1977).

Destructive sampling is the most accurate way to measure biomass and does not require extensive training for observers. However, it is time consuming and laborious, especially if biomass by fuel size is required, and can be difficult to implement in remote areas and with large shrubs.

Non-destructive sampling includes multiple techniques such as relative estimates, percent cover translation, and allometric relationships (Bonham, 2013). Relative estimates involve weighing representative units of a plant (i.e., a branch), and training observers to recognize these "weight units" within the sample area or of an individual shrub (Bonham, 2013). Relative estimates can allow for a larger sample size, but extensive training and skill is required for precise observations (Bonham, 2013). Biomass can also be translated from percent cover values, as implemented by Riccardi et al. (2007) in their guide to characterize wildland fuel beds, though this may not consider the influence of shrub height on fuel bed structure. Percent cover translation techniques are also used to calculate biomass across Long Term Ecological Research sites (Herrick et al., 2017). A primary technique used to non-destructively sample shrub biomass is allometric relationships. Shrub height and two perpendicular longest crown intercepts are measured and converted to canopy volume based on shrub shape, and then translated to biomass via regression equations (Rittenhouse and Sneva, 1977; Ursic et al., 1997). The primary disadvantage of allometric methods is the assumption of consistent shrub shape through time, which can be altered by multiple factors, such as grazing (Karl et al., 2020).

Drones

Drones (unpiloted aerial vehicles) are increasingly being used for remote ecological measurements. The availability of low-cost consumer drones with high-quality imaging sensors makes it possible to collect very-high-resolution imagery easily and inexpensively (Anderson and Gaston, 2013; Westoby et al., 2012). Further, photogrammetric techniques can create high-quality 3-dimensional models and orthomosaics from drone imagery (Westoby et al. 2012).

Several studies have demonstrated the high value of drone-acquired imagery for non-destructive sampling shrub volume or biomass (e. g., Cunliffe et al., 2021, 2016; Gillan et al., 2020; Karl et al., 2020). For example, Cunliffe et al. (2021) estimated above-ground biomass in non-forested ecosystems based on drone-photogrammetry-derived canopy height and compared biomass across plant species. The authors reported canopy height as a strong predictor of above ground biomass across all species (median adjusted $R^2 = 0.87$) with variability of biomass occurring among plant functional types (Cunliffe et al., 2021).

Karl et al. (2020) used two techniques to estimate canopy volume from drone-collected data. The first method was a user-interactive measurement of canopy dimensions using predefined views based on cardinal directions and the second method used the height of each point on the topmost layer of the point cloud and calculated the volume under the topmost layer. However, these methods

consistently underestimated canopy volume due to obstruction of ground surface elevation from underneath the dense vegetation caused by the sensor's overhead vantage point and inability to see through plant canopies (Cao et al., 2019). Since vegetation height is calculated from ground surface elevation, accuracy in detecting ground surface elevation must first be verified by comparing drone results with field measurements.

Previous studies clearly demonstrate drone-based methods as a viable approach to estimate shrub volume. Both land managers and researchers require cost-effective methods to monitor canopy volume across the broader sagebrush shrublands. However, there is currently a lack of studies assessing the utility of drone-based measurements specifically for species-specific measurements of shrubs in upland sagebrush shrublands. Therefore, it remains uncertain which methodology is superior and more useful for different shrub species.

The objective of this paper was to assess the suitability of surveying shrub volume of upland sagebrush shrublands using drones compared with *in situ* measurements. Specifically, we compared allometric and volumetric methods of measuring shrub volume from point clouds to traditional field-based measurements. Secondarily, we examined how the accuracy of point cloud-based methods may differ among the eight species in our study in terms of variation in size of individuals. Finally, we considered techniques to automate shrub volume estimates across a subset of the study area using crown detection algorithms.

Methods

Study Area

This study was conducted at the University of Idaho's Rinker Rock Creek Ranch in southern Idaho (43.4139 °N, 114.3946 °W, Fig. 3.1). The 9-ha study area was located on the south end of the ranch and was selected due to abundance of multiple shrub species, and accessibility for drone flights and field measurements.

Field measurements of canopy size

Eight species of shrubs from upland sagebrush shrublands were included in this study: low sagebrush (*Artemisia arbuscula*), basin big sagebrush (*Artemisia tridentata* subsp. *tridentata*), mountain big sagebrush (*Artemisia tridentata* subsp. *vaseyana*), Wyoming big sagebrush (*Artemisia tridentata* subsp. *wyomingensis*), yellow rabbitbrush (*Chrysothamnus viscidiflorus*), rubber rabbitbrush (*Ericameria nauseosa*), antelope bitterbrush (*Purshia tridentata*), and spineless horsebrush (*Tetradymia canescens*). 2 - 15 individuals of each shrub species were identified within the study area, for a total of 105 shrubs (Table 3.1). Individuals were selected to represent the range of sizes for each species observed at the site. Only two individuals of *A. tridentata* subsp. *tridentata* were sampled due to limited abundance at the site.

Two individuals, both *P. tridentata*, were larger than all other samples with field measured volumes of 7.94 and 7.27 m^3. We performed a z-test for outliers and both shrubs were significant outliers (z-scores = 6.21 and 6.81, respectively). As such, these two individuals were removed from further analysis, and summary statistics are reported with and without these two individuals in Table 3.1.

Upon selection, shrubs were marked with plastic flagging tape and assigned a unique identifying number. Tallest height and two perpendicular canopy widths for each shrub were measured to the nearest whole centimeter using a 2-m ruler (Fig. 3.2).

From height and canopy widths, canopy volume was calculated for each individual shrub. First, following Karl et al. (2020), canopy volume was calculated using the equation [3.1] for an ellipsoid modified by Thorne et al. (2002):

Equation 3.1. Modified volume of an ellipsoid

$$V = \frac{2}{3}\,\pi * H * \frac{D_1 * D_2}{2}$$

where H is shrub height, D_1 is the longest canopy diameter, and D_2 is the longest diameter perpendicular to D_1 (Fig. 3.2). However, initial data exploration indicated a poor fit between field and drone-based measurements, therefore an alternative shape for volume calculation was considered for this project. Following the Bourne & Bunting (2011b) guide for characterizing fuels in sagebrush steppe and juniper woodlands of the Great Basin, canopy volume was then calculated using the equation for volume of a frustrum (a truncated pyramid) [3.2],

Equation 3.2. Volume of a frustrum

$$V = \frac{\pi}{6}\,H * D_1 * D_2.$$

To prepare for drone flights and improve model accuracy at predicting ground elevation and thus plant height (see Karl et al. 2020), vegetation at the base of each shrub was removed. Point locations surrounding each individual shrub (four corners) were collected using an Emlid Reach RS+ real-time kinematic geographic navigation satellite system (RTK-GNSS) (absolute accuracy < 4cm, Emlid, https://emlid.com), to aid in identification of each shrub in final image products.

Image Acquisition

Drone flights took place on June 27, 2022. The imaged area was established in the field, and a double-overlap grid pattern consisting of parallel flight lines in north-south and east-west directions was created. We flew a DJI Mavic 2 Pro drone with a 20-megapixel RGB camera 50 meters above ground level. Images collected during drone flights had at least 80% endlap and sidelap. This drone flight resulted in 1,302 images.

Seventeen ground control points (GCPs) were placed throughout the study area to improve model building, point cloud and orthomosaic accuracy and scaling, and identification of shrubs in the point clouds and orthomosaics. Precise location (absolute accuracy < 4cm) of each marker was recorded using the Emlid Reach RS+ RTK-GNSS. All RTK-GNSS points (one for each GCPs and four for each shrub) were post-processed using rover and base tracking within Emlid Studio version 1.3 (https://docs.emlid.com/emlid-studio) for point correction.

Photo processing and model building

The photos collected from the drone were used to produce a point cloud, digital elevation model, and orthomosaic using structure-from-motion (SfM) photogrammetry in Agisoft Metashape Professional (version 1.8.4 build 14671; herein referred to as 'Metashape'). A SfM-based approach allows for the creation of a stereo model that represents the orientation and location of the drone camera for every collected photo and a 3-dimensional (3D) model of the area photographed (Westoby et al., 2012). The photo processing workflow in Metashape followed methods outlined by James et al. (2017) and implemented by Karl et al. (2020). All 1,302 photos were imported and aligned with Metashape's highest accuracy setting and a maximum of 40,000 key points and 6,000 tie points per image.

The post-processed locations of the GCPs were imported into Metashape as markers for geolocation and scaling of the stereo model. Marker locations were identified and manually adjusted for at least 20 photos per marker. Stereo model alignment parameters were re-optimized with adaptive model fitting and tie point covariance estimations based on the manually assigned marker locations. The sparse cloud representing the tie point locations was then optimized using the 'gradual selection' tool in Metashape to select and remove low-quality tie points followed by re-optimization of the photo bundle-block following techniques outlined by James et al. (2017). Marker corrections and sparse point cloud optimization reduced positional errors in X, Y, and Z from 1.03, 1.06, and 2.19 to 0.04, 0.03, and 0.47 m respectively, and reduced the total positional error from 2.64 to 0.48 m (Table 3.2).

After model optimization, a dense point cloud was generated in Metashape using the optimized sparse point cloud as the base model with 'high' quality and 'mild' point filtering options. The dense cloud contained over 311 million points (~2,020 points/m^2). A digital elevation model (DEM) was created based on the dense point cloud with a resolution of 2.22 cm/pix, and an orthomosaic was generated based on the DEM product.

The orthomosaic generated from Metashape was displayed in ArcGIS Pro (V 3.0.2, ESRI, Redlands, CA; herein referred to as 'ArcGIS') using NAD83 / UTM zone 11N coordinate reference system (EPSG:26911). The post-processed locations representing the four points surrounding each

shrub were also imported onto ArcGIS. These points were used as guides to manually digitize areas of interest (AOIs) around each shrub (Fig. 3.3). Once all the sampled sample shrub boundaries were manually digitized, a polygon feature class containing a total of 105 AOIs (individual polygons) was exported as a shapefile.

Canopy estimates from point clouds

The dense point cloud generated from Metashape and AOI polygons were imported into RStudio (R Core Team, 2023) using the '*lidR'* package (Roussel et al., 2020, 2022a). The shapefile with polygons created in ArcGIS was imported using the '*sf"* package (Pebesma, 2018). The point cloud was clipped to polygons resulting in a unique point cloud for each field-measured shrub using package '*lidR'* (Roussel et al., 2020, 2022a). The result was a unique point cloud for each field-measured shrub.

The clipped point cloud profiles of individual shrubs were imported into CloudCompare (version 2.12.4, http://www.cloudcompare.org/, accessed September 2022) for volume estimations. Two distinct methods were used to estimate shrub canopy volume: allometric and volumetric.

The allometric method replicates the field method by calculating canopy volume from user-measured height and canopy widths. To measure height and width, distances between points were measured for each shrub using the CloudCompare XY distance tool (Fig. 3.4a). First, the height of the shrub was estimated by measuring the distance from the lowest point to the highest point on the point cloud profile (Fig. 3.4b). We used two allometric methods to estimate canopy widths: 'CC-snap' and 'Top-down'. The 'CC-snap' method followed Karl et al. (2020), where the orientation functions in CloudCompare were used to 'snap' point cloud data sets to pre-defined views (i.e., viewing the shrubs from the side via a south-facing direction and east-facing direction). Distances between points for the 'CC-snap' method were measured at the widest part of the point cloud profile of the shrub assessed on-screen by the technician (Fig. 3.4d). The 'top-down' method attempted to closely mimic the field-based measurements, where a top-down view was used as the fixed perspective in CloudCompare and the observer measured the longest canopy width (D_1, Fig. 3.4c) and width perpendicular to D_1 (D_2, Fig. 3.4c). Shrub canopy volumes for each allometric method were calculated using equation [2].

Volumetric methods used a generalized raster surface model of each shrub created by overlaying a grid on the point cloud and calculating shrub either mean or maximum height of each grid cell based on difference between the shrub model elevations and a fixed elevation (Karl et al., 2020). The fixed elevation value for each model was set to the minimum elevation (i.e., ground) of the point cloud data set of each shrub. Volume was estimated using two different cell dimensions (one side of each cell either 0.05m or 0.025m) and two height rules (average point height or maximum

point height within each cell). Volumetric analysis was completed with CloudCompare using the 2.5D volume tool.

Statistical analysis

Statistical analysis was performed in R (version 4.0.3; R Core Team, 2021). Ordinary least-squares regression was used to compare field and drone-based estimates of shrub volume shrub height, and canopy widths. R^2 and slope values were used to compare different CloudCompare techniques to estimated volume and canopy width. We examined these trends across all species sampled, but also within each species to assess suitability of drone techniques for multiple upland sagebrush steppe shrub species across the range of size variability within each species. Based on fundings by Karl et al. (2020), we expected that drone-based measurements of shrub canopy volume may be underestimated compared to field measurements, but still strongly correlated. Further, regression estimators could be used to estimate point cloud measurements with limited field data if there is a consistent relationship between field and drone estimates, and thus they will be reported here.

Individual shrub detection

We relied on field-placed GCPs to locate and then extract each shrub within the point-cloud scene. We performed analyses on a subset of shrubs within the landscape which represented the size range of shrubs present at the site. These techniques provided us with the ability to compare field and drone-based measurements but could limit application when scaled-up to larger areas or integrated in larger monitoring programs. To address this limitation, we tested the potential use of raster and point cloud-based automatic individual shrub detection (ISD) algorithms derived from tree detection algorithms (Fig. 3.5).

Structure-from-motion -derived point cloud data are commonly used in drone-based remote sensing of forests to derive height information such as digital terrain model (DTM, bare earth elevation), digital surface model (DSM, surface elevation of features in scene), and canopy height model (CHM, canopy elevation) (Ecke et al., 2022). These products can then be used as input for individual tree detection and tree crown delineation algorithms for forest remote sensing applications (Duarte et al., 2022; Guimarães et al., 2020). To test the utility of these techniques with shrubs, we produced a DTM, DSM, and CHM from the subset point cloud data set (230 m^2) and to perform automated shrub detection and delineation by modifying parameters of the tree detection and crown delineation algorithms.

We tested two raster-based ISD algorithms and one point cloud-based ISD algorithm. The raster-based ISD algorithms closely followed steps outlined by Mohan et al. (2021) and used the '*lidR'* (Roussel et al., 2022b) and '*ForestTools'* (Plowright and Roussel, 2021) R packages. The first

raster-based ISD algorithm used a fixed window local maximum filter (herein referred to as 'LMF' method). The LMF method is a common tree detection algorithm used for automatic tree detection in forest remote sensing (Duarte et al., 2022; Ecke et al., 2022; Guimarães et al., 2020). The second raster-based ISD algorithm used a variable window local maximum filter (herein referred to as 'VWF' method, Fig. 3.5a and Fig. 3.5b) following Young et al. (2022) on optimal drone mission parameters for individual tree detection. The point cloud-based ISD algorithm used the '*segment_trees*' function from the '*lidR*' package (Roussel et al., 2022b) with the point cloud segmentation algorithm set as '*li2012*' from Li et al. (2012) (Fig. 3.5c and Fig. 3.5d). This function performs a direct point cloud segmentation and returns point cloud data set where each point has a 'treeID' attribute, points with the same 'treeID' attribute are segmented points for a distinct object, which is in this case a distinct shrub. The most important parameter adjusted for all three algorithms was the default minimum height for object detection. These algorithms were designed to detect trees that are taller than shrubs. Hence, the minimum height threshold was changed from 2 meters (default) to 0.10 meters for all three algorithms. R code for all three methods is available in a public github repository: https://github.com/gharrison159/UAVShrubVolume.

Results

All six point-cloud volume estimation techniques showed strong relationships between field- and point-cloud-estimated volume (Fig. 3.6). Among the two allometric methods, the CC-snap method outperformed the top-down method, by having both a better model fit (R^2 = 0.77 vs 0.74; Mean Square Error (MSE) = 0.0671 vs 0.0559) and slope closer to 1 (slope = 1 vs 0.88; Fig. 3.6).

Canopy widths and height as measured with the two allometric methods can be directly compared to field measurements. CloudCompare estimates of height had good model fit to field measurements (R^2 = 0.87) but were slightly and consistently underestimated (slope = 0.91; Fig. 3.7). Model fit varied by shrub height. Shorter shrubs (field height <1m) had decreased model fit (R^2 = 0.81), but slope improved (slope = 0.96) compared to the model for all individuals, suggesting underestimation was greater for taller shrubs (Fig. 3.7). CloudCompare allometric techniques better fit field measurements of D_1 (longest diameter) than D_2 (perpendicular to longest diameter; Fig. 3.8). This difference suggests that field and CloudCompare techniques for identifying and measuring D_1 are more similar than those for D_2, potentially due to challenges to accurately identify perpendicularity to D_1 in the field. Within canopy width measurements, measurements of shrub canopy widths differed by CloudCompare allometric technique (Fig. 3.8). The top-down method was better correlated to field measurements of D_1 than CC-snap (R^2 = 0.75 vs 0.72; Fig. 3.8). Across both techniques, shrub widths <1 m were overestimated, and >1 m were underestimated (Fig. 3.8). Model fit for allometric methods improved when only considering smaller shrubs (field volume < $1m^3$, 93%

of individuals), suggesting that these methods are more consistent for smaller shrubs (Supplemental Information 3.1).

Among the volumetric techniques, all four iterations of the 2.5D method had similar and good model fit (R^2 range = 0.73 – 0.78; MSE range = 0.0501 – 0.06; Fig. 3.6). All but one (5 cm grid cells using maximum cell rule) of the 2.5D methods overestimated volume for shrubs <1 m^3, but underestimated volume for larger shrubs (Fig. 3.6). Volumetric methods with 2.5 cm cell dimensions had lower slopes than those from 5 cm grid dimensions, suggesting that a smaller cell size underestimated volume (Fig. 3.6. Within each cell dimensions, maximum cell rules yielded better model fit and slopes closer to 1 (Fig. 3.6). With volumetric techniques, maximum values from 5 cm grid cells performed best in terms of both R^2 (0.78), MSE (0.0591), and slope (1; Fig. 3.6). Model fit for volumetric methods decreased when only considering smaller shrubs (field volume < 1m^3, 93% of individuals), suggesting these methods provide more variable estimates for smaller shrubs (Supplemental Information 3.1).

Model fit by volume technique varied by species (Table 3.3, Supplemental Information 3.2). In general, all point cloud estimates were best (in terms of R^2, MSE, and slope) for larger shrub species: *A. tridentata* subsp. *vaseyana*, *A. tridentata* subsp. *wyomingensis*, and *P. tridentata* (R^2 for volumetric techniques ≥ 0.92, MSE ≥ 0.02; Table 3.3). Model fit for all six techniques was also good for *E. nauseosa* (R^2 = 0.82-0.86; MSE = 0.01 – 0.018; Table 3.3). Model fit for *T. canescens* was good, but best for allometric methods (R^2 = 0.71-0.74 and 0.84-0.87 for volumetric and allometric methods, respectively; MSE < 0.001; Table 3.3). Model fit was poorest for C. *viscidiflorus*, the smallest shrub species (maximum R^2 = 0.08, MSE = 0.15 – 0.34; Table 3.3). Model fit for *A. arbuscula* was poor for all volumetric techniques (maximum R^2 = 0.19l; minimum MSE = 0.167) but moderate for allometric techniques (R^2 = 0.78 and 0.53; minimum MSE = 0.001; Table 3.3).

Results from the error matrix and assessment metrics of the ISD algorithms (Supplementary Information 3.3) show the point cloud-based ISD method performed better (overall accuracy (OA) of 76.7%) than the raster-based ISD methods (OA for VWF = 73.3%, LMF = 70.0%). The omission error for detecting shrubs with the point cloud-based ISD method was 7.0% and the commission error was 25.0%.

Discussion

Our results demonstrate measurements of upland sagebrush shrub species canopy volume from drone point clouds are a viable approach when compared with field-based estimates. We outlined non-destructive methods to consistently measure shrub canopy volume, which could be integrated into current rangeland monitoring programs (Gillan et al., 2020). This research improves

upon techniques used by Cunliffe et al. (2021) and Karl et al. (2020) by sampling additional species and considering different techniques to measure point cloud canopy volume.

Our results provide evidence for the suitability of measuring shrub canopy volume from drone point clouds for at least five upland sagebrush steppe shrubs: *A. tridentata* subsp. *tridentata*, *A. tridentata* subsp. *wyomingensis*, *E. nauseosa*, *P. tridentata*, and *T. canescens*. For these species, volume from drone point clouds was most like field-based measurements. Three of those five species, *A. tridentata* subsp. *vaseyana*, *A. tridentata* subsp. *wyomingensis*, and *P. tridentata*, are dominant at the study site and constitute significant proportions of woody fuel in sagebrush steppe ecosystems (Bourne and Bunting 2011b). Drone point cloud methods were less suitable to measure volume of two relatively small shrub species C. *viscidiflorus* and *A. arbuscula*. However, there was some variability in method suitability for in *A. arbuscula* as allometric methods were suitable, but volumetric methods were not.

One technique to potentially mitigate poor model fit for these smaller species is to consider alternate shapes for volume equations. To test if fit between field and point-cloud estimates could be improved especially for smaller species, we examined the results if volume (from field and allometric methods) was calculating using the equation for the volume of a cylinder [3.3],

Equation 3.3 Volume of a cylinder

$$V = \pi * H * maximum(D_1, D_2)^2,$$

Where radius is the greater measurement between D_1 and D_2. Using a cylinder resulted in minor improvements of R2 and MSE for C. *viscidiflorus* (ΔR^2 range from frustrum to cylinder = 0.068 – 0.175; ΔMSE range = -0.0004 – -0.0001). Similarly, model fit was marginally improved for volumetric methods of *A. arbuscula* (ΔR^2 range from frustrum to cylinder = 0.022 – 0.024; ΔMSE = -0.0058 – -0.0049). Through there were some improvements in model fit with this alternative shape, but model fit was poorer than that of suitable species using the original frustrum shape equation.

Suitability of allometric and volumetric methods differed by shrub size. Within allometric methods, drone-based techniques overestimated D_1 and D_2 for smaller shrubs (D_1 or D_2 <1 m). Smaller shrubs represented a majority of our sampling dataset (73% of shrubs had field measured D_1 <1m; 81% for D_2) due to our inclusion of multiple shrub species and attempts to sample across each species' size range. For shrubs with field-measured widths greater than 1m, point cloud estimates of width were more variable, and neither were consistently over nor underestimated. Karl et al. (2020) implemented similar methods to estimate willow (*Salix* spp.) canopy volume from drone derived point clouds. However, they did not observe any bias based on size classes, which could be because the shrubs they studied were distributed more evenly across a wider size range, less variable, and

generally larger in size (Karl et al. 2020). Finally, for the ‘top-down’ allometric technique, it is worth mentioning that this technique does not require the 3-D rendering of point cloud data on CloudCompare and could be executed using a 2-D (point-cloud derived) orthomosaic imagery on other image analysis or geospatial software.

Allometric and volumetric methods can vary in their repeatability. Allometric methods require high amounts of user interaction and time, and we (similar to Karl et al. 2020) aimed to standardize these measurements using fixed views (CC-snap method). Volumetric methods, however, required relatively low amounts of manual interaction to obtain measurements and have the potential to be more easily standardized. Volumetric techniques were simpler and less time consuming to perform and would have less bias toward technician error or differences in judgement. Additionally, volumetric methods can be automated using a scripting-based approach (e.g., Greaves et al. (2015)).

We observed systematic model underestimation of shrub volume using point-cloud models. Karl et al. (2020) observed a similar trend and noted underestimation was likely due to dense vegetation obstructing bare ground and impeding the ability to model ground height. Understory vegetation height, especially when completely obstructing the ground surface, can be adjusted for in the model but may create additional variability in height estimates (see Karl et al. 2020). We suspect that the abundance of bare ground and deliberate vegetation removal around shrubs prior to drone data collection may have contributed to our improved accuracy in estimating height. However, previous studies (Cunliffe et al., 2021) did not remove vegetation and still obtained highly accurate estimates of shrub biomass in semi-arid systems where some bare ground was present. Therefore, we do not believe that vegetation removal at the base of shrubs is necessary for all applications of these methods.

Further, it is important to consider how field methods may or may not translate to point cloud measurements and potentially lead to underestimation. In the field, canopy height and diameter are both measured along the greatest perennial, live plane of a shrub, which could be an individual branch depending on the shrub (Bourne and Bunting 2011b, Bonham 2013). Points within the point cloud for that individual branch could be sparser or potentially even removed during the quality control and point filtering processes during model building. This means that estimates for that individual branch may not be included for both allometric and volumetric methods, and potentially contribute to underestimation compared to field estimates.

Our analysis focused on comparing point cloud and field measurements, but these are both estimates, and are indirect measures of volume. Field measurements are based on assumptions of canopy shape (in this case, a frustrum). This assumption confers inherent limitations, such as the top of each shrub is flat, the top is the maximum width, and there are no gaps within the canopy. Our

allometric methods were also subject to these same assumptions. Volumetric methods were only partially limited as they allowed for differential heights but did not take into account gaps or decreases in canopy width throughout the plant. One potential benefit of point cloud data is the ability to adjust the classification and calculation methods to those which have assumptions which are suitable for the analysis scenario. For example, another approach which could address some of these shape-based limitations is the voxel-counting method implemented by Greaves et al. (2015). Voxel-based approaches increment biomass into voxels, which are cubic volumes of space, or 3D pixels, and then calculate volume by counting the number of voxels for each shrub or across the region of interest. Voxel-counting methods may better account for canopy openings, but can be computationally more intensive than the methods we implemented (Greaves et al., 2015). Overall, it is important to consider assumptions and limitations of indirect measurements, especially those of field-based data, and drones may allow for greater flexibility in selecting an appropriate method with acceptable limitations.

An additional component of the study by Karl et al. (2020) was a cost-comparison of time spent on field measurements versus processing time of drone data for estimating canopy volumes. The study reported that collection of field measurements took more time (approximately 10 hours per sampling event for field-based measurements compared to about four hours per sampling event for drone-based estimates) than the photogrammetric estimations via drone data (Karl et al., 2020). While our study did not explicitly track time, similar outcomes can be inferred since the same model building methods were employed. Although the addition of GCPs added approximately one hour of time in the field (placing markers and recording RTK GNSS locations) and one hour of additional processing time (to identify marker locations in photos and rebuild models) in the lab, these points increased model accuracy and therefore were key to overlaying images/models over time in the same monitoring location.

Drones could also provide time savings if used in a double sampling technique. Double sampling requires that attributes be measured for all individuals using one technique, and a subset to be re-measured using a different technique (Karl et al., 2014). The sub-sampled method is generally more time and labor intensive but provides higher accuracy. A relationship between the sampling techniques methods is generated using linear regression analysis, and the fit or ability for the model to predict further outputs must be verified using reserved or new data (Karl et al., 2014). Although our study did not entail subsampling, such techniques could be implemented using drone estimates of shrub volume. Site and/or species-specific relationship could be derived to improve accuracy of drone-collected data, while maintaining the added benefit of increasing sample distribution with drones.

Semi-automated landscape-level surveys could supplement current field-based monitoring of shrub canopy volume-based metrics and increase reproducibility across spatial and temporal scales. Visual assessment of the point cloud segmentation results indicates a better individual shrub delineation for larger, taller shrubs than small ones. From these results we suggest that this workflow might be useful as an initial first pass before a technician can perform on-screen assessment and digitization, and overall increase efficiency of the process. For example, in this scenario, the use of an automatic individual shrub detection algorithm detected 75% of all shrubs with 93% accuracy, which could result in around 70% less digitization needed by technicians. These methods could also increase reproducibility across both spatial and temporal scales. Additionally, this automatic crown detection workflow provides an added benefit for estimating shrub canopy volume across a site. The volume of each shrub can be aggregated across the scale of interest and then translated to informative ecological metrics, such as fuel load, carbon stock estimation or total above ground biomass. The integration of individual shrub detection and subsequent point cloud-based volume estimates can be used to perform semi-automated landscape-level surveys, and could augment current field-based monitoring of shrub canopy volume-based metrics.

As the point cloud-based ISD method operates on an individual point level, the algorithm took a longer time to execute than the raster-based methods (approximately 427 times slower; approximately 6.5 min total runtime for the direct point-cloud segmentation method vs 0.9 sec for VWF and LMF methods). One way to increase the efficiency of the point cloud-based ISD method is by filtering all ground classified points and implementing the algorithm on only non-ground classified points. In our case, filtering out ground classified points resulted in a decrease in runtime from 6.5 minutes to 1.5 minutes. Among the raster-based methods, the VWF algorithm performed slightly better with a higher overall accuracy compared to the LMF algorithm for detecting shrubs. Furthermore, as parameters for the VWF algorithm can be fine-tuned, and our initial results indicate that the VWF algorithm is a better raster-based option.

An alternative method to using drone-photogrammetry-derived point clouds would be to use an active sensor, such as a light detection and ranging (LiDAR) sensor. A recent study by Zhao et al. (2021) used drone-acquired multispectral and LiDAR data for shrub above ground biomass estimations. The study identified shrubs by thresholding their spectral signatures and used the height data from the LiDAR sensor to derive canopy heights for volumetric estimation (Zhao et al., 2021). The shrub volume estimates were used in predictive regression models, where Zhao et al. (2021) reported a promising R^2 of 0.86 and RMSE of 101.97 g.

The cost of purchasing and maintaining a LiDAR sensor remains relatively prohibitively high compared to an RGB camera similar to the one used in this study (Prošek and Šímová, 2019). Additionally, the acquisition of a LiDAR system would require the availability of a larger drone due to the sensor's larger weight, further increasing the cost (Karl et al., 2020). Therefore, using drone-photogrammetry derived data might be appropriate from a cost-benefit perspective when a program aims to assess vegetation over large spatial extents with intermediate volume estimation accuracy. Moreover, the use of LiDAR data does not necessarily guarantee increased accuracy. In Zhao et al. (2021), the multispectral only model performed similarly to the multispectral and LiDAR combined model, and better than the LiDAR only model, demonstrating that simply adding LiDAR data may not increase the accuracy and performance relative to the increased cost and complexity of the instrument.

Drones offer comparable data products at a fractional cost of similar LiDAR outputs. Research by Olsoy (2014) explored the potential of terrestrial laser scanning (TLS), or ground-based LiDAR, in the same southern Idaho sagebrush ecosystem. In this study, sagebrush biomass was estimated from TLS-derived volume to detect seasonal variations in biomass. While TLS results are more accurate than those of airborne laser scanning (ALS) by way of generating denser point clouds, TLS instruments are bound to the same constraints as traditional field sampling in terms of site access and relative spatial coverage.

Management Implications

This study is part of a growing collection of research in drone-based vegetation measurements that adds common sagebrush shrubland species to the species directory for drone methods (Cunliffe et al., 2021). Drone-imagery methods for rangeland monitoring have the potential to supplement or potentially replace field methods in some but not all instances (Gillan et al., 2020; Laliberte et al., 2011, 2010; Rango et al., 2009). Drone-based methods may also allow managers to estimate metrics not measurable from the ground and at sampling frequencies and extents not currently feasible, such as bare ground cover immediately post-wildfire or 3-D representations of canopy gaps (Gillan et al., 2020). Further refinements may be needed to develop methods for measuring low-stature species that showed lower accuracy in drone-measurements, notably *A. arbuscula* and C. *viscidiflorus*. Findings suggest that obtaining canopy volume using drones may be an attractive strategy for shrubland managers to expand their spatial catalogue and/or increase measurement frequency without increasing costs. Doing so would allow for more accurate monitoring of land cover changes that would highlight areas where management projects would be most impactful and further damage could be most effectively prevented.

References

Anderson, J.E., Inouye, R.S., 2001. Landscape-scale chanes in plant species abundance and biodiversity of a Sagebrush Steppe over 45 years. Ecological Monographs 71, 531–556. https://doi.org/10.1890/0012-9615(2001)071[0531:LSCIPS]2.0.CO;2

Anderson, K., Gaston, K., 2013. Lightweight unmanned aerial vehicles will revolutionize spatial ecology. Frontiers in Ecology and the Environment 11, 138–146.

Bonham, C.D., 2013. Measurements for terrestrial vegetation, Second edition. ed. Wiley-Blackwell, Chichester, West Sussex, UK ; Hoboken, NJ.

Bourne, A., Bunting, S.C., 2011. Post-treatment Fuels in the Sagebrush Steppe and Juniper Woodlands of the Great Basin. Bureau of Land Management, Denver, CO.

Cao, L., Liu, H., Fu, X., Zhang, Z., Shen, X., Ruan, H., 2019. Comparison of UAV LiDAR and Digital Aerial Photogrammetry Point Clouds for Estimating Forest Structural Attributes in Subtropical Planted Forests. Forests 10, 145. https://doi.org/10.3390/f10020145

Chambers, J.C., Urza, A.K., Board, D.I., Miller, R.F., Pyke, D.A., Roundy, B.A., Schupp, E.W., Tausch, R.J., 2021. Sagebrush recovery patterns after fuel treatments mediated by disturbance type and plant functional group interactions. Ecosphere 12, e03450. https://doi.org/10.1002/ecs2.3450

CloudCompare (version 2.12.4), 2022. . GPL Software. Retrieved from http://www.cloudcompare.org/.

Cunliffe, A.M., Anderson, K., Boschetti, F., Brazier, R.E., Graham, H.A., Myers-Smith, I.H., Astor, T., Boer, M.M., Calvo, L.G., Clark, P.E., Cramer, M.D., Encinas-Lara, M.S., Escarzaga, S.M., Fernández-Guisuraga, J.M., Fisher, A.G., Gdulová, K., Gillespie, B.M., Griebel, A., Hanan, N.P., Hanggito, M.S., Haselberger, S., Havrilla, C.A., Heilman, P., Ji, W., Karl, J.W., Kirchhoff, M., Kraushaar, S., Lyons, M.B., Marzolff, I., Mauritz, M.E., McIntire, C.D., Metzen, D., Méndez-Barroso, L.A., Power, S.C., Prošek, J., Sanz-Ablanedo, E., Sauer, K.J., Schulze-Brüninghoff, D., Šímová, P., Sitch, S., Smit, J.L., Steele, C.M., Suárez-Seoane, S., Vargas, S.A., Villarreal, M., Visser, F., Wachendorf, M., Wirnsberger, H., Wojcikiewicz, R., 2021. Global application of an unoccupied aerial vehicle photogrammetry protocol for predicting aboveground biomass in non-forest ecosystems. Remote Sens Ecol Conserv 8, 57–71. https://doi.org/10.1002/rse2.228

Cunliffe, A.M., Brazier, R.E., Anderson, K., 2016. Ultra-fine grain landscape-scale quantification of dryland vegetation structure with drone-acquired structure-from-motion photogrammetry. Remote Sensing of Environment 183, 129–143. https://doi.org/10.1016/j.rse.2016.05.019

Davies, K.W., Boyd, C.S., Beck, J.L., Bates, J.D., Svejcar, T.J., Gregg, M.A., 2011. Saving the sagebrush sea: An ecosystem conservation plan for big sagebrush plant communities. Biological Conservation 144, 2573–2584. https://doi.org/10.1016/j.biocon.2011.07.016

Duarte, A., Borralho, N., Cabral, P., Caetano, M., 2022. Recent Advances in Forest Insect Pests and Diseases Monitoring Using UAV-Based Data: A Systematic Review. Forests 13, 911. https://doi.org/10.3390/f13060911

Ecke, S., Dempewolf, J., Frey, J., Schwaller, A., Endres, E., Klemmt, H.-J., Tiede, D., Seifert, T., 2022. UAV-Based Forest Health Monitoring: A Systematic Review. Remote Sensing 14, 3205. https://doi.org/10.3390/rs14133205

Ellsworth, L.M., Newingham, B.A., Shaff, S.E., Williams, C.L., Strand, E.K., Reeves, M., Pyke, D.A., Schupp, E.W., Chambers, J.C., 2022. Fuel reduction treatments reduce modeled fire intensity in the sagebrush steppe. Ecosphere 13. https://doi.org/10.1002/ecs2.4064

Entwistle, P.G., DeBolt, A.M., Kaltenecker, J.H., Steenhof, K., 1999. Proceedings: Sagebrush Steppe Ecosystems Symposium (No. BLM/ID/PT-001001+1150). Boise State University, Boise, ID, USA.

Germino, M.J., Torma, P., Fisk, M.R., Applestein, C.V., 2022. Monitoring for adaptive management of burned sagebrush-steppe rangelands: addressing variability and uncertainty on the 2015 Soda Megafire. Rangelands 44, 99–110. https://doi.org/10.1016/j.rala.2021.12.002

Gillan, J.K., Karl, J.W., Duniway, M., Elaksher, A., 2014. Modeling vegetation heights from high resolution stereo aerial photography: An application for broad-scale rangeland monitoring. Journal of Environmental Management 144, 226–235. https://doi.org/10.1016/j.jenvman.2014.05.028

Gillan, J.K., Karl, J.W., van Leeuwen, W.J.D., 2020. Integrating drone imagery with existing rangeland monitoring programs. Environ Monit Assess 192, 269. https://doi.org/10.1007/s10661-020-8216-3

Greaves, H.E., Vierling, L.A., Eitel, J.U.H., Boelman, N.T., Magney, T.S., Prager, C.M., Griffin, K.L., 2015. Estimating aboveground biomass and leaf area of low-stature Arctic shrubs with terrestrial LiDAR. Remote Sensing of Environment 164, 26–35. https://doi.org/10.1016/j.rse.2015.02.023

Guimarães, N., Pádua, L., Marques, P., Silva, N., Peres, E., Sousa, J.J., 2020. Forestry Remote Sensing from Unmanned Aerial Vehicles: A Review Focusing on the Data, Processing and Potentialities. Remote Sensing 12, 1046. https://doi.org/10.3390/rs12061046

Herrick, J.E., Van Zee, J.W., McCord, S.E., Ericha M., C., Karl, J.W., Burkett, L.M., 2017. Monitoring manual for grassland, shrubland, and savanna ecosystems, 2nd edition. ed. USDA - ARS Jordnada Experimental Range, Las Cruces, N.M.

James, M.R., Robson, S., d'Oleire-Oltmanns, S., Niethammer, U., 2017. Optimising UAV topographic surveys processed with structure-from-motion: Ground control quality, quantity and bundle adjustment. Geomorphology 280, 51–66. https://doi.org/10.1016/j.geomorph.2016.11.021

Karl, J.W., Taylor, J., Bobo, M., 2014. A double-sampling approach to deriving training and validation data for remotely-sensed vegetation products. International Journal of Remote Sensing 35, 1936–1955. https://doi.org/10.1080/01431161.2014.880820

Karl, J.W., Yelich, J.V., Ellison, M.J., Lauritzen, D., 2020. Estimates of Willow (Salix Spp.) Canopy Volume using Unmanned Aerial Systems. Rangeland Ecology & Management 73, 531–537. https://doi.org/10.1016/j.rama.2020.03.001

Laliberte, A.S., Herrick, J.E., Rango, A., Winters, C., 2010. Acquisition, Orthorectification, and Object-based Classification of Unmanned Aerial Vehicle (UAV) Imagery for Rangeland Monitoring. photogramm eng remote sensing 76, 661–672. https://doi.org/10.14358/PERS.76.6.661

Laliberte, A.S., Winters, C., Rango, A., 2011. UAS remote sensing missions for rangeland applications. Geocarto International 26, 141–156. https://doi.org/10.1080/10106049.2010.534557

Li, W., Guo, Q., Jakubowski, M.K., Kelly, M., 2012. A New Method for Segmenting Individual Trees from the Lidar Point Cloud. photogramm eng remote sensing 78, 75–84. https://doi.org/10.14358/PERS.78.1.75

Mohan, M., Leite, R.V., Broadbent, E.N., Jaafar, W.S.W.M., Srinivasan, S., Bajaj, S., Corte, A.P.D., Amaral, C.H. do, Gopan, G., Saad, S.N.M., Kamarulzaman, A.M.M., Prata, G.A., Llewelyn, E., Johnson, D.J., Doaemo, W., Bohlman, S., Zambrano, A.M.A., Cardil, A., 2021. Individual tree detection using UAV-lidar and UAV-SfM data: A tutorial for beginners. Open Geosciences 13, 1028–1039. https://doi.org/10.1515/geo-2020-0290

Olsoy, P., 2014. Aboveground total and green biomass of dryland shrub derived from terrestrial laser scanning. ISPRS Journal of Photogrammetry and Remote Sensing 88, 166–173. https://doi.org/10.1016/j.isprsjprs.2013.12.006

Padgett, P.E., 2020. Weeds, Wheels, Fire, and Juniper: Threats to Sagebrush Steppe (General Technical Report No. RMRSGTR-409). USDA Forest Service Rocky Mountain Research Station, Fort Collins, CO.

Pebesma, E., 2018. Simple Features for R: Standardized Support for Spatial Vector Data. The R Journal 10, 439–446.

Plowright, A., Roussel, J.-R., 2021. ForestTools: Analyzing Remotely Sensed Forest Data.

Prošek, J., Šímová, P., 2019. UAV for mapping shrubland vegetation: Does fusion of spectral and vertical information derived from a single sensor increase the classification accuracy? International Journal of Applied Earth Observation and Geoinformation 75, 151–162. https://doi.org/10.1016/j.jag.2018.10.009

R Core Team, 2023. R: A Language and Environment for Statistical Computing. R Foundation for Statistical Computing, Vienna, Austria.

Rango, A., Laliberte, A., Herrick, J.E., Winters, C., Steele, C., Browning, D., 2009. Unmanned aerial vehicle-based remote sensing for rangeland assessment, monitoring, and management. J. Appl. Remote Sens 3, 033542. https://doi.org/10.1117/1.3216822

Riccardi, C.L., Prichard, S.J., Sandberg, D.V., Ottmar, R.D., 2007. Quantifying physical characteristics of wildland fuels using the Fuel Characteristic Classification System. Can. J. For. Res. 37, 2413–2420. https://doi.org/10.1139/X07-175

Rittenhouse, L.R., Sneva, F.A., 1977. A Technique for Estimating Big Sagebrush Production. Journal of Range Management 30, 68–70.

Roussel, J.-R., Auty, D., Coops, N.C., Tompalski, P., Goodbody, T.R.H., Meador, A.S., Bourdon, J.-F., de Boissieu, F., Achim, A., 2020. lidR: An R package for analysis of Airborne Laser Scanning (ALS) data. Remote Sensing of Environment 251, 112061. https://doi.org/10.1016/j.rse.2020.112061

Roussel, J.-R., documentation), D.A. (Reviews the, features), F.D.B. (Fixed bugs and improved catalog, segment_snags()), A.S.M. (Implemented wing2015() for, track_sensor()), B.J.-F. (Contributed to R. for, track_sensor()), G.D. (Implemented G. for, management), L.S. (Contributed to parallelization, code), S.A. (Author of the C. concaveman, 2022a. lidR: Airborne LiDAR Data Manipulation and Visualization for Forestry Applications.

Roussel, J.-R., documentation), D.A. (Reviews the, features), F.D.B. (Fixed bugs and improved catalog, segment_snags()), A.S.M. (Implemented wing2015() for, track_sensor()), B.J.-F. (Contributed to R. for, track_sensor()), G.D. (Implemented G. for, management), L.S. (Contributed to parallelization, code), S.A. (Author of the C. concaveman, 2022b. lidR: Airborne LiDAR Data Manipulation and Visualization for Forestry Applications.

Sandberg, D.V., Ottmar, R.D., Cushon, G.H., 2001. Characterizing fuels in the 21st Century. Int. J. Wildland Fire 10, 381. https://doi.org/10.1071/WF01036

Thorne, M.S., Skinner, Q.D., Smith, M.A., Rodgers, J.D., Laycock, W.A., Cerekci, S.A., 2002. Evaluation of a Technique for Measuring Canopy Volume of Shrubs. Journal of Range Management 55, 235. https://doi.org/10.2307/4003129

Ursic, K.A., Kenkel, N.C., Larson, D.W., 1997. Revegetation Dynamics of Cliff Faces in Abandoned Limestone Quarries. The Journal of Applied Ecology 34, 289. https://doi.org/10.2307/2404877

Westoby, M.J., Brasington, J., Glasser, N.F., Hambrey, M.J., Reynolds, J.M., 2012. 'Structure-from-Motion' photogrammetry: A low-cost, effective tool for geoscience applications. Geomorphology 179, 300–314. https://doi.org/10.1016/j.geomorph.2012.08.021

Young, D.J.N., Koontz, M.J., Weeks, J., 2022. Optimizing aerial imagery collection and processing parameters for drone-based individual tree mapping in structurally complex conifer forests. Methods Ecol Evol 13, 1447–1463. https://doi.org/10.1111/2041-210X.13860

Zhao, Y., Liu, X., Wang, Y., Zheng, Z., Zheng, S., Zhao, D., Bai, Y., 2021. UAV-based individual shrub aboveground biomass estimation calibrated against terrestrial LiDAR in a shrub-encroached grassland. International Journal of Applied Earth Observation and Geoinformation 101, 102358. https://doi.org/10.1016/j.jag.2021.102358

Tables

Table 3.1. Descriptive summary (mean and range) of field measurements for shrub sampling.

Species	n	Height (m)	D_1 (m)	D_2 (m)	Volume (m^3)
A. arbuscula	15	0.43 [0.24 – 0.60]	0.81 [0.49 – 1.36]	0.62 [0.21 – 1.52]	0.15 [0.02 – 0.54]
A. tridentata ssp. *tridentata*	2*	1.27 [0.99 – 1.54]	1.63 [1.09 – 2.17]	0.96 [0.70 – 1.22]	1.27 [0.40 – 2.13]
A. tridentata ssp. *vaseyana*	15	0.70 [0.52 – 1.02]	1.03 [0.45 – 1.65]	0.89 [0.43 – 1.59]	0.41 [0.07 – 1.10]
A. tridentata ssp. *wyomingensis*	14	0.54 [0.32 – 0.87]	0.76 [0.43 – 1.56]	0.50 [0.19 – 1.21]	0.157 [0.01 – 0.86]
C. viscidiflorus	14	0.36 [0.19 – 0.49]	0.51 [0.24 – 0.69]	0.36 [0.15 – 0.55]	0.04 [0.004 – 0.07]
E. nauseosa	15	0.50 [0.20 – 0.82]	0.79 [0.23 – 1.73]	0.67 [0.17 – 2.50]	0.20 [0.01 – 0.96]
P. tridentata$_1$	15	1.00 [0.31 – 1.78]	1.57 [0.75 – 3.34]	1.31 [0.54 – 2.55]	1.76 [0.07 – 7.94]
P. tridentata$_2$	13	0.88 [0.31 – 1.53]	1.30 [0.75 – 2.03]	1.12 [0.54 – 2.05]	0.86 [0.07 – 2.63]
T. canescens	15	0.37 [0.28 – 0.46]	0.62 [0.31 – 0.97]	0.48 [0.22 – 0.70]	0.06 [0.01 – 0.16]

* only two individuals of *A. tridentata* subsp. *tridentata* were able to be sampled due to limited abundance at the site; this species was excluded from species-specific examinations.

$_{1, 2}$ with *P. tridentata* denotes inclusion and exclusion of large (field volume >7 m^3) shrubs, respectively

Table 3.2. Estimated positional errors for each processing stage.

Processing stage	X error (m)	Y error (m)	Z error (m)	Total error (m)
RTK-GNSS error	1.03148	1.06074	2.19093	2.64373
Final product fit (control points RMSE)	0.068455	0.062268	0.526201	0.534276
Final product accuracy (check points RMSE)	0.04288	0.031412	0.473474	0.476449

Table 3.3. Linear species-specific comparisons between methods to estimate volume from point clouds.

		Species	*A. arbuscula*	***A. tridentata* ssp. *vaseyana***	***A. tridentata* ssp. *wyomingensis***	*C. viscidiflorus*	***E. nauseosa***	***P. tridentata***	***T. canescens***
		n	14	**15**	**14**	15	**13**	**13**	**15**
2.5D Method: 2.5 cm	Average	m	1.18	0.86	2.09	0.79	0.85	0.80	1.22
		R^2	0.18	0.95	0.94	0.08	0.82	0.92	0.73
		MSE	0.167	0.004	0.013	0.004	0.010	0.031	0.001
		Sig	0.11	**	**	0.34	**	**	**
	Maximum	m	1.20	0.93	2.14	0.81	0.90	0.85	1.26
		R^2	0.19	0.94	0.94	0.08	0.83	0.93	0.74
		MSE	0.167	0.005	0.014	0.004	0.011	0.032	0.001
		Sig	0.11	**	**	0.33	**	**	**
2.5D Method: 5 cm	Average	m	1.21	0.90	2.18	0.87	0.92	0.89	1.27
		R^2	0.16	0.94	0.94	0.08	0.83	0.92	0.71
		MSE	0.205	0.005	0.014	0.005	0.011	0.037	0.001
		Sig	0.14	**	**	0.34	**	**	**
	Maximum	m	1.28	1.01	2.31	0.95	1.03	0.97	1.39
		R^2	0.18	0.94	0.94	0.08	0.83	0.93	0.73
		MSE	0.205	0.007	0.016	0.005	0.014	0.038	0.001
		Sig	0.12	**	**	0.32	**	**	**
CC height and width	CC-snap	m	1.04	0.90	2.27	0.40	1.28	1.28	1.47
		R^2	0.97	0.81	0.95	0.08	0.86	0.89	0.77
		MSE	0.001	0.020	0.013	0.001	0.016	0.113	0.001
		Sig	**	**	**	0.32	**	**	**
	Top-down	m	1.22	0.83	2.37	0.62	1.11	0.99	1.59
		R^2	0.84	0.92	0.94	0.16	0.81	0.85	0.86
		MSE	0.007	0.006	0.016	0.001	0.018	0.092	0.001
		Sig	**	**	**	0.15	**	**	**

****** = P<0.0001

Bold text represents species whose linear relationship between field and all drone-based techniques was highly significant.

Figures

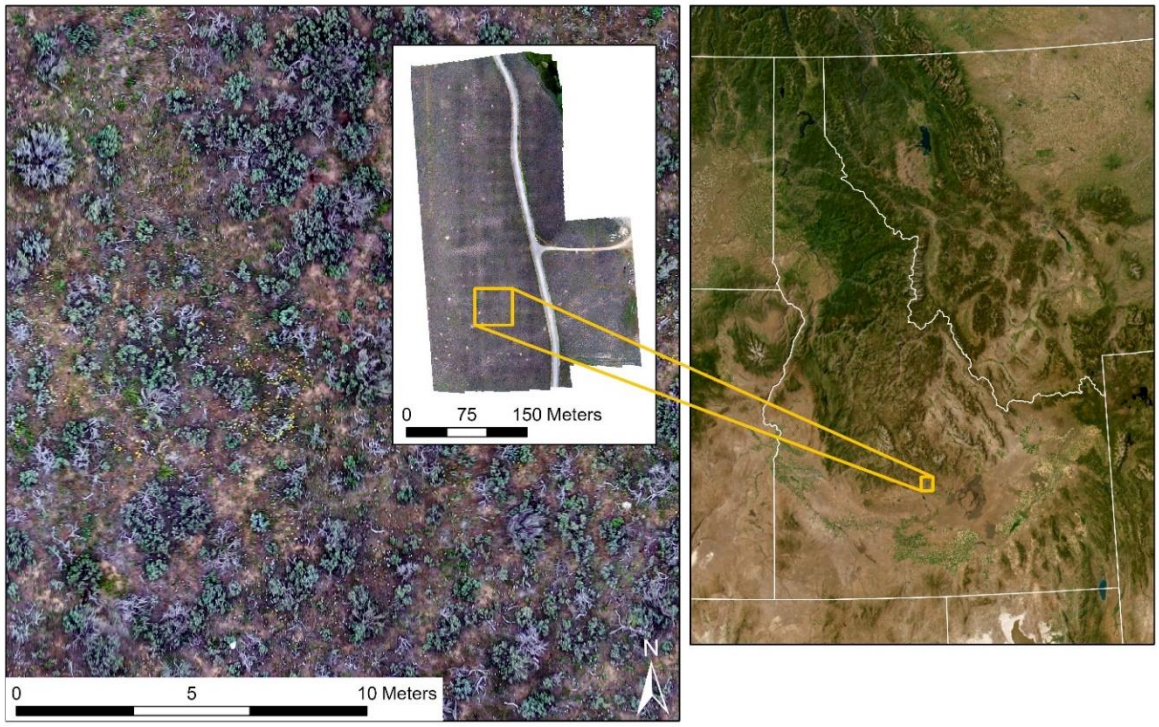

Figure 3.1. Location of the study area in southern Idaho (43.4139 °N, 114.3946 °W) and a close-up aerial orthomosaic view of shrubs created from drone imagery.

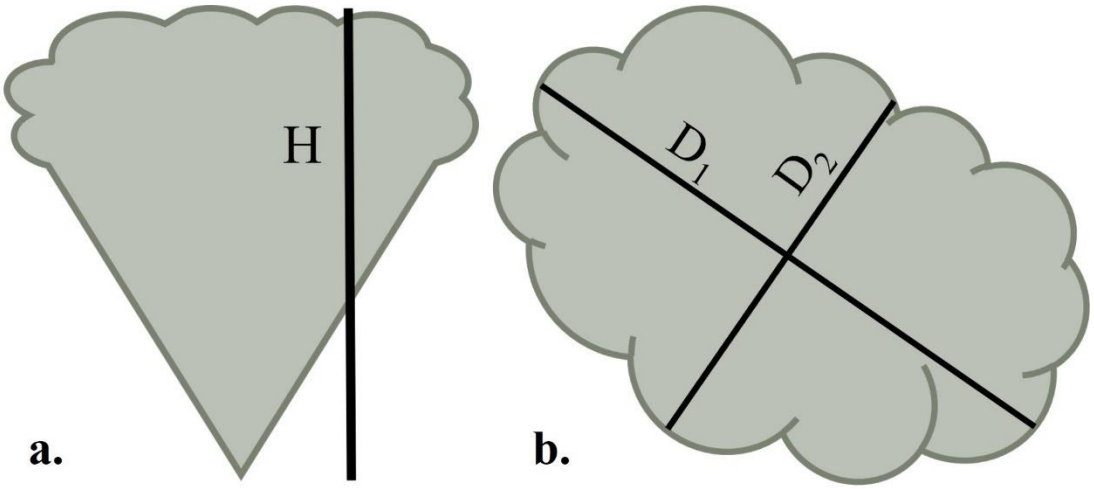

Figure 3.2. Shrub canopy volume was estimated from field-collected data on shrub maximum height (a) and two measures of canopy width (b) following Bourne & Bunting (2011).
H is shrub height, D_1 is the longest canopy width, and D_2 is the greatest canopy width perpendicular to D_1.

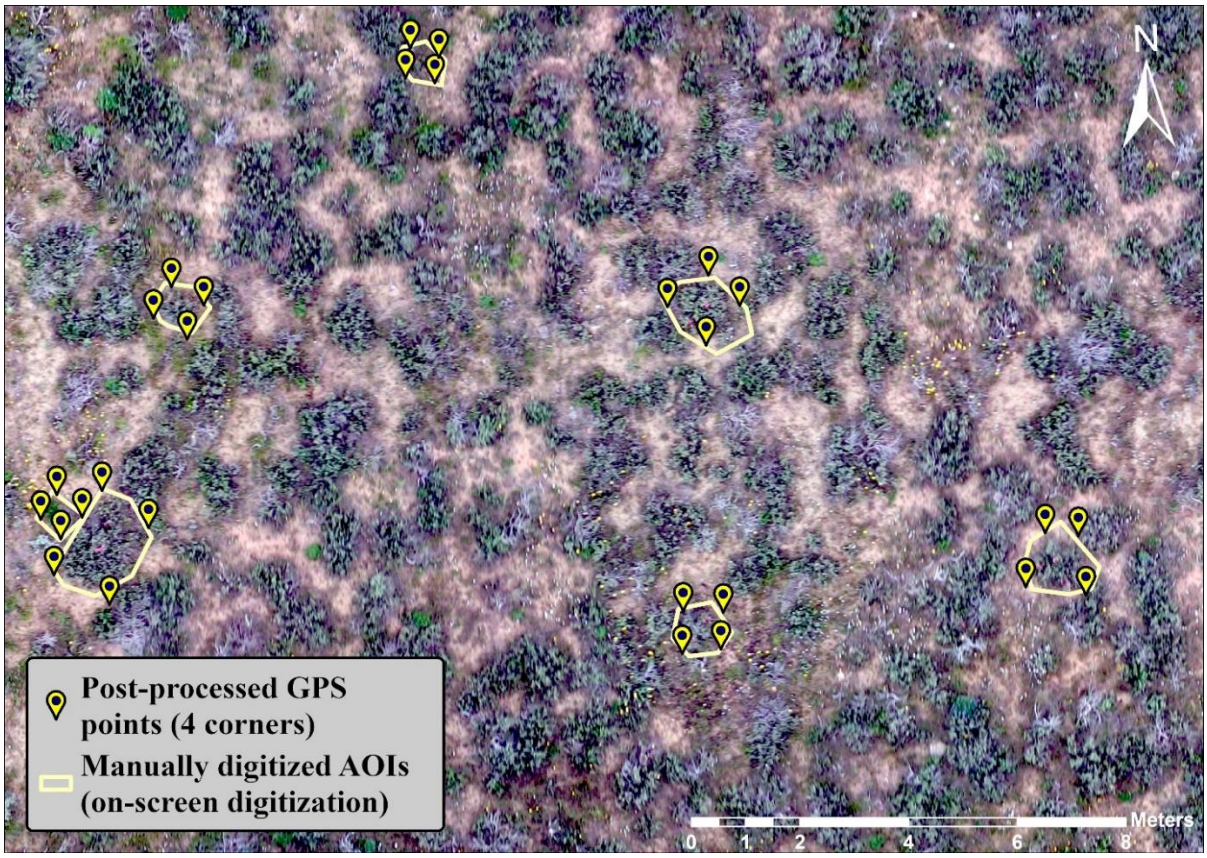

Figure 3.3. Post-processed point locations representing the four corners of each shrub were overlaid on the orthomosaic created from the drone imagery.
Shrub areas were manually digitized on screen in ArcGIS and exported for extracting each shrub from the point cloud in R.

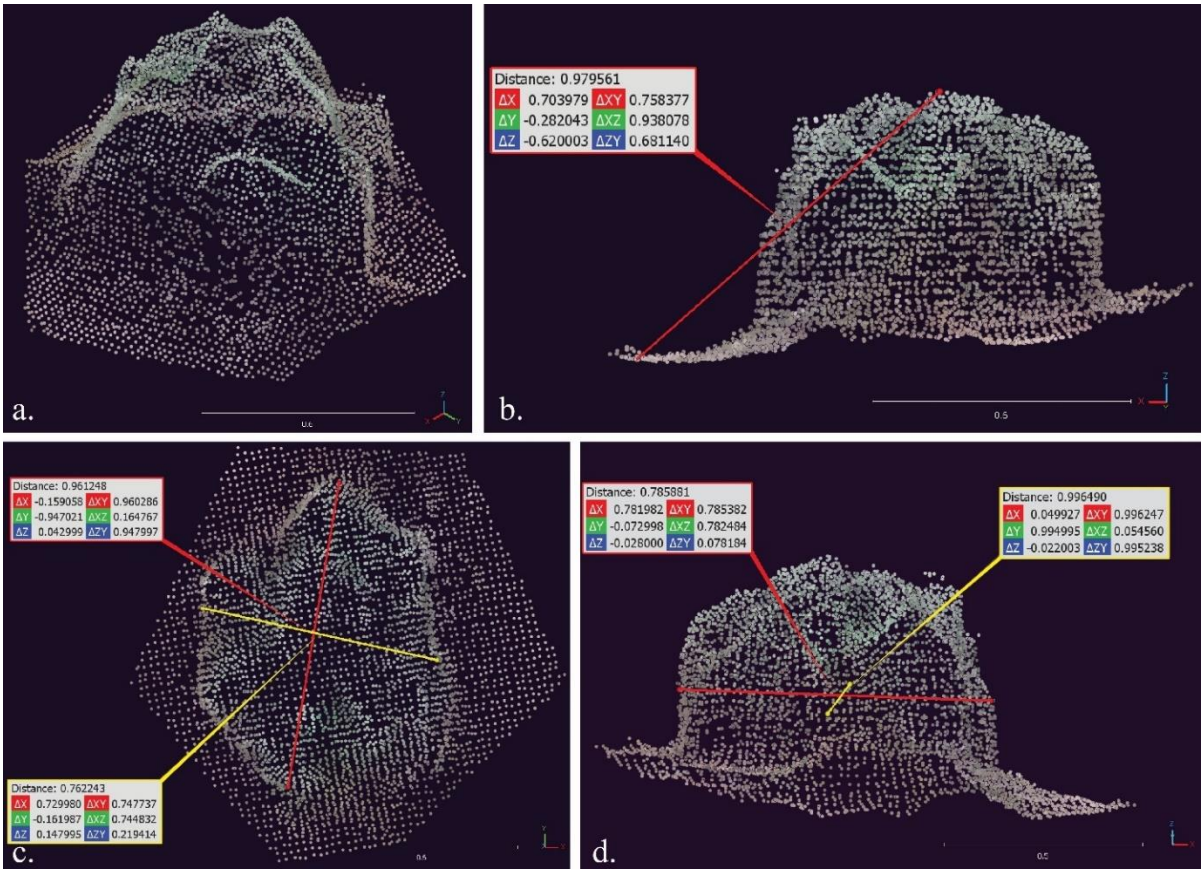

Figure 3.4. On-screen allometric methods to estimate volume of structure-from-motion-generated photogrammetric point cloud of each shrub (a) using the distance tool in CloudCompare.
For both 'top-down' and 'CC-snap' methods, height (ΔZ) was measured by selecting a point from the top-most layer of the shrub canopy and a point from the lowest layer of the shrub canopy (b). For the 'top-down' method (c), D_1 was the longest canopy width (red) and D_2 (yellow) was the greatest canopy width perpendicular to D_1. For the 'CC-snap' method (d), the shrub widths were measured using preset snap settings in CloudCompare with a south (red) and east view (yellow).

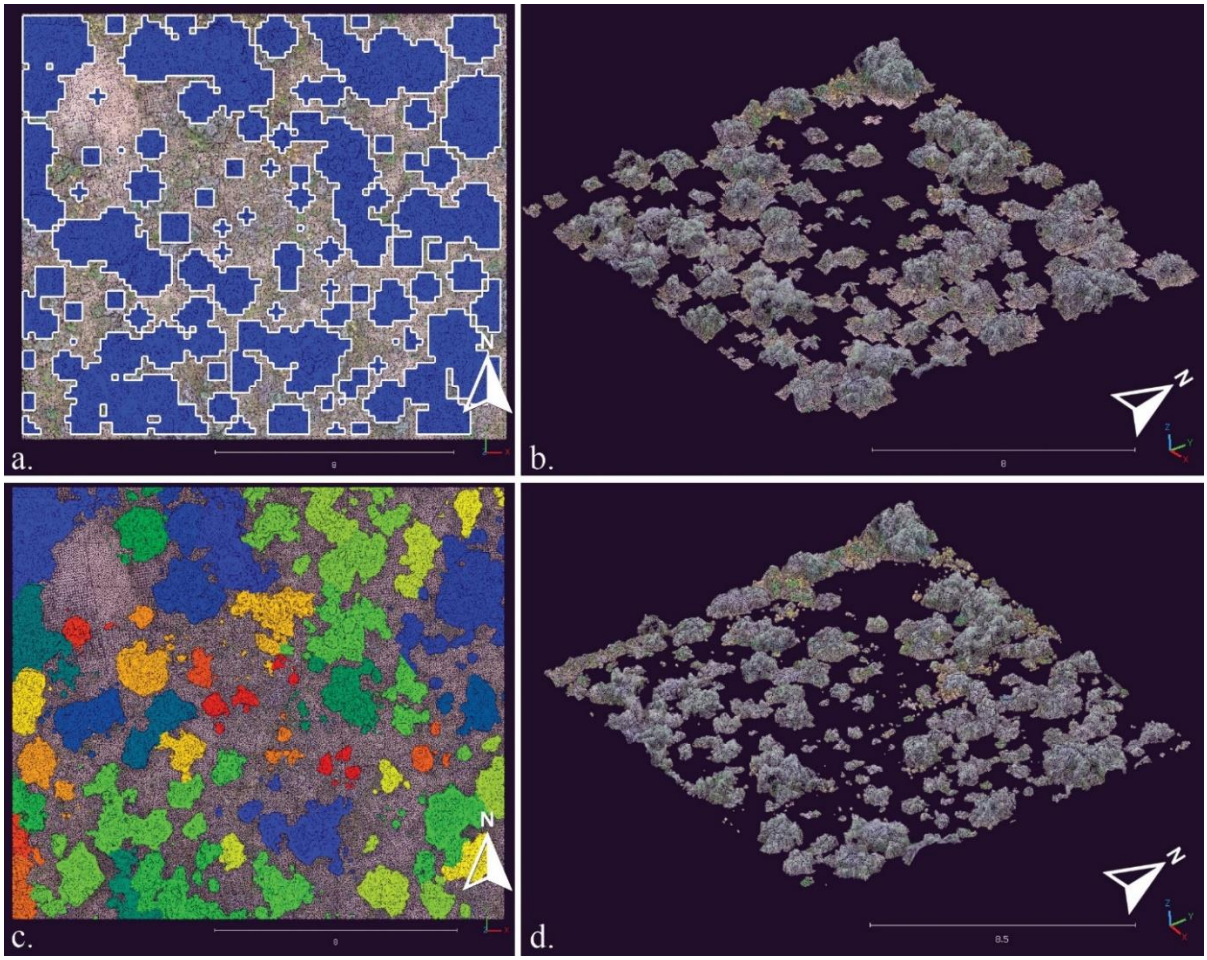

Figure 3.5. Shrub crown delineations on a subset of the study site (16.2 m by 14.2 m) using the variable window filter (VWF) algorithm outlined as blue polygons with white borders (a) are used to clip the point cloud of the study area into individual shrub point clouds (b).
Direct point cloud segmentation of individual shrubs on the same subset of the study site (16.2 m by 14.2 m) represented by a set of repeating colors (c). The individual shrubs can be filtered by their ID attribute and exported (d).

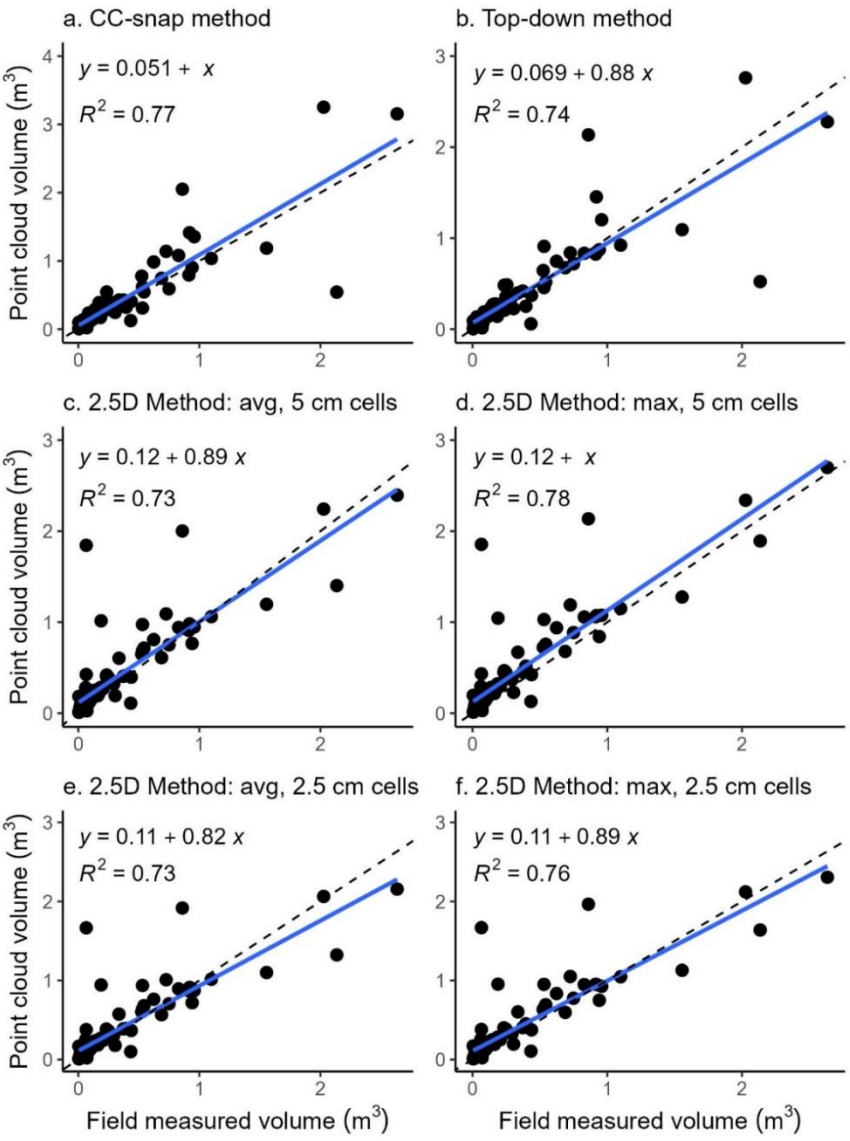

Figure 3.6. Comparing field and allometric (a-b) and volumetric (c-f) point cloud-based measurements of canopy volume.
Model fit varied by shrub size: allometric methods better fit field estimates for smaller shrubs, whereas all 2.5D methods better fit field methods for larger (>1 m^3) shrubs. All but two methods (a and d) underestimated canopy volume for larger shrubs and tended to slightly overestimate canopy volume for smaller shrubs. Blue line is linear regression line of best fit, dashed line is 1:1. For species-specific graphs for each method, see Supplemental Information 3.2. For similar comparisons between field and point cloud-based measurements but with subsets of the data based on field volume, see Supplemental Information 3.1.

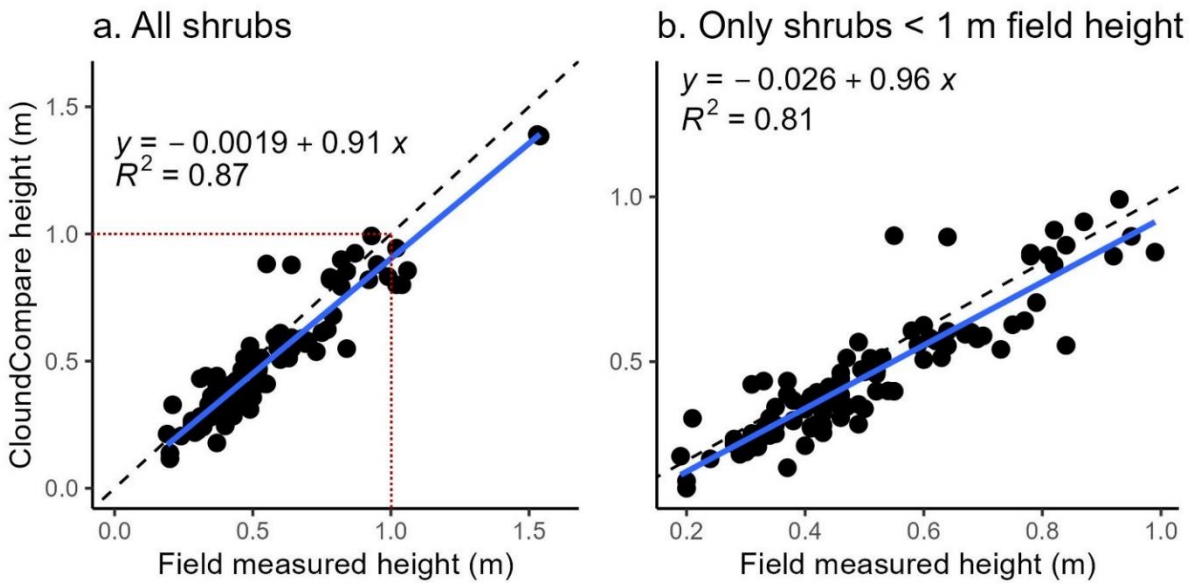

Figure 3.7. Field measured height for (a) all shrubs and (b) only shrubs whose field heights were <1 m (n = 97) compared to CloudCompare (CC) heights which were used in allometric calculation of shrub canopy volume (cc-snap and top-down).
CloudCompare height was overestimated and more variable for shrubs taller than 0.74 m. Shrubs taller than 1 m were uncommon in the study area (7.6% of shrubs measured), and the ability to accurately estimate shrub height in CC versus field-measured height was variable. In the field, the tallest perennial vegetation of each shrub (which may be a single branch) was measured for height. Thin or sparse portions of shrubs may not be well represented in the drone-based point clouds and thus not included in measurements (see Gillan et al. (2014)). Blue line is linear regression line of best fit, dashed line is 1:1.

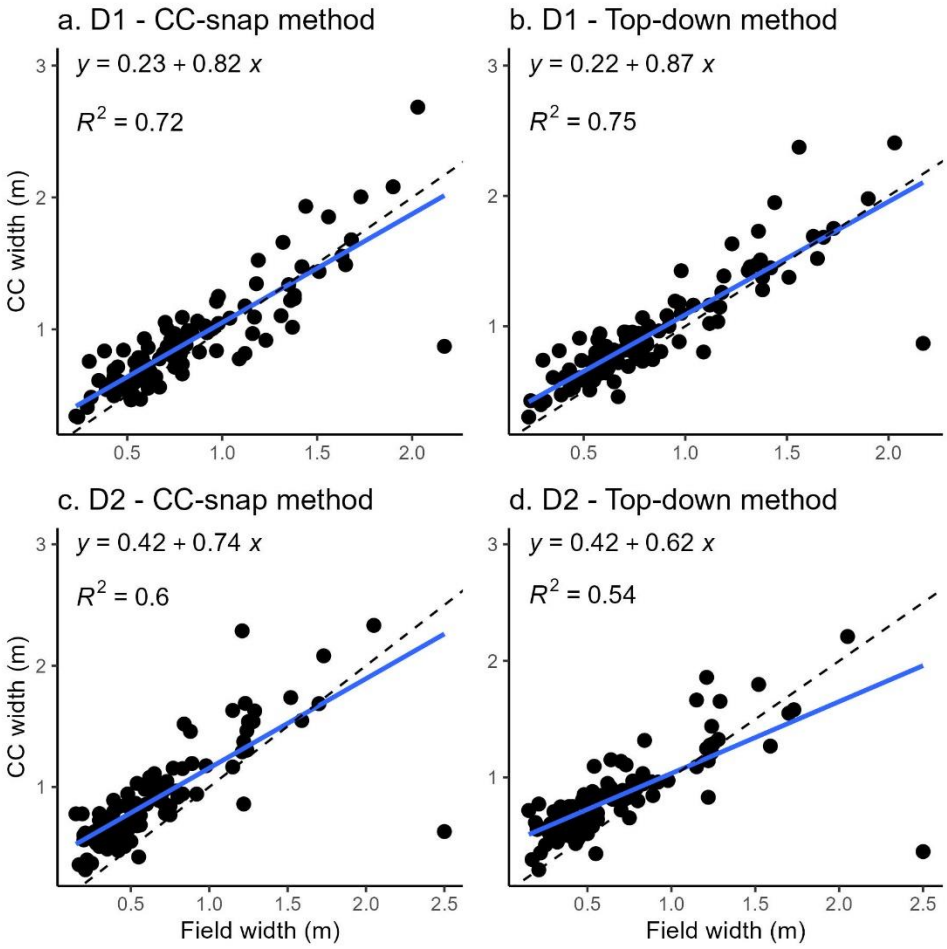

Figure 3.8. Direct comparison of field and CloudCompare measurements of shrub widths using two methods.
These two methods differ in their reliance on technician decision-making to perform measurements: the cc-snap method introduces less bias. CC-snap estimates of D_1 were slightly poorer than those from the top-down method, but measurements of D_2 were superior from cc-snap method. Blue line is linear regression line of best fit, dashed line is 1:1.

Supplemental Information

Supplemental Information 3.1. Comparison of field to point cloud estimates of canopy volume only with shrubs less than 2 m^3 and 1 m^3 volume

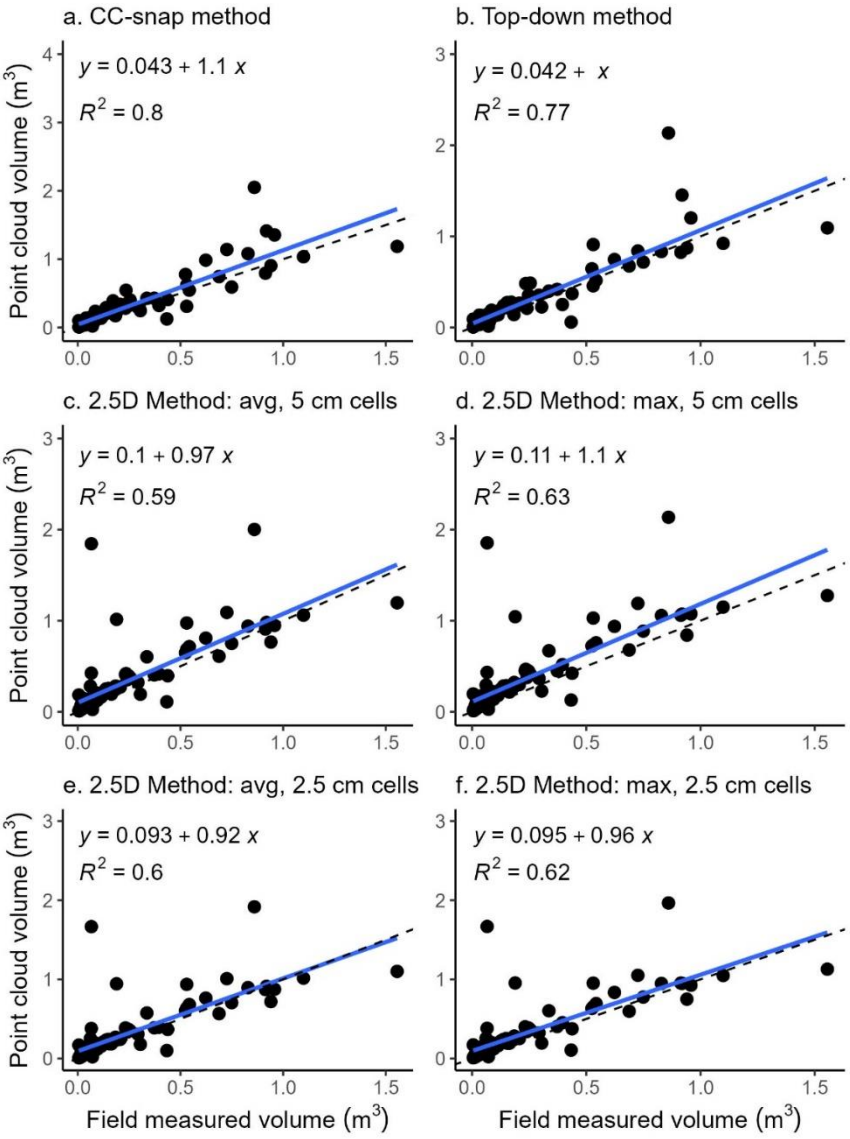

Comparing field and allometric and volumetric point cloud-based measurements of canopy volume for shrubs with field volume < 2m^3 (100/105 individuals). R^2 for 2.5D methods were poorer than when same analysis is run on all individuals, suggesting that 2.5D methods are more variable and less consistent in estimates of volume for smaller shrubs.

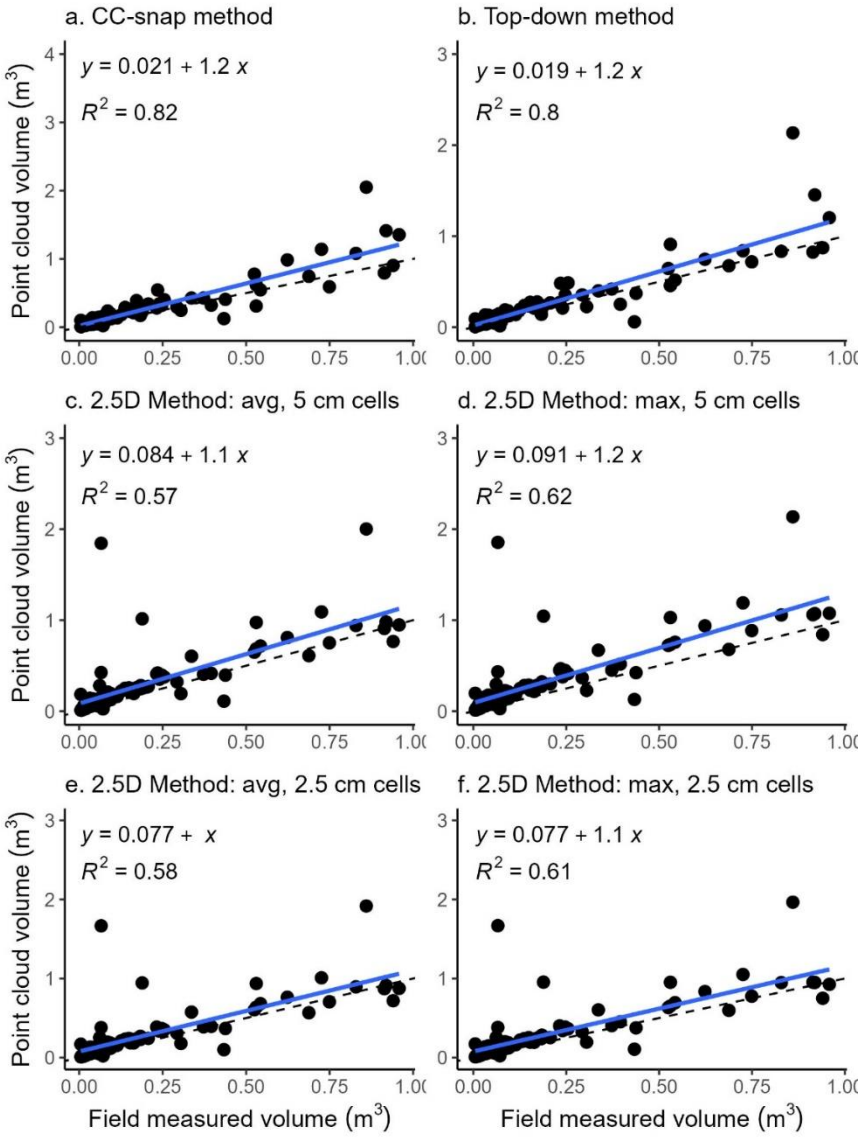

Comparing field and allometric and volumetric point cloud-based measurements of canopy volume for shrubs with field volume < $1m^3$ (98/105 individuals). R^2 estimates for allometric methods (a-b) were improved from when same analysis is run on all individuals, suggesting that these methods are more consistent for smaller shrubs. R^2 estimates for volumetric methods (c-f) were poorer than when larger shrubs were included, suggesting these methods provide more variable estimates for smaller shrubs.

Supplemental Information 3.2. Species-specific comparisons of field to point cloud estimates of canopy volume.

Species codes follow USDA PLANTS database, and are the first two letter of the genus and specific epithet and the first letter of the subspecies name, if applicable.

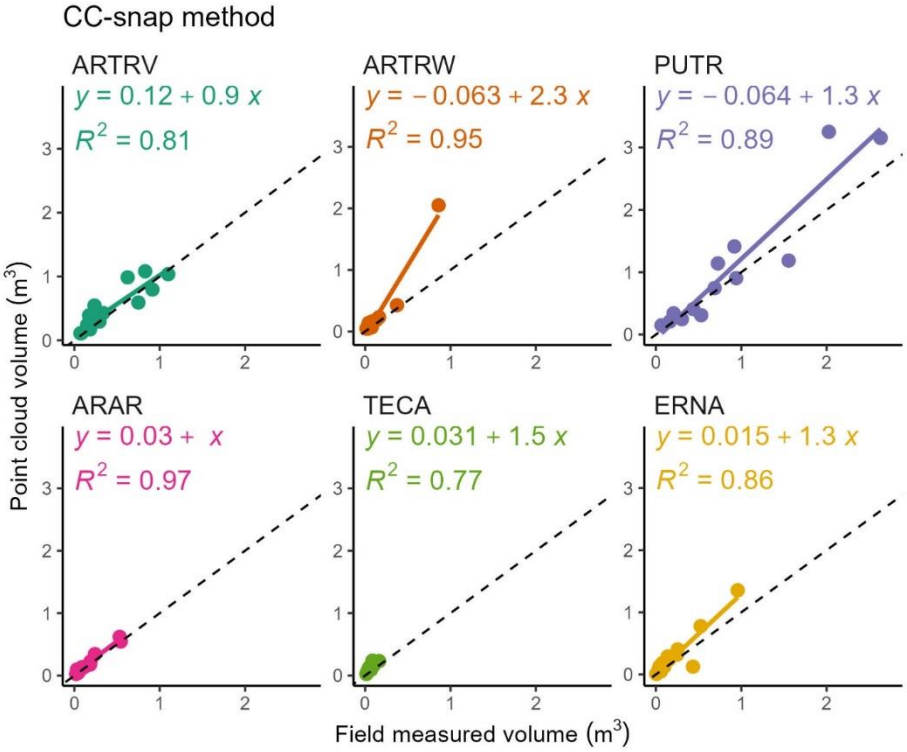

Species-specific comparisons for the cc-snap allometric method for point cloud-based volume estimates.

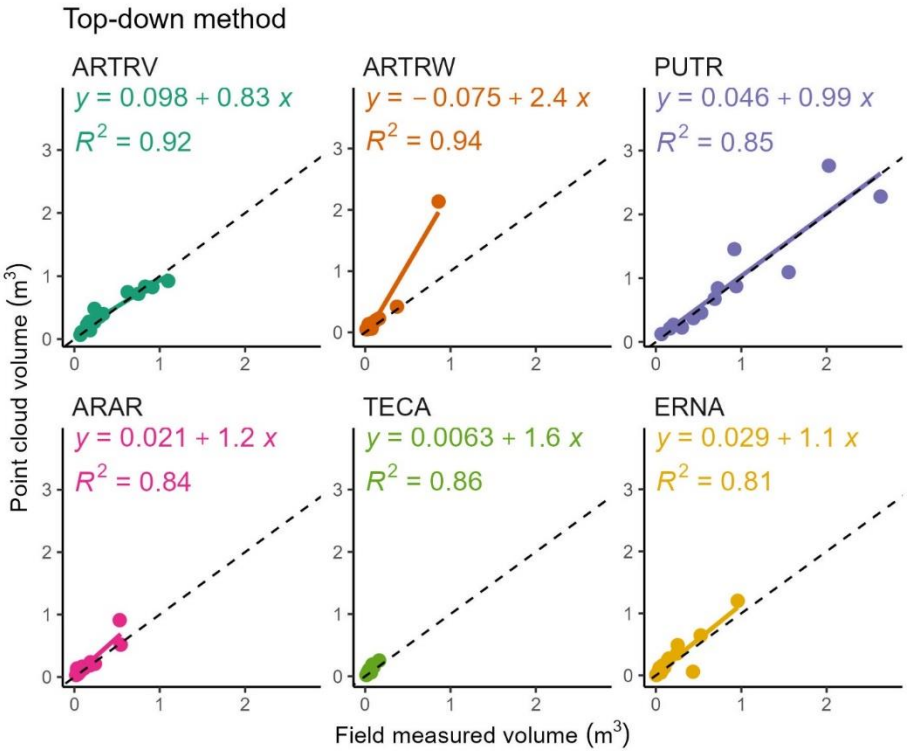

Species-specific comparisons for the top-down allometric method for point cloud-based volume estimates.

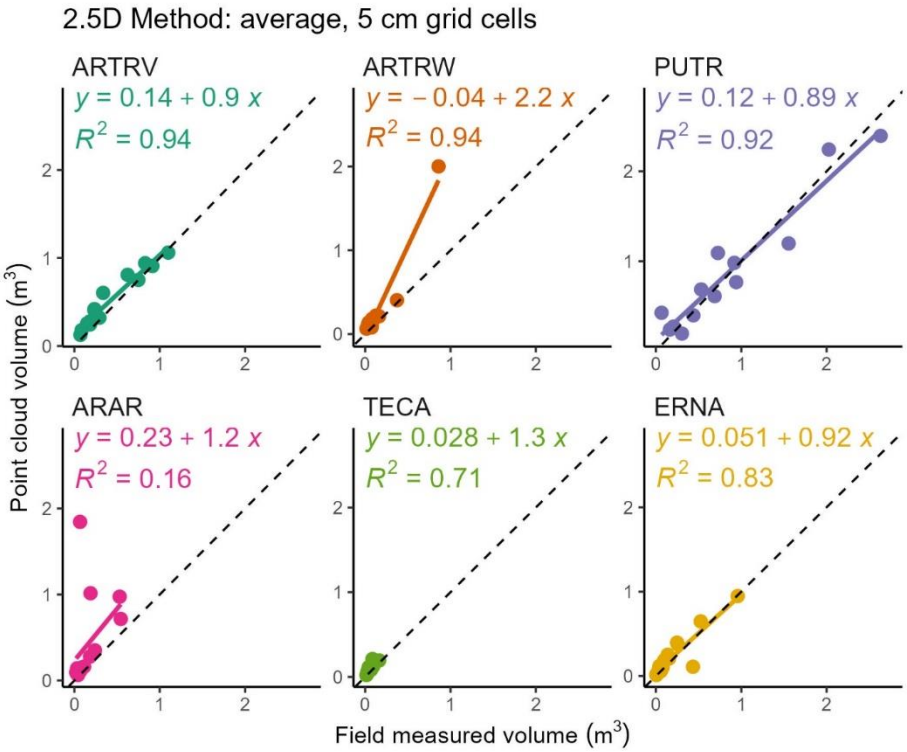

Species-specific comparisons for the volumetric method with average cell height for 5 cm cell dimensions for point cloud-based volume estimates.

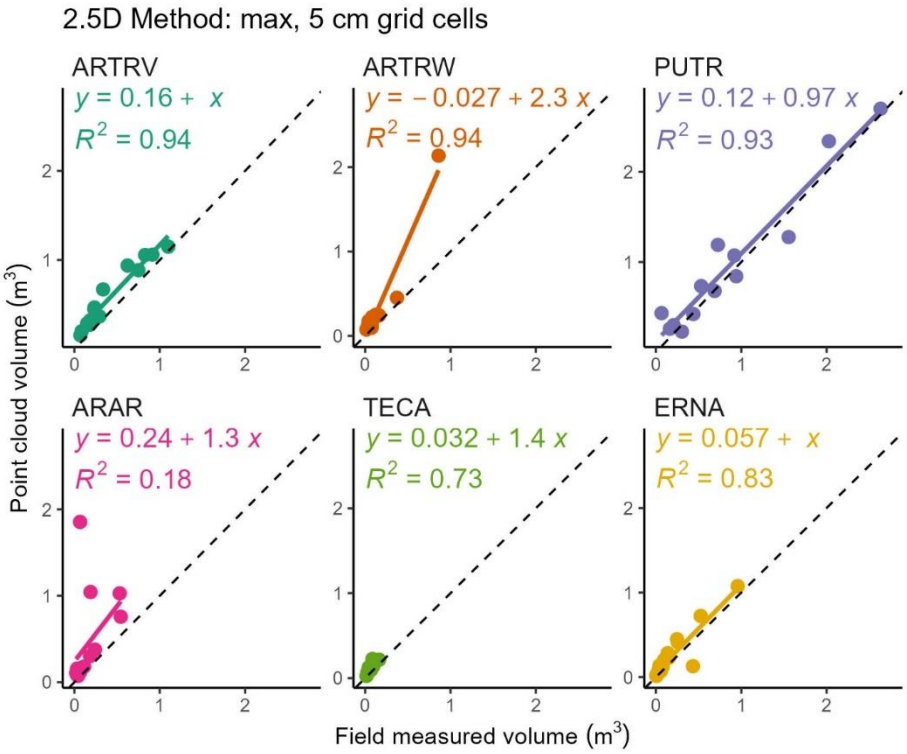

Species-specific comparisons for the volumetric method with maximum cell height for 5 cm cell dimensions for point cloud-based volume estimates.

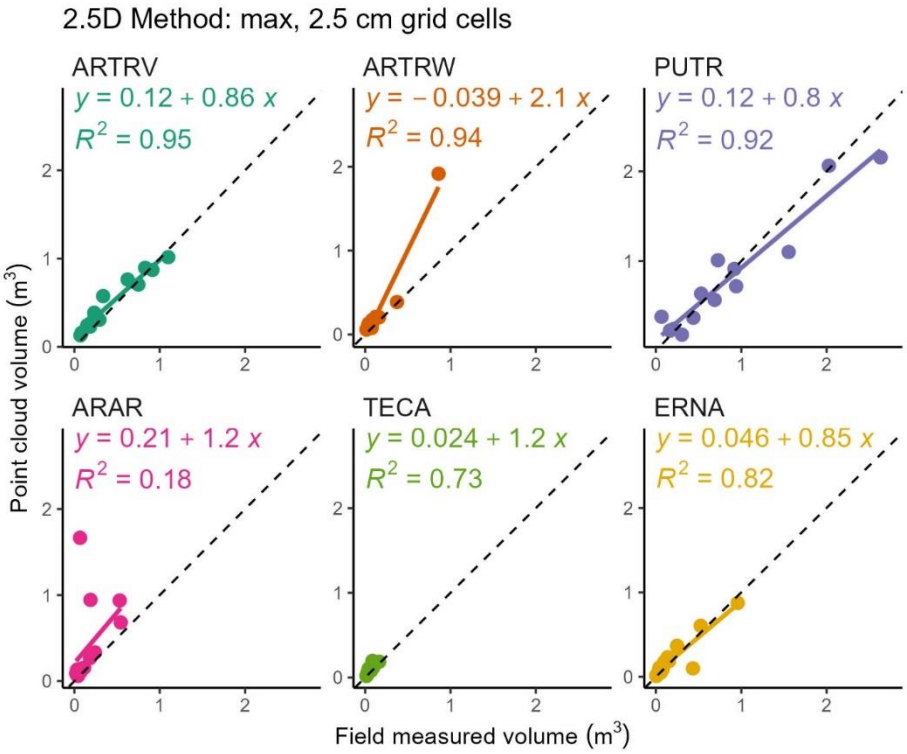

Species-specific comparisons for the volumetric method with average cell height for 2.5 cm cell dimensions for point cloud-based volume estimates.

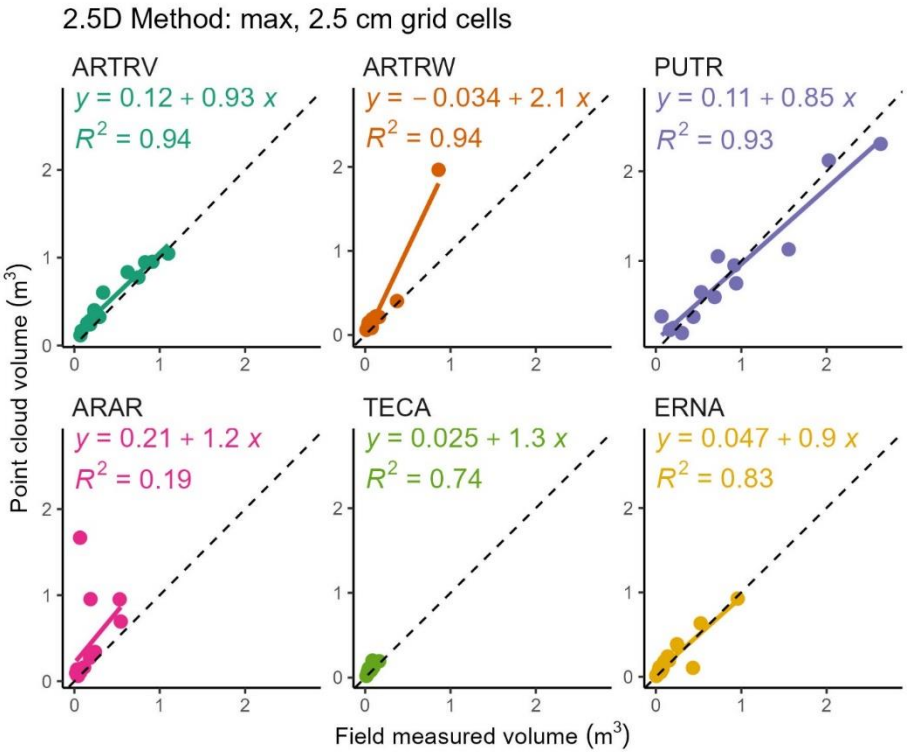

Species-specific comparisons for the volumetric method with maximum cell height for 2.5 cm cell dimensions for point cloud-based volume estimates.

Supplemental Information 3.3. Automatic shrub detection and delineation error matrices and accuracy metrics.

Variable window filter (VWF) error matrix and accuracy metrics

Reference data				
Predicted data	Not shrub	Shrub	Row Total	**Commission error**
Not shrub	35	22	57	38.60%
Shrub	10	53	63	15.87%
Column Total	45	75	120	
Omission error	22.22%	29.33%	**Overall Accuracy**	73.33%

Fixed window local maximum filter (LMF) error matrix and accuracy metrics

Reference data				
Predicted data	Not shrub	Shrub	Row Total	**Commission error**
Not shrub	40	30	70	42.86%
Shrub	6	44	50	12.00%
Column Total	46	74	120	
Omission error	13.04%	40.54%	**Overall Accuracy**	70.00%

Direct point cloud segmentation error matrix and accuracy metrics

Reference data				
Predicted data	Not shrub	Shrub	Row Total	**Commission error**
Not shrub	23	5	28	18.00%
Shrub	23	69	92	25.00%
Column Total	46	74	120	
Omission error	50.00%	7.00%	**Overall Accuracy**	76.67%